Effectiveness of Ecosystem-based Adaptation Measures Subject to Sea Level Rise & Land Subsidence

Modelling Report of 'Ecosystem-based Adaptation at Scale Through Building with Nature Towards Resilient Coasts in Indonesia' project in Demak

Effectiveness of Ecosystem-based Adaptation Measures Subject to Sea Level Rise & Land Subsidence
Modelling Report of 'Ecosystem-based Adaptation at Scale Through Building with Nature Towards Resilient Coasts in Indonesia' project in Demak

Authors
Bob Smits
Miguel de Lucas Pardo
Bregje van Wesenbeeck

Project statement
This report was written in the context of the Building with Nature Indonesia programme by Ecoshape, Wetlands International, the Indonesian Ministry of Marine Affairs and Fisheries (MMAF), and the Indonesian Ministry of Public Works and Human Settlement (PU), in partnership with Witteveen+Bos, Deltares, Wageningen University & Research Centre, UNESCO-IHE, Blue Forests, and Von Lieberman, with support from the Diponegoro University, and local communities.
"Building with Nature Indonesia" is supported by the Dutch Sustainable Water Fund, the German Federal Ministry for the Environment, Nature Conservation and Nuclear Safety (BMU) as part of the International Climate Initiative (IKI), Waterloo Foundation, Otter Foundation, Topconsortia for Knowledge and Innovation, and Mangroves for the Future.
The cover photo is a drone picture showing permeable structures in Bedono, Demak district, by Building with Nature Indonesia.

Disclaimer
Project partners are committed to drive the current Building with Nature innovation trajectory, by demonstrating the approach in a case study site in Demak. Successful implementation requires in-depth system understanding, extensive stakeholder engagement, and adaptive management on the basis of monitoring and evaluation. We stimulate and support upscaling of the approach by disseminating knowledge, lessons learned and implementation guidance. Stakeholders interested to replicate our approach are strongly recommended to adhere to this guidance and bear full responsibility for the success and sustainability of the approach.

Effectiveness of Ecosystem-based Adaptation Measures Subject to Sea Level Rise & Land Subsidence

Modelling Report of 'Ecosystem-based Adaptation at Scale Through Building with Nature Towards Resilient Coasts in Indonesia' project in Demak

Opdrachtgevers	Wetlands International and EcoShape
Contactpersoon	Femke Tonneijck and Fokko van der Goot
Referenties	Contract number WI-NL 1354
Trefwoorden	Sediment modelling, Nature-Based Solutions, Sea Level Rise, Land Subsidence, Building with Nature

Documentgegevens	
Versie	3.0
Datum	December 2020
Projectnummer	1220476
Document ID	1220476-004-ZKS-0011
Pagina's	36
Status	definitief

Auteur(s)		
	Bob Smits Miguel de Lucas Pardo Bregje van Wesenbeeck	

Doc. Versie	**Auteur**	**Controle**	**Akkoord**	**Publicatie**
1.0	Bob Smits	Bas van Maren, Han Winterwerp		November 2019
2.0	Bob Smits	Bas van Maren		Juli 2020
3.0	Bob Smits	Bas van Maren	Toon Segeren	December 2020

Executive summary

In many places in South East Asia low-lying coastal areas are increasingly densely populated through expanding populations and migration to coastal megacities. These low-lying areas are becoming increasingly vulnerable to flooding through sea level rise and land subsidence, threatening coastal communities and ecosystems. The coastal zone of Demak district (Central Java, Indonesia) provides an example of such a threatened coastal zone, where severe erosion was observed for the last 20 years as a result of subsidence caused by groundwater extraction. The replacement of mangrove forests with aquaculture ponds and embankment of rivers resulted in declining sediment input and sediment trapping, exacerbating the erosion problems. This study assesses the effectiveness of the permeable structures implemented to restore eroding mangrove mud coastline near Demak under various rates of relative sea level rise.

To mitigate erosion, enhance accretion and restore the mangrove ecosystem, permeable bamboo structures were implemented in the intertidal zone near Demak. These structures were designed to attenuate waves and create sheltered conditions suitable for sediment accretion and mangrove recruitment. The design and construction of these semi-permeable structures was part of the ongoing projects funded by SWF and IKI. These projects also aimed to rehabilitate aquaculture to improve livelihoods of coastal communities and focused strongly on building capacity in the community and on knowledge transfer to different government levels. In the present study, the effectiveness of these structures is investigated using a numerical model.

The study area is characterised by a shallow muddy coastline of 20 km with a mixed, diurnal tide (tidal range of 40-60 cm). The wave climate is dominated by the northwest monsoon season, with average significant wave heights around 50 cm. On a timescale of five to ten years, land subsidence and sea level rise are likely the most important drivers of coastal change in the area. Based on those drivers, the effectiveness of the implemented permeable structures was assessed under various scenarios of sea level rise and land subsidence by simulating morphodynamic development of the coastal zone. A process-based numerical model was used to compare the 10-year development of the coast under these scenarios for conditions with and without the implementation of permeable structures.

In this scenario study, eustatic sea level rise (based on RCP scenarios by IPCC) and land subsidence (based on local observations) were combined in a rate of relative sea level rise. Note that the rate of land subsidence (~8-13 cm/year) is roughly twenty times larger than the rate of eustatic sea level rise (~0.4-0.6 cm/year). As land subsidence was assumed linear over time and spatially uniform, the model will not provide spatially-varying patterns in relative sea level rise at the scale of the entire project area. The following scenarios were considered in this study:

- Best-case scenario: relative sea level rise rate of 8.2 cm per year
- Intermediate scenario: relative sea level rise rate of 10.5 cm per year
- Worst-case scenario: relative sea level rise rate of 13.6 cm per year

A 2-dimensional depth-averaged Delft3D Flexible Mesh model was used to simulate flow, waves, sediment transport and morphology. Local bathymetry data (based on a combination of sources) and tidal boundary conditions (extracted from a global tidal model) were used to simulate the local flow pattern. The model was coupled to a SWAN wave model with time-varying wave boundaries (significant wave height between 0.4 and 1.0 m; peak wave period between 4.8 and 5.2 s). Two fine sediment fractions were included in

the model to simulate sediment deposition and erosion. Model results were not significantly affected by the initial sediment distribution and seaward boundary conditions for suspended sediment (within the studied ranges).

This model is used as a tool to gain more insight into the behaviour of the Demak coastal system under relative SLR and the effect of implementing permeable structures. The model does not exactly predict flooding and bed level changes but does provide indicative trends and developments in the Demak Coastal zone through user's expert judgement. Model results showed that without implementing permeable structures the intertidal area eroded, decreasing the bed level by roughly 0.4 m over a ten-year period (Autonomous development in Table 1). However, to keep up with relative sea level rise, accretion of intertidal areas is required. Thus, without implementing permeable structures, the Demak coastal zone was submerged for all investigated scenarios of relative sea level rise. With implementation of permeable structures, the bed level behind the structures increased by 0.3-0.4 m (Permeable structures in Table 1). Consequently, the final bed level behind the structures was 0.8 m higher for the scenarios with structures compared to the scenario without structures (Difference in Table 1). The difference plot (Figure 1) was created by substracting the final bed level with permeable structures from the final bed level without structures. Furthermore, results indicated that for higher rates of relative sea level rise, sediment trapping behind structures increased. Thus, the permeable structures trap sediment for all scenarios, but not enough to keep pace with sea level rise, i.e. relative sea level rise is only partly compensated by sediment accretion. Without permeable structures, on the other hand, the increase in water depth would have been much larger than the amount of relative sea level rise.

Another important conclusion from this modelling study was that bed level behind permeable structures managed to keep up with relative sea level rise until a critical threshold of sea level rise was exceeded. This critical threshold is linked to the transition from net accretion to net erosion and can be identified by the inflection point in the bed level development in Figure 2. For the specific structure highlighted here, the critical total amount of sea level rise was roughly 50-60 cm (independent of the scenario), but this value should not be taken as a reference for all structures, because it is location dependent. After exceeding this threshold, permeable structures were no longer able to capture enough sediments for the bed level to keep pace with relative sea level rise. This was caused by insufficient wave damping: larger water depths result in higher waves, initiating larger bed shear stresses. Once these higher bed shear stresses result in net bed erosion (instead of accretion) the water depth increases rapidly, and the intertidal area drowns.

Table 1: Average bed level change after 10 years at observation points behind the permeable structures for different scenarios and simulations with and without permeable structures. Positive values indicate accretion, negative values indicate erosion of the sea bed.

Scenario	**Average bed level change [m]**		**Difference Δz [m]**
	Autonomous development	**Permeable structures**	
Best-case (0.82 m rSLR)	-0.44	+0.34	+0.78
Intermediate (1.05 m rSLR)	-0.45	+0.38	+0.84
Worst-case (1.36 m rSLR)	-0.44	+0.44	+0.88

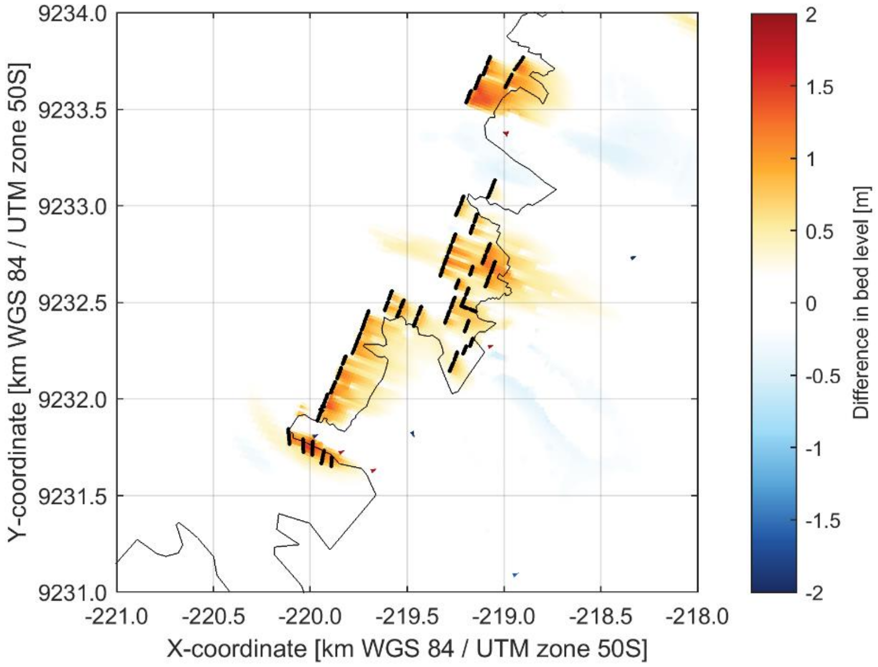

Figure 1: Difference plot between final bed level with and without permeable structures for the intermediate scenario, showing a zoom around the area of the structures. Red colours indicate higher bed levels in the simulation with permeable structures, blue colours indicate lower levels.

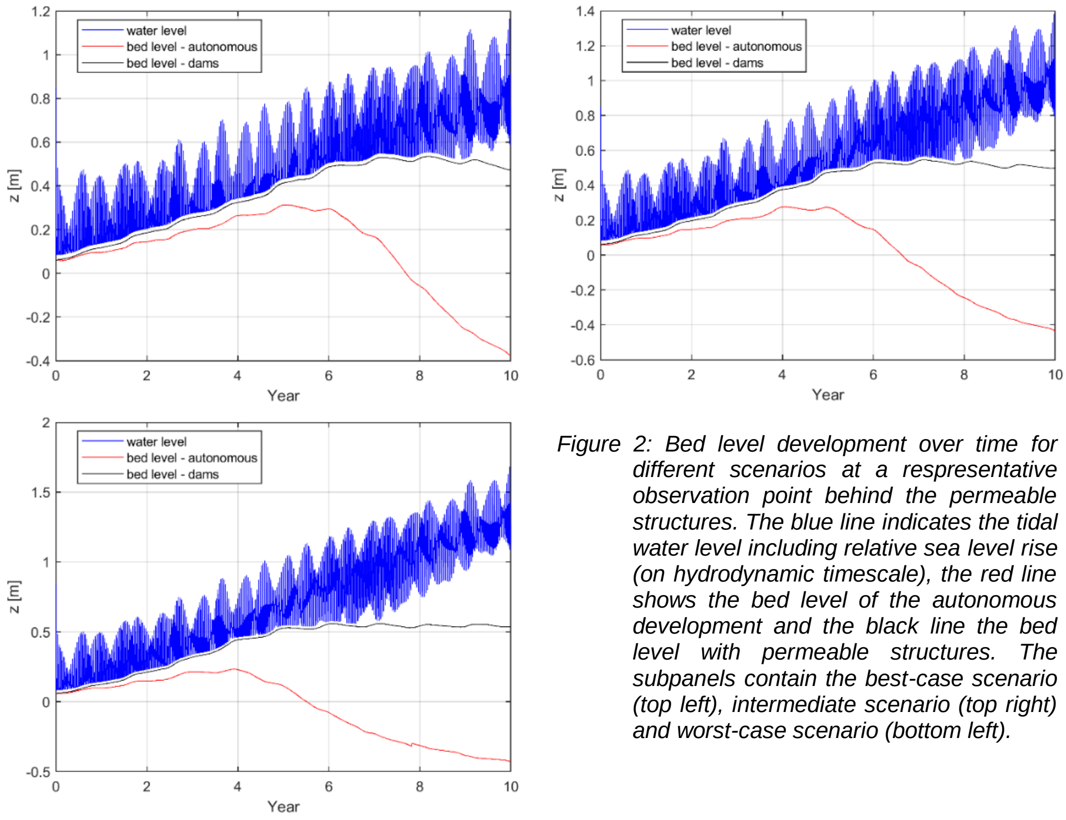

Figure 2: Bed level development over time for different scenarios at a representative observation point behind the permeable structures. The blue line indicates the tidal water level including relative sea level rise (on hydrodynamic timescale), the red line shows the bed level of the autonomous development and the black line the bed level with permeable structures. The subpanels contain the best-case scenario (top left), intermediate scenario (top right) and worst-case scenario (bottom left).

This modelling study therefore suggests that without mitigating measures (such as the permeable structures) the high land subsidence rates in Demak will result in rapid loss of coastal areas. Permeable structures to reduce wave impact and trap sediment may help in mitigating the effects of relative sea level rise. Model simulations showed that permeable structures locally stimulate sediment accretion, and even enable the bed level to keep up with relative sea level rise for a number of years (based on the assumptions in this study a period of 5-7 years, depending on the scenario). However, on the long term and with the extreme subsidence rates typical for our project area, this positive effect of structures is not sufficient to protect the coastline from eroding and submerging in the long-term.

The main recommendations derived from the current study to mitigate coastal erosion are:

- To use this model as a tool to assess the potential of new coastal interventions on a time scale of 5 to 10 years and optimise the spatial design of such interventions.
- To mitigate land subsidence. The model results show that relative sea level rise can cause a lot of erosion and flooding. As about 90% of the relative sea level rise is caused by land subsidence, efforts should be undertaken to minimise the amount of land subsidence. The model results substantiate this statement.

Contents

1 Introduction

1.1 Problem description: global trend

The long-term sustainability of mangroves is threatened by sea level rise, putting these valuable ecosystems, as well as coastal communities, at risk (Nicholls & Cazenave, 2010; Woodruff *et al*, 2013). Mangrove forests have the capacity to keep pace with sea-level rise and to avoid inundation through vertical accretion of sediments, which allows them to maintain bed level elevations suitable for plant growth (Kirwan & Megonigal, 2013; Allongi, 2008). In many coastal systems throughout Asia, however, sediment availability is declining due to anthropogenic activities, such as damming of rivers and deforestation. Analysis of recent trends in mangrove surface elevation changes across the Indo-Pacific region by Lovelock *et al.* (2015) showed that for 69% of their study sites the current rate of sea level rise exceeded the sediment accretion rates. Using a model based on field data, Lovelock *et al.* (2015) suggest that sites with low tidal range and low sediment supply could be submerged as early as 2070 (even without considering land subsidence). Hence, sediment availability is a key factor to achieve bed level elevation gains and to enable mangroves to maintain their elevation above mean sea level.

Though mangroves are rather resilient to sea level rise in a natural state, the impact may be detrimental where combined with land subsidence. Reported subsidence rates up to 2.5 cm per year in the Mekong Delta (Minderhoud *et al.*, 2017), around 12 cm per year near Bangkok (Phien-Wej *et al.*, 2006) and 9 cm per year in Manila Bay (Rodolfo & Siringan, 2006; MBSDMP, 2019), indicate that land subsidence rates are outpacing global sea level rise by an order of magnitude. For each of these examples excessive groundwater extraction is the main driver of land subsidence.

To combat mangrove loss and restore the sediment balance, large scale restoration efforts are implemented across the world. Permeable structures made of bamboo piles and brushwood have successfully reduced erosion and stimulated sedimentation in comparable muddy environments in Vietnam, Thailand and the Philippines. In the Mekong delta this approach successfully reduced wave energy and achieves up to 20 cm of sediment accretion per year (Schmitt *et al*., 2013; Van Cuong *et al*., 2015). In Chachoengsao province (near Bangkok) deposition rates of 20-25 cm per year were measured behind such structures (Saengsupavanich, 2013). Ultimately, the future potential for persistence of sustainable mangrove forests along heavily disturbed coastlines under influence of sea level rise depends on the success of these type of ecosystem-based adaptation measures.

1.2 Problem analysis: local characteristics

The coastal zone of Demak district (Central Java, Indonesia) suffers from severe erosion. The coastline retreated hundreds of meters in recent decades (Ecoshape, 2015) as a result of land subsidence, removal of mangrove forests, installation of aquaculture ponds in the intertidal and disconnecting rivers from the floodplains. The present-day eroding coastline of Demak is characterized by an irregular pattern of protruding sections of land, often around rivers and flooded inlets, at some locations an offshore chenier is present (Figure 1.1).

Figure 1.1: Drone image of the project location made in February 2016, showing the heavily eroded coastline, as well as the permeable structures that have already been implemented (courtesy of Tom Wilms, Witteveen+Bos)

Historically, the coastal zone of Demak district was fronted by a mangrove greenbelt that attenuated waves and captured and stabilised sediment. However, the conversion of mangrove belts into aquaculture ponds has impeded this protective function (Winterwerp, *et al.*, 2013; Van Wesenbeeck *et al*., 2015). Additionally, the sediment supply to the intertidal area is diminished, as aquaculture pond systems disconnect the river from the natural floodplain. Storm surges, high tides and periods of excessive rainfall have severely increased flood risk in the area. Over the past decades rapid shoreline degradation and erosion have been recorded to amount up to 1.4 km of retreat in certain areas (Winterwerp *et al*., 2014). Moreover, the removal of mangroves has led to loss of other ecosystem services (i.e. economic, environmental and social services), such as carbon capture and storage.

On a timescale of five to ten years, however, land subsidence and sea level rise are likely the most important drivers of coastal change in the area. Therefore, these are the two variables considered in this study as relative sea level rise (i.e. the sum of eustatic sea level rise and land subsidence). Other climate change effects, apart from sea level rise (e.g. increased frequency and intensity of storms and rainfall), are not considered. It is important to note that the rate of land subsidence (between 5-10 cm/year, see section 2.6) is roughly one order of magnitude larger than worst-case projections for regional sea level rise (Chaussard *et al*, 2013). So, land subsidence currently dominates coastal flooding and erosion problems in the study area.

A coastline restoration project was setup and executed under the umbrella of EcoShape and Wetlands International, targeting to restore the coastal area by installing permeable structures (e.g. Arentz & Van Wesenbeeck, 2013; Winterwerp, *et al.*, 2014; Ecoshape, 2015). The project aims to stimulate regrowth of a healthy mangrove ecosystem by restoring the fine sediment balance. So far, however, rapid mangrove recovery as a result of implementation of permeable structures, has not yet been observed. It should be noted that during the first implementation phase, the extreme land subsidence rates, which certainly affects the potential to restore mangroves, were unknown. Nevertheless, the project still remains a very relevant opportunity for studying the efficiency of permeable structures in capturing sediment, particularly under the extreme local subsidence rates. In this study the effectiveness of the permeable structures to restore eroding mangrove mud coastlines is assessed on a time scale of five to ten years under the influence of sea level rise and land subsidence.

1.3 Project area

The area of interest is Demak district, located on central Java (Indonesia) at the Java Sea coast. Figure 1.2 shows the location and definition of the project area. Sediment dynamics are mainly driven by tides and waves, which largely depend on the local meteorology. The area is subject to monsoons, which determine prevailing wind directions and rainfall intensities. The northwest monsoon occurs between November and April, with prevailing western winds over the Java Sea. The wind speed peaks in the months December, January and February, typically around 10-15 m/s. The southeast monsoon occurs between May and October, with winds over land from east and southeast directions. The southeast monsoon reaches its greatest strength in July and August with wind speeds of about 5-10 m/s (Wyrtki, 1961). More information on wind data (courtesy of Boskalis) is provided in appendix A.

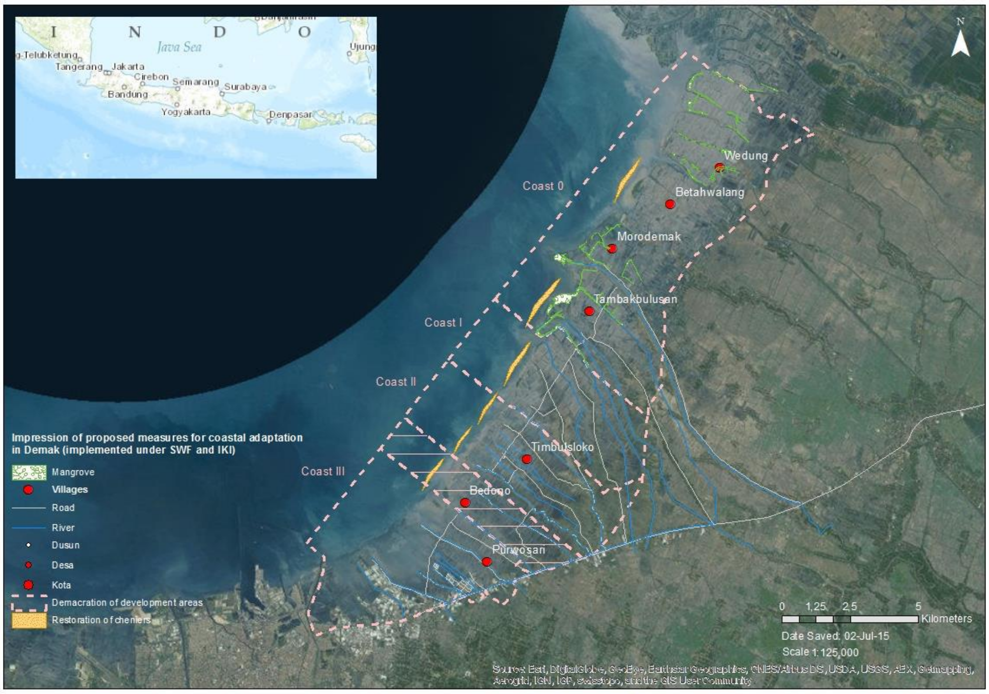

Figure 1.2: Location and definition of project area (Ecoshape, 2015)

The tide at Demak coast is mixed, mainly diurnal. The resulting variation in tidal water levels over time is highly irregular, with daily inequalities and monthly variations of the spring-neap cycle. The tidal range is approximately 0.60 m at spring tide and 0.40 m at neap tide. The spring tide can be a bit larger when semi-diurnal spring tides overlap with diurnal spring tides (MMAF, 2012). During the northwest monsoon, the strongest wind waves develop. Based on fourteen years of wave data from a measuring station near Semarang, the mean significant wave height in the area equalled 0.54 m. The maximum offshore wave height was about 2.5 m with a wave period of about 5.5 s. The predominant offshore wave direction was northwest. More information on wave data is provided in appendix B.

These mud coasts typically have a convex (rounded) profile when stable, but the profile can be reshaped to concave (hollow) due to erosion. The Demak coastal zone is very shallow, with slopes of about 1:1000 or even 1:1500 in areas without erosion, which is typical for muddy mangrove coasts (Augustinus, 1999). Erosion caused the slope to steepen to about 1:600 and reshape to concave. Close to the coast the substrate is extremely muddy (anecdotal evidence) with mud densities of 1300 to 1500 kg/m³ in the top 60 cm of the bed (Koster, 2019). Just in front of the coast several *cheniers* are present at a number of locations. Cheniers are thin, narrow lenses of sand that overly a muddy substrate. The cheniers cause wave breaking, thereby reducing the wave impact on the coastline directly behind. The cheniers are included in the model bathymetry, causing wave energy dissipation. The dynamics of these cheniers are not taken into account in this study.

Mangrove species that prevail in the area are *Avicennia marina* and *Rhizophora apiculata*. In the past a more diverse mangrove vegetation was encountered. Currently, about 21 species are still present (Wetlands International Indonesia, 2015). The colonisation behaviour of *Avicennia Marina*, a pioneer species, is most important for mangrove re-establishment.

1.4 Objectives

This study aims to assess the effectiveness of ecosystem-based adaptation measures subject to scenarios of sea level rise and land subsidence. For this purpose, the effects of relative sea level rise on the morphodynamic development of the Demak coastal zone are simulated using a process-based numerical model. Based on the model results, the effectiveness of the permeable structures is assessed by their capacity to capture sediments.

1.5 Approach

For these objectives, a process-based numerical model is used as a tool to gain more insight into the behaviour of the Demak coastal system. An existing Delft3D Flexible Mesh model, which was developed to study the application of semi-permeable dams in the area (Smits, 2016), is improved for the purpose of this study. The model includes the effects of tides, waves, cohesive sediment transport and morphology. This model is utilised to assess the effectiveness of the permeable structures in capturing sediments under scenarios of sea level rise and subsidence and should be used only in combination with interpretation by experts.

Sea level rise and land subsidence are subject to large uncertainty, hence their effect is evaluated through scenarios. As especially long-term future land subsidence rates are unknown, the scenarios are restricted to a five to ten-year horizon. The selected scenarios are in line with the IPCC scenarios for regional sea level rise and local land subsidence observations.

1.6 Outline

Chapter 2 describes the methodology, including the model setup and scenarios for sea level rise and land subsidence. The results of the scenario study are presented in chapter 3, describing the autonomous development of the area as well the effectiveness of the permeable structures, all for the scenarios of sea level rise and land subsidence. The methodology and model results are further interpreted and discussed in chapter 4. Finally, the chapter ends with the conclusions for this study, as well as recommendations for further research.

2 Method

The numerical model Delft3D Flexible Mesh (DFM) is used as a tool to gain more insight into the behaviour of the Demak coastal system and to assess the morphological changes in response to relative sea level rise and permeable structures. In this chapter first the general model concepts are described in section 2.1. The model set-up is discussed in detail in section 2.2. Moreover, this section explains how long-term projections are schematised in the model. Section 2.3 describes the model updates made for the purpose of this study, including improvements of the computational grid and bathymetry. Sections 2.4 and 2.5 explain how the model hydrodynamics were verified and how the sediment model was calibrated, based on monitoring results. Finally, the setup of the scenario study is described in section 2.6.

2.1 Model description

The Delft3D Flexible Mesh suite is the successor of the structured Delft3D 4.01 suite (Deltares, 2015). The software can be used to simulate flows, waves, water quality, ecology, sediment transport and morphology. Three modules were used for the model in this project: the flow module (D-Flow FM), the SWAN wave module (within D-Waves) and the sediment & morphology module (D-Morphology), which are described in more detail in appendix D.1. The version number that was used for this study is version 2.06.02_61208. It should be noted that the present implementation of Delft3D Flexible Mesh was still under development during the execution of this work and therefore has some limitations (see discussion in section 4.1).

2.2 Model set-up

The model set-up is described in detail in this section. First, section 2.2.1 explains which simplifications and assumptions were made to schematise long term projections in the model. The computational grid and bathymetry, boundary conditions and parameter settings are described in subsequent sections.

2.2.1 Simplifications & assumptions

The real world is more complex than a process-based numerical model. Models are affected by limited process knowledge and time constraints, so schematisations of reality and assumptions are needed to work with them. In order to achieve the objectives of this study, the following simplifications are made for the model setup:

- A 2-dimensional depth-averaged model is used for hydrodynamics and morphodynamics with (cohesive) sediment transport. This means that all computations are depth-averaged and 3D effects (e.g. density differences and associated currents) are neglected.
- The effect of mangroves on flow and waves is not accounted for in the model. In reality, mangroves will protect the coast by attenuating waves and thereby prevent erosion. Moreover, mangrove seedlings are known to spread and grow on fresh sediment deposits and to stimulate sedimentation. The model will therefore only give an indication of sedimentation and erosion areas, thereby underestimating the capacity of the coastline to keep up with sea level rise.
- Chenier dynamics are not taken into account (no sand fraction). As explained in section 1.2, cheniers are located just in front of the mangrove greenbelt along some parts of the coast and provide shelter for these parts against wave impact thereby inducing sedimentation. The cheniers are only considered in the initial bathymetry, but not in the sediment composition (i.e. no sand fraction is included). Consequently, the cheniers erode more easily in the model than they would in reality and the actual dynamics of these cheniers (which are observed in the field) are lacking.

- Land subsidence is simplified as a spatially uniform process that is linear over time, although in reality the land subsidence varies spatially (but how is insufficiently known to implement in the model) and may also develop non-linearly over time. Land subsidence is schematised as a relative sea level rise, as explained in section 2.3.
- Fluid mud layers are known to attenuate waves through viscous energy dissipation (Winterwerp, *et al.,* 2007*)*. This wave energy dissipation process is not included in the model. Consequently, the simulated wave height near the surf zone will be slightly overestimated.

Based on these simplifications, the model is set up. First, the underlying assumptions of the model and consequences for the model setup are described:

i. Sediment transport in the Demak coastal zone is dominated by local redistribution (erosion and sedimentation)

Sediment sources and sinks in the model are local exchanges between water column and bed, the model results are independent of the initial and boundary conditions. Other sediment sources (e.g. influx of sediment from offshore or from river outflows) are not considered. This assumption is based on the sensitivity study by Smits (2016) with sediment influx from the boundaries. The sediment concentration on the boundary did not significantly affect the results. Moreover, the sediment inputs from rivers are expected to be small. Thus, this assumption is justified.

ii. Net morphodynamic developments occur only during the northwest monsoon season.

From the initial monitoring results and a reference project in Vietnam (Van Cuong *et al*., 2015), it was concluded that the northwest monsoon season is the most dynamic season. Therefore, following the approach of Smits (2016), only the northwest monsoon season is modelled for a time period of three months in which the monsoon has developed its full strength (December, February and January). It is assumed that during the rest of the year little deposition or erosion occurs. The amount of deposition after three months is assumed to be representative for the total deposition after an entire year (including the southeast monsoon period). and consolidation & compaction effects[1]. So, essentially only three months are simulated per year.
This assumption does not fully hold since bed level changes have occurred outside of the northwest monsoon season, presumably mainly due to land subsidence and consolidation. Nevertheless, our previous experience in modeling this study area proved that this approach, though schematised, is able to produce realistic and comprehensive results.

iii. The net morphodynamic developments within a northwest monsoon season can be assumed to be linear over time.

The bed level changes after three months can be approximated by multiplying the bed level change of one month by a factor three. This is implemented in the model software through the morphological upscaling factor (Morfac) and standard modelling practice with a maximum Morfac of 3. Applying a larger Morfac is unfavourable for this model, as the tidal and seasonal effects would not be properly represented. This assumption is reasonable for small values for the morphological upscaling factor. Hence, a value of 3 is used, which is relatively small (compared to standard modelling practice of applying morphological upscaling factors up to 40 (Roelvink, 2006)) and appropriate for cohesive sediments.

---

[1] *In order to take into account consolidation effects in the model, once sediment is deposited on the bed, it is instantly assumed to be in a compacted/consolidated state (with a dry bed density increased from 300 kg/m^3 to 500 kg/m^3).*

2.2.2 Computational grid

Waves and hydrodynamics are computed on different computational grids (see Figure 2.1). The domain for the wave grid is larger than the flow grid to prevent boundary instabilities. As the used SWAN model can only be used for rectangular or curvilinear grids, a nesting approach is applied for the wave module using three domains, with cell sizes decreasing from 500 m (outer domain) down to 60 m (middle domain) and 20 m (inner domain).

The grid in the flow module was refined using flexible meshes to achieve a resolution of 16 m locally at the Demak coast. The offshore resolution is much lower (with a cell size of about 1 km) to save computation time, in line with our modelling experience (Kernkamp *et al*, 2011; De Goede, 2020). The computational grid that was used for the flow module is visualized in Figure 2.2. More detailed figures of the flow and wave grids are included in Appendix D.1, also showing the extent of the inner wave domains.

2.2.3 Bathymetry

Two sets of local bathymetry data were available from depth measurements (Smits, 2016). This local nearshore bathymetry data is assumed to be representative for the entire coastline, as the bottom profile has a very gentle slope. For the depth in offshore grid cells an offshore bathymetry database by GEBCO was used. The bathymetry that was used is visualised in Figure 2.3. More information on the bathymetry datasets is provided in appendix C.

The cheniers were not included in the depth measurements. Instead, they are artificially included by increasing the bed level by 20 cm over a width of 30 m width at locations where cheniers are present, as obtained from Google Earth images, and consistent with field observations from our project. Chenier behaviour and migration are beyond the scope of the current study.

In order minimise model initialisation effects, the model is spun up for 4 years with the same settings, but no sea level rise imposed at the boundaries. Figure 2.4 shows the result of this spin-up simulation and thus the initial bed level that was used in the scenario simulations after this spin-up period.

2.2.4 Initial & boundary conditions

The boundary conditions of the flow module are water level boundaries, created from tidal constituents. These tidal boundaries were obtained from the OSU TOPEX/Poseidon Global Inverse Solution (Egbert & Erofeeva, 2001) through Delft Dashboard. Version TPXO 10 was used. Note that the large-scale water level setup due to wind at the scale of the entire Java sea is not included in the model.

Representative values for the wave and wind parameters during the northwest monsoon period (December up to February) were based on an aggregated dataset from a range of local observations between 1997 and 2013, following the data analysis by Smits (2016). A time-varying wind speed is imposed of 3.5-8.0 m/s from west-northwest direction. For the waves a time-varying JONSWAP spectrum was used with a peak enhancement factor of 3.3 with waves coming from northwest direction and a directional spreading of 15 degrees. The significant wave height varies between 0.4 and 1.0 m with a peak wave period between 4.8 and 5.2 s. This is further explained in section 2.3.2.

The initial sediment concentration of the water column was set to 0.1 g/L and no sediment concentration was imposed at the open boundaries. Sensitivity tests (not presented here) indicated no significant impact of the initial and boundary conditions on the results in the area of interest. The initial bed layer thickness is 3.0 m.

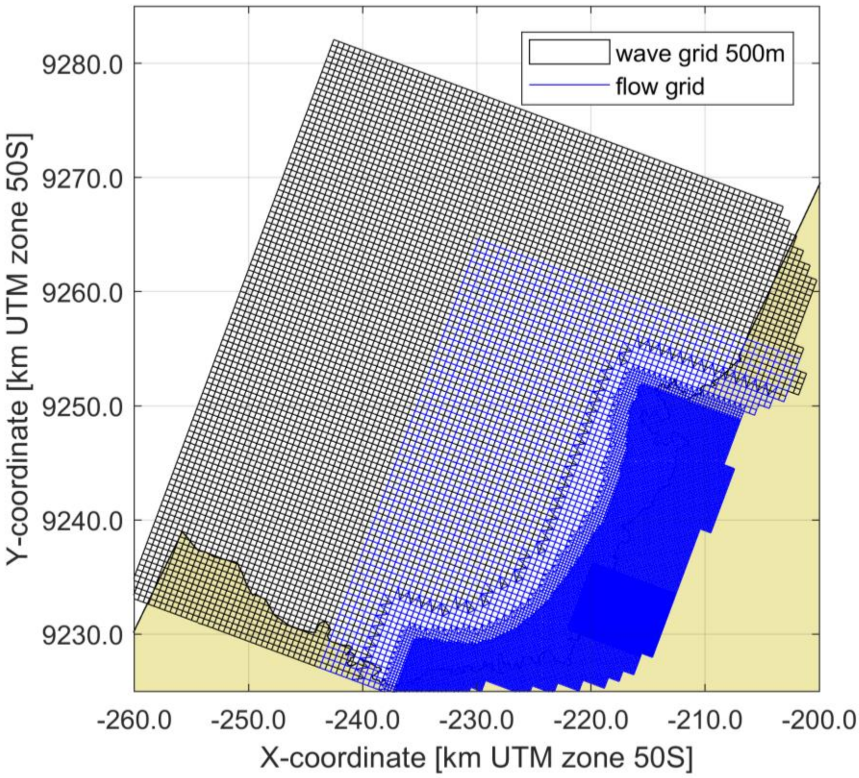

Figure 2.1: Extent of the flow grid (blue) and outer wave grid (black). The flow grid resolution follows the local bathymetry and varies between roughly 1 km offshore and 16 m in the area of interest. The outer wave grid has a cell size of 500 m.

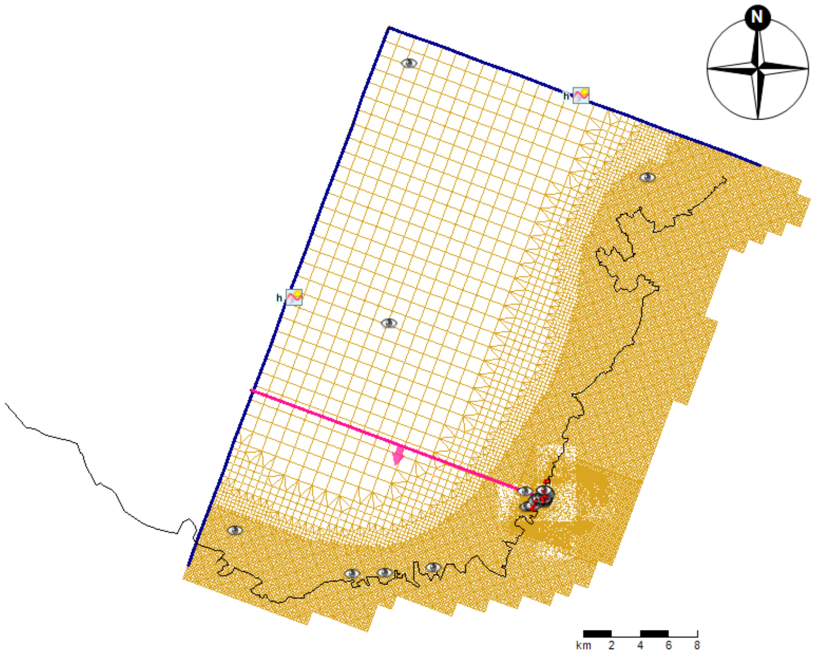

Figure 2.2: The computational grid as used in the D-Flow Flexible Mesh simulations. The grid cell size varies between roughly 1 km offshore and 16 m in the area of interest. Tidal boundaries in the north and west are represented by blue lines. Observation points and cross-sections are represented by eye icons and the pink line. For reference, the coastline is visualised with a black line.

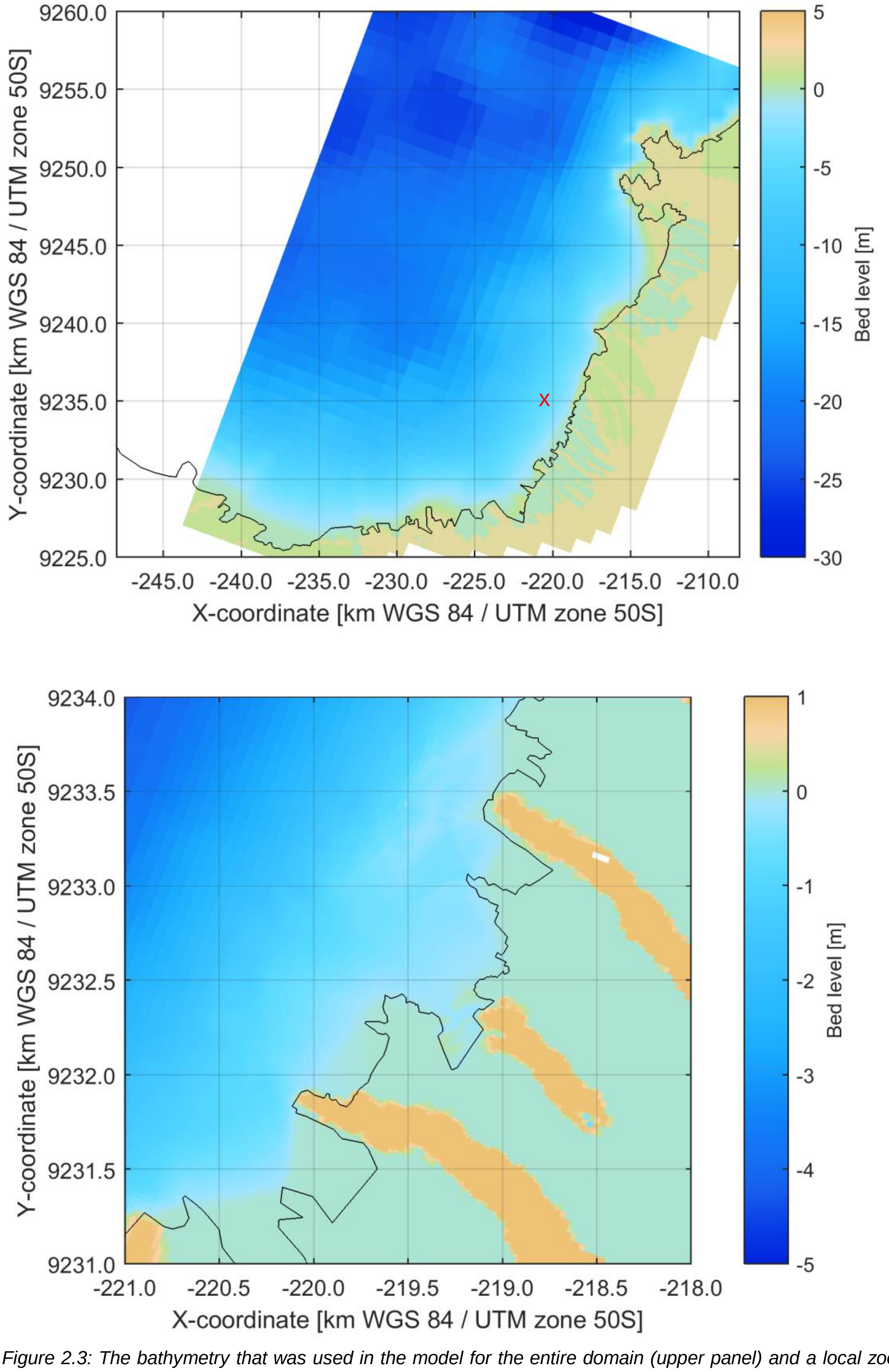

Figure 2.3: The bathymetry that was used in the model for the entire domain (upper panel) and a local zoom around the area of interest (lower panel). Note the different colour scales. The red cross in the upper figure represents the location of the wave buoy.

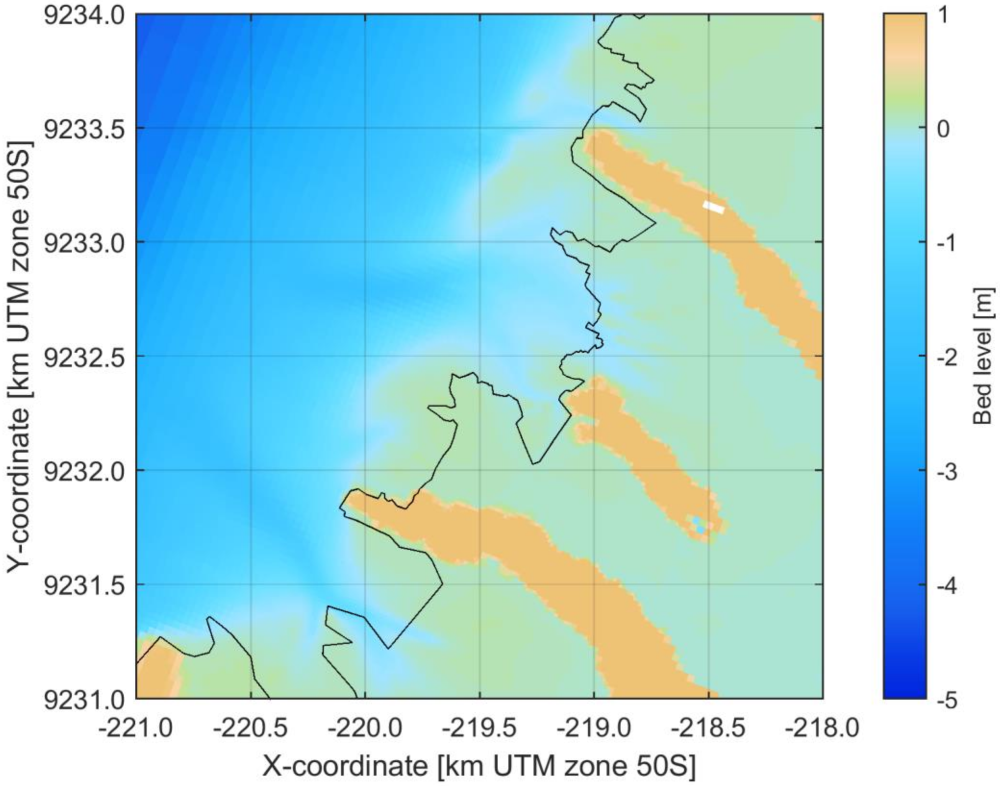

Figure 2.4: Bed level after the spin-up period

2.2.5 Parameter settings

Bed roughness in the flow module was computed using a Manning coefficient of 0.012 s/m$^{1/3}$, representative for a smooth, muddy bed. The water density was assumed to be 1025 km/m^3 (standard for sea water). For the horizontal eddy viscosity and eddy diffusivity uniform values of 1.0 m^2/s are used. All other values are D-Flow FM defaults.

Bottom friction in the wave module, was computed with the JONSWAP formulation and a constant friction coefficient of 0.019 m^2/s^3 (as recommended for smooth sea floors). For depth-induced breaking a gamma of 0.78 was used. The approach of Fredsoe (1984) is followed to compute the combined bed shear stress by waves and currents.

Erosion and deposition in the sediment module are computed using the Partheniades erosion equation and a permanent settling flux (no critical shear stress for sedimentation). Two cohesive mud fractions are prescribed, one representing a more mobile fraction that sits on top of the seabed and is more easily resuspended, the other representing a less mobile fraction that attains a weakly consolidated state during most tidal conditions. The settling velocities applied for these fractions are 0.05 and 0.1 mm/s respectively. The critical shear stress for erosion[2] of these sediment fractions were set at 0.1 N/m^2 and 0.5 N/m^2 (Van Maren *et al.*, 2015). For the erosion parameter in the Partheniades formulation values of 4.3*10^{-6} kg/m^2/s and 1.2*10^{-5} kg/m^2/s were used. The dry bed density was 300 kg/m^3, which assumes a weakly consolidated state. As explained in section 2.2.1, a morphological upscaling factor of 3 was applied. During the first 36 hours, bed level changes are not taken into account to prevent hydrodynamic spin-up effects from influencing the morphology.

---

[2] *Note that the computed bed shear stresses are a combination of the current-induced bed shear stress and the wave-induced bed shear stress, where the maximum wave-induced bed shear stress within a wave period is used.*

2.3 Model updates

For the purpose of this study, some model updates were made compared to the DFM-model of Smits (2016):

- The computational grid and bathymetry of the flow and wave modules were improved;
- Time-varying wind and wave forcings were implemented;
- Sediment parameter settings were improved;
- New permeable structures, which were constructed after 2016, were added.

2.3.1 Computational grid & bathymetry

In order to evaluate the effects of sea level rise, the model domain was extended landward to include the entire project area as defined by Ecoshape (2015). Thus, potential flooding of the hinterland can be computed, including sedimentation and erosion effects. Figure D.1 in the appendix shows the extent of the computational grid on a map. For the wave module, an extra high-resolution domain was included with grid cell size of 20 m to improve the resolution around the permeable structures. The extent of the wave grids can be seen in Figure D.2.

Next, the topography of the hinterland was also included, based on SRTM data. The vertical error in this data is around 3 m, which is relatively large for application in the model. Where possible, vertical errors in the bottom level were manually removed, e.g. where man-made structures or vegetation is present. As a consequence of the relatively large vertical error, the topography of the hinterland is not very accurate and thus results of hinterland flooding should be interpreted with care.

Finally, the bathymetry around the offshore boundary was improved. The original bathymetry at the boundary was rather coarse, causing unrealistically large gradients in the bed profile and boundary instabilities. In order to improve the hydrodynamic performance of the model, the bathymetry around the boundary was smoothened to obtain a more realistic coastal profile, based on expert judgement and admiralty charts.

2.3.2 Time-varying wind and wave forcing

At the start of the monsoon season the meteorological forcing is relatively small, representative for the transition period in November. The intensity of the monsoon gradually increases until the monsoon reaches its peak around mid-January. The meteorological forcing then decreases to the relatively calm transition period in March.

In order to more adequately represent these meteorological characteristics throughout the monsoon season, the wind and wave forcing are now imposed using time-varying parameters (but still spatially uniform). The wind speed, wave height and wave period are represented by a Gaussian shape which is repeated for every monsoon season.

The final model boundaries conditions are time-variable with values based on the data analysis by Smits (2016). The wind speed varies between 3.5 and 8.0 m/s. The significant wave height varies between 0.4 and 1.0 m with a peak wave period that varies simultaneously between 4.8 and 5.2 s. Figure 2.5 shows the seasonal variations of wave height and wind speed throughout two monsoon seasons.

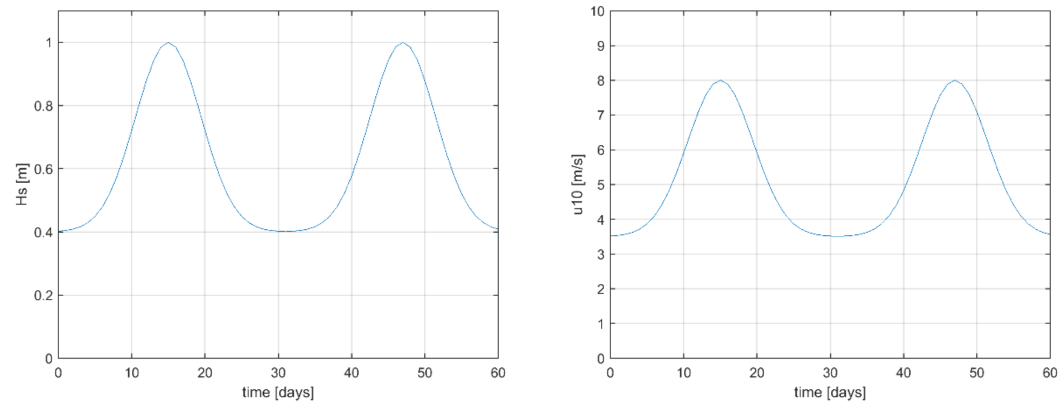

Figure 2.5: Seasonal variations in wave height (left panel) and wind speed (right panel) visualised throughout two monsoon seasons as included in the model. Note that a duration of 60 days with morphologic upscaling factor of 3 is representative for 180 days.

2.3.3 Sediment parameter settings

The initial sediment layer thickness is 1.5 m per sediment fraction. In order to approximate the effect of strength development in the mud deposits, the erosion rates linearly decrease when the available mass of sediment reduces to 0.5 meter (so the erosion rates become less when the top layer has been removed by erosion). For the critical bed shear stress for erosion, which is a property of the sediment, values of 0.5 and 0.1 N/m^2 are applied after extensive calibration efforts, see section 2.5.

2.3.4 Permeable structures

New permeable structures, which were constructed after 2016, were added. Now all permeable structures that have been constructed by January 2019 were included in the model.

Following the approach in the existing model, the permeable structures are simulated in the flow and sediment modules as ‘thin dams’, which close off a cell edge completely (i.e. impermeable over an infinite height). In the wave module, the structures are added as obstacles by which most of the wave energy is dissipated and through which only a small part of the wave energy is transmitted. For all structures in the wave module the height is 2.0 m above the reference level.

Figure 2.6 provides an overview of the locations and names of the permeable structures. Behind all the structures an observation point was placed for which the model results are studied. So, also in autonomous simulations (without permeable structures included), the same observation points are used for comparison. In the field, sediment poles were placed at the same locations as part of the monitoring campaign. However, comparison to these field measurements has turned out to be difficult due to various reasons. For example, in the model the permeable structures stay in good condition, whereas they may deteriorate under rough conditions in the field.

Figure 2.6: Map with the locations and names of the permeable structures and clusters used in the analysis

2.4 Verification of hydrodynamics

2.4.1 General circulation pattern

The large-scale circulation pattern is governed by the large-scale wind-driven monsoon circulation (Wyrtki, 1961). The local circulation pattern at the scale of the permeable structures, on the other hand, is governed by the tidal flow, which causes shoreward flood currents and seaward ebb currents. This is evident from Figure D.5, showing very similar results with or without wind effects (only offshore the wind-driven alongshore current can be distinguished). Thus, large-scale circulation patterns do not have to be reproduced in too much detail. The circulation pattern at the scale of the model domain is reproduced by including the wind (Figure D.4 in the appendix). Even though the setup of water level at the scale of the entire Java Sea is not included in the model, nor enforced from the boundaries, the simulated large-scale simulation pattern is roughly in the right direction and order of magnitude (KOICA, 2012; MMAF, 2012).

2.4.2 Wave transformation

As part of the BioManCo field measurement campaign a wave buoy was deployed 3 km offshore at 12 m water depth, where the waves are unaffected by the depth. The location of the wave buoy is indicated in Figure 2.1. The wave data collected at this wave buoy is used as means of verification of the wave model.

The wave heights measured during the northwest monsoon season ranged between 0.2 m and 2.0 m. In the model wave heights between 0.4 m and 1.1 m were computed at the same location. As the model is forced at the boundaries with a specific set of wave characteristics, it was not possible to cover all the observed combinations of wave height and wave period. The average conditions mainly govern the long-term morphodynamics, whereas storm conditions drive short term deviations from this long-term trend. Since the model aims to simulate the long-term morphodynamic deverlopment, storm conditions and very small waves were neglected. Wave heights in between were reasonably well reproduced, covering the wave height density function between 34% and 80%, see Figure 2.7.

To conclude, the modelled wave characteristics fit well within the observed spread of wave characteristics, although it does not cover the complete observed spectrum of wave characteristics. The modelled wave characteristics are realistic enough to get a good estimate of the sediment transport under average conditions.

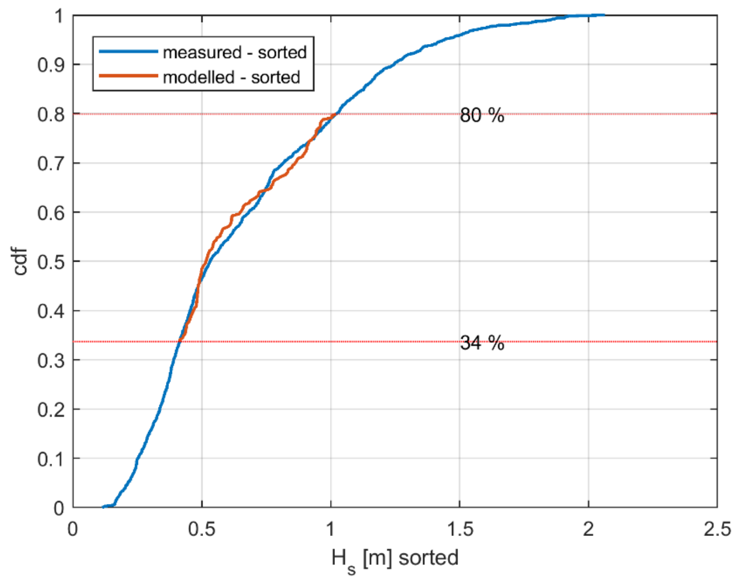

Figure 2.7: The distribution of the significant wave height is shown on the x-axis and the cumulative density function (or probability of non-exceedance) on the y-axis. The blue line represents the measured wave height at the wave buoy as part of BioManCo field campaign and the red line is the modelled wave height at the same location.

2.5 Calibration of sediment transport model

The existing DFM model was originally calibrated based on very little observation data in combination with expert judgement. With the use of new monitoring data from monthly field monitoring, the existing model was re-calibrated for short term hydro- and morphodynamics (yearly and seasonal development). Based on a sensitivity analysis (not reported here), the critical shear stress for erosion and the erosion parameter *M* from the Partherniades erosion formulation were tuned, following the approach described below.

The combination of the critical shear stress and the erosion parameter determines the erosive behaviour of the sediment. The critical shear stress for erosion is a threshold parameter beyond which the bed starts to erode. It thereby affects the spatial patterns of erosion. Since erosion of the bed seaward provides fine sediment that can deposit behind the permeable structures, higher erosion rates of the bed result in higher deposition rates behind the permeable structures. For the existing DFM model, the critical shear stress for erosion was optimised to resemble spatial patterns of erosion and deposition as understood from analysis of field observations.

The erosion parameter (M) determines how much erosion occurs once the critical shear stress has been reached. It can roughly be said that the erosion parameter has a simple linear effect on the erosion and deposition rates, because it just uniformly increases erosion rates. Hence, *M* was used to scale erosion and deposition in the entire domain.

During calibration very distinct areas of erosion with sharp gradients were initially observed. These patterns did not resemble the more gradual patterns observed in the field. Therefore, the critical shear stress for erosion was reduced (creating a lower threshold for onset of erosion), combined with a lower erosion parameter (lower rate of erosion). Eventually, values of 0.5 Pa and 0.1 Pa for the critical shear stress and values of $1.2*10^{-5}$ $kg/m^2/s$ and $4.3*10^{-6}$ $kg/m^2/s$ for the erosion parameter delivered the best results.

2.6 Setup of scenario study

The scenarios that were simulated with the model are based on sea level rise and land subsidence. First, sea level rise and land subsidence projections and observations from literature are summarised. These projections are combined in relative sea level rise rates for the model scenarios.

2.6.1 Sea level rise

According to IPCC 5 report, the sea level rise for the period 2046–2065 (relative to 1986–2005) will *likely* be in the ranges of 0.17-0.32 m (for RCP2.6), and 0.22-0.38 m (for RCP8.5), see Table 2.1 and Figure 2.8 (IPCC, 2014). So, the projections vary between 17 cm and 38 cm sea level rise over a time period of 60 years. Assumed linearly over time, this would correspond to a rate of global sea level rise of 0.28-0.63 cm per year.

Table 2.1: Projected global mean sea level rise [m] for the mid- and late 21st century, relative to the 1986-2005 period, courtesy of IPCC (2014) (WGI Table SPM.2, 12.4.1, 13.5.1, Table 12.2, Table 13.5)

		2046–2065		2081–2100	
	Scenario	Mean	*Likely* range [d]	Mean	*Likely* range [d]
Global Mean Sea Level Rise (m) [b]	RCP2.6	0.24	0.17 to 0.32	0.40	0.26 to 0.55
	RCP4.5	0.26	0.19 to 0.33	0.47	0.32 to 0.63
	RCP6.0	0.25	0.18 to 0.32	0.48	0.33 to 0.63
	RCP8.5	0.30	0.22 to 0.38	0.63	0.45 to 0.82

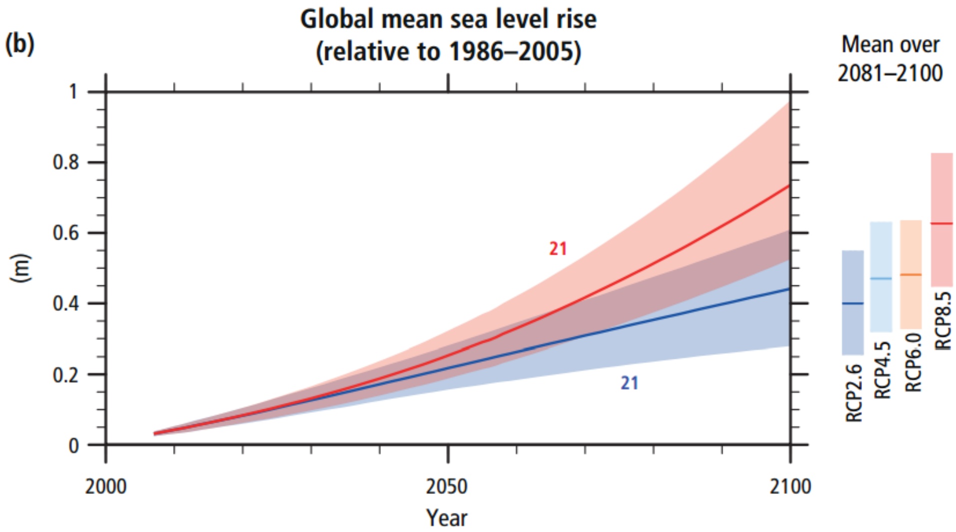

Figure 2.8: IPCC projections for global mean sea level rise (IPCC, 2014)

However, IPCC also reports that “sea level rise will not be uniform across regions. About 70% of the coastlines worldwide are projected to experience a sea level change within ±20% of the global mean” (IPCC, 2014*).* Slangen *et al.* (2012) report a regional sea level rise of 38-58 cm for Jakarta by 2100 (based on IPCC4 instead of IPCC5). These projections roughly correspond to global mean sea level rise projections from IPCC4 (between 40 cm and 63 cm by 2100 depending on the CO_2-scenarios). As regional sea level rise projections for Jakarta are similar to the global mean value, the regional sea level rise for Demak is assumed to roughly correspond to global-mean sea level rise projections of IPCC 5, likely ranging between 0.17-0.38 m for the period 2045-2065. Assuming a linear trend over 60 years, the Sea Level Rise rate ranges between 0.28 and 0.63 cm per year.

Local observations give a current average rate of sea level rise near Semarang of 0.42 cm per year (KOICA, 2012) based on satellite observations. As best-case scenario, this rate of sea level rise is assumed for the entire period. As intermediate scenario the mean projections of IPCC scenarios RCP 4.5 and RCP6.0 are taken, which would be a rate of 0.50 cm per year on average. As worst-case scenario the mean projection of IPCC scenario RCP8.5 is used, which would be a rate of 0.60 cm per year on average. This value of 0.60 cm per year is also used in the Masterplan for Jakarta (Van der Wulp *et al*, 2016).

2.6.2 Land subsidence

The Demak coastal area suffers from severe land subsidence. Literature on land subsidence rates in Demak and Semarang areas gives a range of observed subsidence rates:

- Marfai & King (2007) discuss 38 benchmark data measurements with land subsidence rates between 2.0 and 10 cm per year. The average rate was 4.82 cm per year.
- Lubis (2011) reports observations in Semarang with subsidence rates of about 8 cm per year, although the spatial pattern shows increasing land subsidence rates in northeastern direction, suggesting that higher rates may occur in the Demak coastal area.
- Remote sensing of several Indonesian cities by Chaussard, *et al.* (2013) gives an average vertical rate of 4.8 cm per year for Semarang and a maximum vertical rate of 13.0 cm per year. At the site closest to Demak (location B in Figure 2.9) a subsidence rate of about 7.8 cm per year is observed.

However, all these projections are 10 to 5 years old. The population of Semarang has shown a steady increase from 1.482 million in 2010 to 1.763 million in 2015 (most recent data available from Indonesia Central Bureau of Statistics; Hadi & Buchori, 2018). This has obviously increased water demand in the region. Moreover, industrial development has increased considerably and groundwater extraction rates are expected to keep rising. Consequently, subsidence dates likely accelerated in the past 5 to 10 years and therefore, we here assumed a rate of 7.8 cm per year for the lowest scenario. For the worst-case scenario, the maximum rate observed in the area of 13.0 cm per year is used. As intermediate scenario 10.0 cm per year is used.

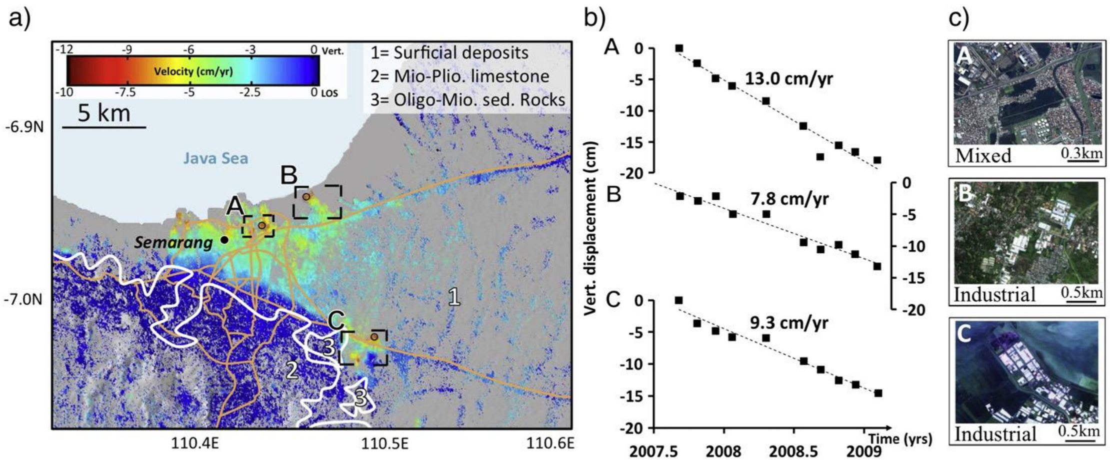

Figure 2.9: Panel (a) shows a subsidence map by Chaussard, et al. *(2013) in and around Semarang (redder colours correspond to larger subsidence rates). For locations A, B and C the measurements over time are plotted in panel (b) and areal images shown in panel (c) give an indication of the type of land use.*

2.6.3 Model scenarios

In this study relative sea level rise is defined as the sum of the eustatic sea level rise and land subsidence, under the assumption that the subsidence occurs linearly in time and spatially uniform. This is quite a safe assumption to make for relatively small spatial and temporal scales (up to several tens of kilometers and up to around a decade). Relative sea level rise (including subsidence) is implemented by linearly increasing the water level at the model boundary. Table 2.2 gives an overview of the relative sea level rise scenarios imposed in the model (relative to the current Mean Sea Level). Note that the total relative sea level rise is larger than the tidal range (0.60 m at spring tide, see section 1.3).

Table 2.2: Sea level rise and land subsidence scenarios that are applied in the model with the total relative sea level rise in cm after 10 years in the column furthest on the right

Scenarios	**Sea level rise rate [cm/year]**	**Land subsidence rate [cm/year]**	**Total rel. SLR rate [cm/year]**	**Total rel. SLR after 10 years [cm]**
Best-case	0.42	7.80	**8.22**	**82.2**
Intermediate	0.50	10.0	**10.5**	**105**
Worst-case	0.60	13.0	**13.6**	**136**

2.6.4 Potential model responses

The way in which the system reacts to the effects of relative sea level rise is generally categorised into three potential responses (Fitzgerald *et al*, 2008):

- 'Keeping up with sea level rise': the sedimentation rate equals the rate of relative sea level rise.
- 'Partial drowning': sedimentation rate is (initially) smaller than rate of relative sea level rise, but later reaches the stabilised or more slowly rising sea level. Some authors refer to this response as 'catching up'.
- 'Drowning': the sediment accretion cannot follow the rising sea level. Some authors refer to this response as 'giving up'.

3 Results of scenario study

The model is used as a tool to gain more insight into the behaviour of the Demak coastal system, which helps to study the effectiveness of the permeable structures in capturing sediments under the scenarios of sea level rise and land subsidence described in section 2.6.3. Note that relative sea level rise (i.e. the sum of eustatic sea level rise and land subsidence) is considered in these scenarios. In this chapter the results are presented and analysed. Interpretation of these results will follow in chapter 4.

For each scenario two model simulations were performed: a simulation without permeable structures, indicating the autonomous development of the coast for a particular relative sea level rise scenario, and a simulation with the permeable structures. A synthesis of general results is presented in section 3.1. In the subsequent sections the results of best-case, intermediate and worst-case scenarios are described in more detail. In section 3.2 the spatial patterns of bed level changes in the Demak coastal zone are reported, for simulations with and without permeable structures, as well as comparisons between these simulations. Next, section 3.3 zooms in at the locations of the permeable structures, presenting time series of the bed level changes at the observation points behind the permeable structures. Finally, the structures are analysed as clusters with neighbouring structures to obtain insights into spatial patterns in section 3.4.

3.1 Synthesis of results

The model results indicate that the autonomous development of the coast (without permeable structures) will eventually lead to bed erosion in the intertidal area and flooding of the hinterland under all scenarios for relative sea level rise. Without permeable structures, the average erosion of the sea bed at the observation points (located behind the – absent – structures, as described in section 2.3.4) is approximately 0.4 m after 10 years for all sea level rise scenarios. When permeable structures are included, large-scale patterns are identical, since these structures only exert influence on small scales. Locally, however, sedimentation prevails behind the permeable structures. Averaged over all observation points behind structures, the total sedimentation after ten years ranges between +0.3 m to +0.4 m for the different scenarios (Table 3.1). Based on the average bed level change, the permeable structures manage to trap sediment for all scenarios, but not enough to keep pace with sea level rise. So, part of the relative sea level rise is compensated by sediment accretion, implying that the increase in water depth will be less than the amount of relative sea level rise. Without permeable structures, on the other hand, the increase in water depth would have been much larger than the amount of relative sea level rise.

Table 3.1: Average bed level change after 10 years at observation points behind the permeable structures for different scenarios and simulations with and without permeable structures. Positive values indicate accretion, negative values indicate erosion of the sea bed.

Scenario	Average bed level change [m]		Difference Δz [m]
	Autonomous development	Permeable structures	
Best-case (0.82 m rSLR)	-0.44	+0.34	+0.78
Intermediate (1.05 m rSLR)	-0.45	+0.38	+0.84
Worst-case (1.36 m rSLR)	-0.44	+0.44	+0.88

To illustrate these findings, the best-case scenario is used as an example. The permeable structures trap on average 34 cm sediment, which is less than the 82 cm relative sea level rise; hence the water depth behind the permeable structures will on average increase by (82-34=) 48 cm relative to the present state. However, since erosion occurs during autonomous development (average erosion of 44 cm), the increase in water depth without permeable structures is predicted to be (82+44=) 126 cm relative to the present state. Therefore, structures manage to bring the water level increase (caused by rSLR) down by almost 60% for this particular scenario.

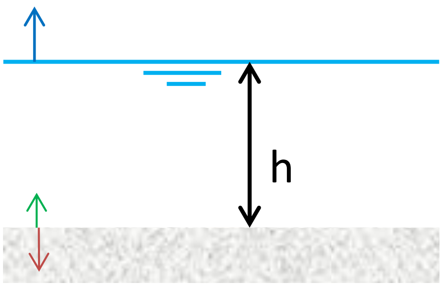

Figure 3.1 Schematisation of water level increase due to rSLR (blue arrow), bed accretion (green arrow) and/or erosion (red arrow)

The bed level development behind a representative permeable structure (Figure 3.2) is analysed to gain insight in time-dependency. Already from the start of simulation, the autonomous bed level development (red line) cannot keep up with sea level rise: the bed accretion is not fast enough and reverts to net erosion after four to six years. The permeable structures manage to trap sediments throughout a part of the simulation, allowing the bed level to keep up with sea level rise for about 7 years in the best-case scenario (top left panel of Figure 3.2). Only in the last three years, the bed level cannot keep up anymore. For the intermediate and worst-case scenarios, the bed level seems to keep up with sea level rise for about 6 and 5 years respectively (see Figure 3.2, middle and lower panels). So, it can be concluded that the permeable structures help to trap sediments, allowing the bed level to keep up with relative sea level rise until a certain threshold has been exceeded. The processes responsible for this behaviour are elucidated in section 3.3.

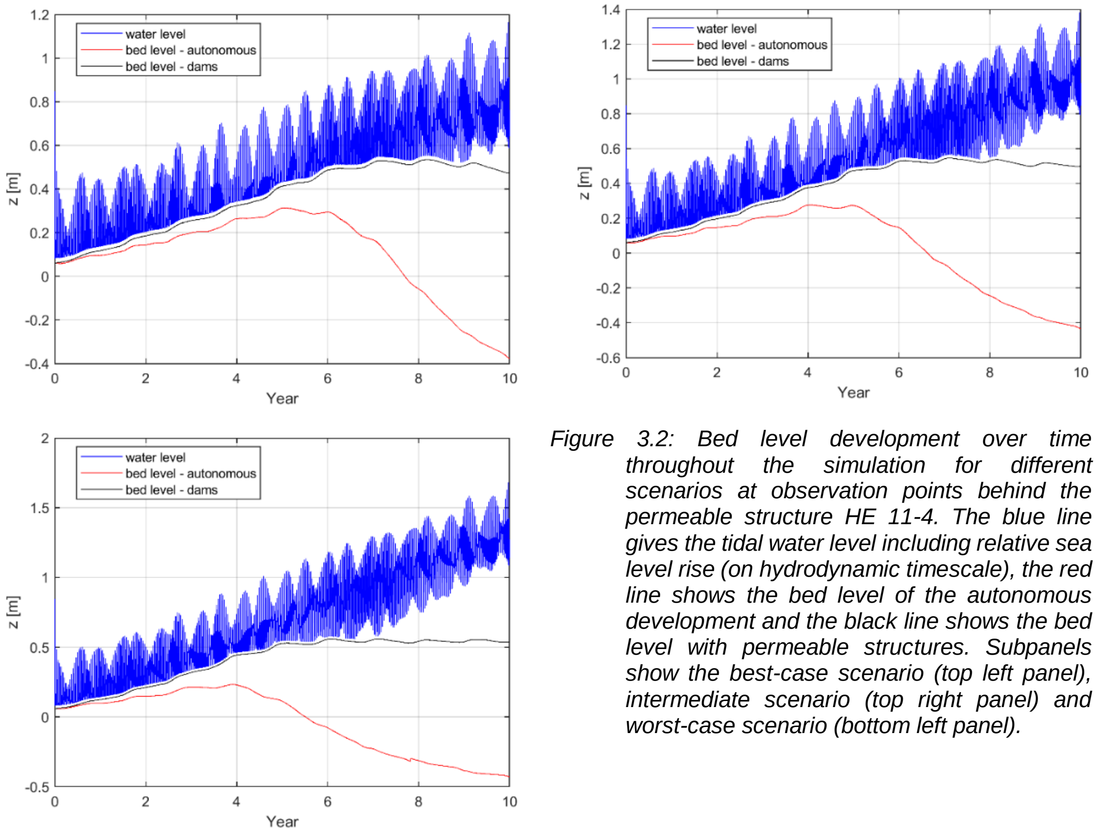

Figure 3.2: Bed level development over time throughout the simulation for different scenarios at observation points behind the permeable structure HE 11-4. The blue line gives the tidal water level including relative sea level rise (on hydrodynamic timescale), the red line shows the bed level of the autonomous development and the black line shows the bed level with permeable structures. Subpanels show the best-case scenario (top left panel), intermediate scenario (top right panel) and worst-case scenario (bottom left panel).

3.2 Spatial bed level changes in the Demak coastal zone

The total relative sea level rise after 10 years is 0.82 m, 1.05 m and 1.36 m for the best-case, intermediate and worst-case scenarios respectively. For all scenarios this increase in water depth affects the wave field, allowing large waves to penetrate further landward. Figure 3.3 indicates that the wave height increased nearshore (initial wave field during the peak of the monsoon in the upper panel and the differences between the start and the end of the simulation in the lower panel). For increasing rate of relative sea level rise, the wave height increases slightly more (Figure E.14 and Figure E.30).

As a consequence of the increased wave heights, bed erosion occurs in the intertidal areas (blue colours in Figure 3.4), where wave dissipation causes stirring up of sediments. Sediment is then deposited on the landward areas (red colour tones). When permeable structures are included, sediment is trapped behind the structures instead (lower panels of Figure 3.4). These figures also indicate that the main sediment source is the seabed in the foreshore. The bed level changes are visualized again in Figure 3.5, this time with a colour scale created to reveal bed level change with respect to sea level rise. The trapping effect of the structures (green colours) and the erosion areas (blue colours) can be distinguished. Moreover, it can now be observed that the accretion rate is less than the rate of relative sea level rise (i.e. no brown colours). Enlarged versions of these figures per scenario, as well as the bed level changes at the scale of the entire project area (using the colour scale of Figure 3.5) are provided in appendix E. For different scenarios the spatial patterns of sedimentation and erosion areas are very similar, but the amount of accretion behind the structures is slightly larger (on average 0.34 m for the best-case scenario, 0.38 m for the intermediate scenario and 0.44 m for the worst-case scenario) and located somewhat further landward. For all scenarios the sedimentation rate is less than the rate of relative sea level rise (i.e. no brown colours in Figure 3.5).

Difference plots are created by substracting the final bed level for a simulation without permeable structures from that of a simulation with permeable structures. From such difference plots the influence of the permeable structures can be distinguished (Figure 3.6). Sediment is captured behind the structures, locally resulting in higher bed levels (in the best-case scenario on average 0.78 m higher than for the autonomous development). For increasing rate of sea level rise this difference becomes larger (0.84 m for the intermediate scenario and 0.88 m for the worst-case scenario). Based on these results, the permeable structures only have a very local effect and almost no negative effect on the surrounding bed level, compared to the autonomous development (only a limited number of blue patches).

The final bed level for the simulation of the autonomous development for the best-case scenario of relative SLR is shown in the left panels of Figure 3.7. Note that the vertical reference level (z=0) of these figures has changed, so the mean sea level at the end of the simulation is located at z=0 m. Comparison of this figure to the initial bed level (Figure 2.4), reveals that the coastline has severely retreated with only some small strips of land left, due to the increase in the water level. This is not an effect of coastal erosion, but simply the direct effect of relative sea level rise that submerges low-lying lands. For increasing rate of sea level rise the coastline retreats slightly further. The seaward areas are not very different from the best-case scenario, but at the landward areas sediments are deposited slightly further landward (green colour tones in Figure E.17 and Figure E.33).

The average concentration behind the permeable structures is roughly 0.1 g/L (Figure 3.8, Figure E.20 and Figure E.36). No large differences in sediment concentration were found between the scenarios. Such concentrations would allow for roughly 20 cm of accretion per year (assuming continuous sedimentation, equally distributed between the two sediment fractions). As the results depict 40 cm accretion over 10 years, sediment availability does not seem to be a limiting factor for sedimentation.

The differences between the scenarios that were identified are a consequence of the increase in relative sea level rise (ranging between 0.82 and 1.36 m). Larger rates of relative sea level rise result in slightly more sediment deposition behind the structures, but not enough to fully compensate for the additional amount of relative sea level rise (i.e. the water depth increases and a larger area is flooded).

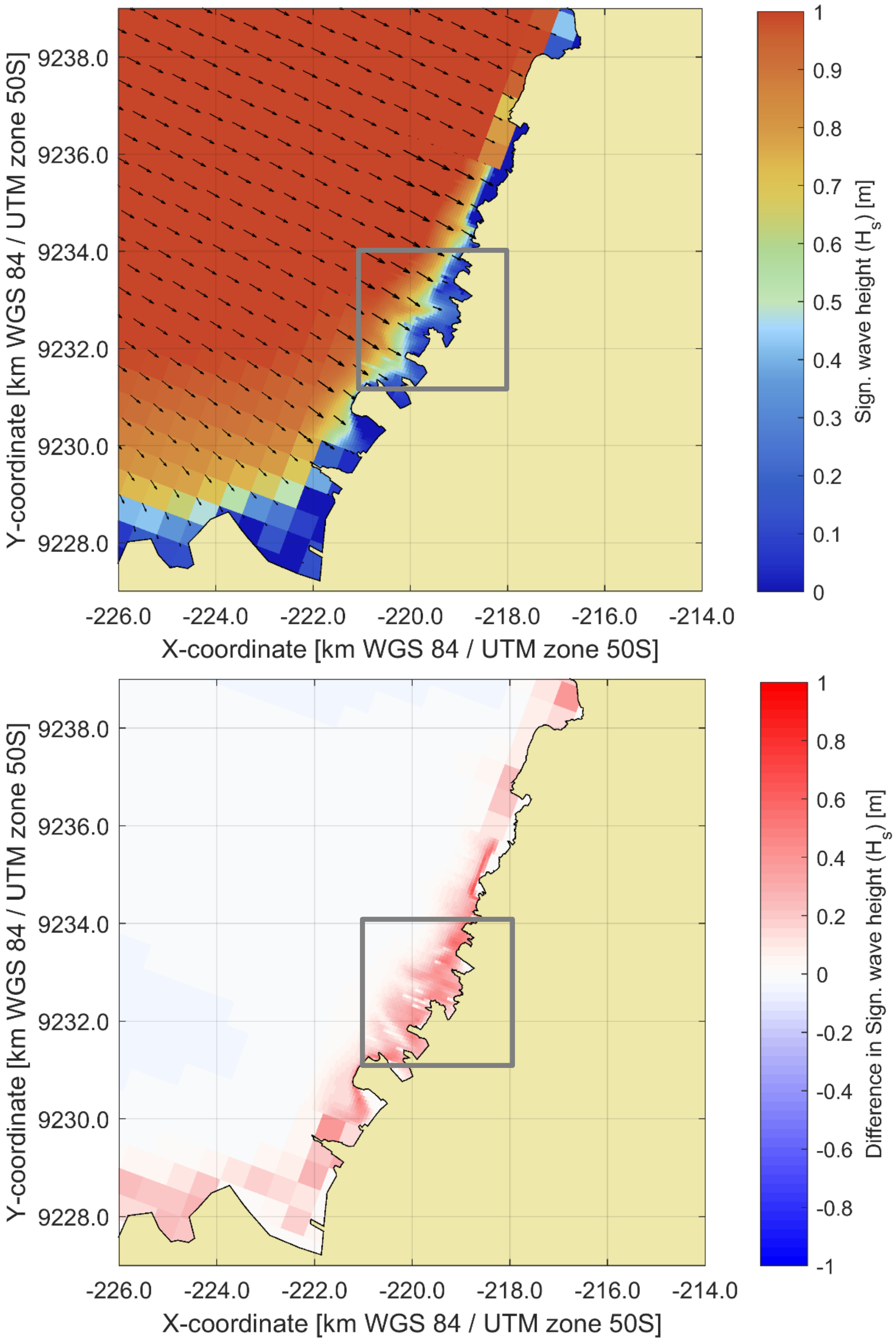

Figure 3.3 Significant wave height during the peak of the monsoon for the best-case scenario (upper panel) and differences in significant wave height between the start and the end of the simulation (lower panel). The land boundary is only used for visualisation in these figures, but was not included in the model (flooding and drying is computed by the model). The boxes indicate the zoom area for the subsequent figures.

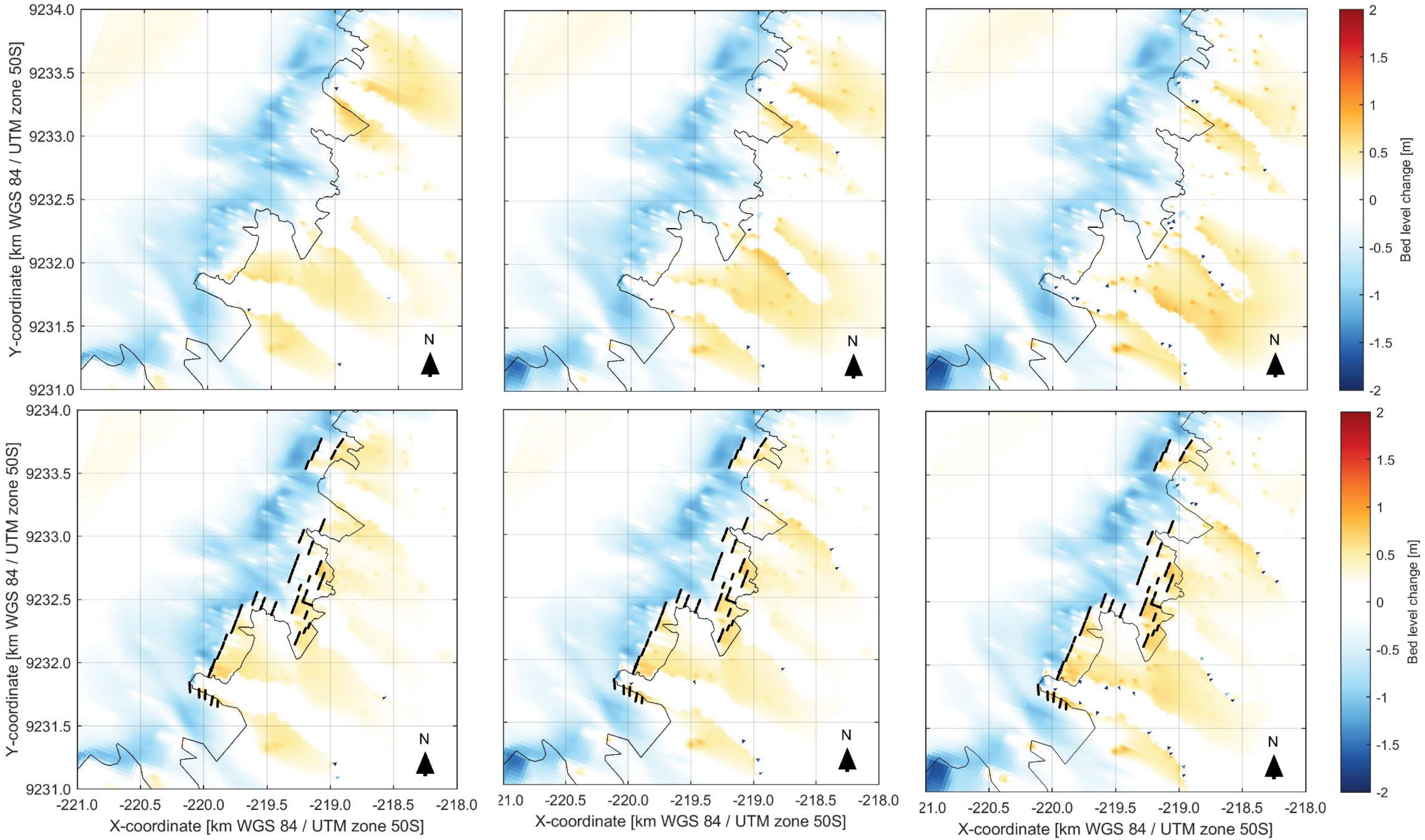

Figure 3.4 Total bed level change after 10 years for the best- (left), intermediate (centre) and worst-case (right) scenario simulations. The upper panels show the autonomous development and the lower panels show the results of the simulations with permeable structures. Red colours indicate sedimentation areas and blue colours indicate erosion areas. The thin black line indicating the coastline is included in these figures for reference only, but was not included in the model (flooding and drying is computed by the model).

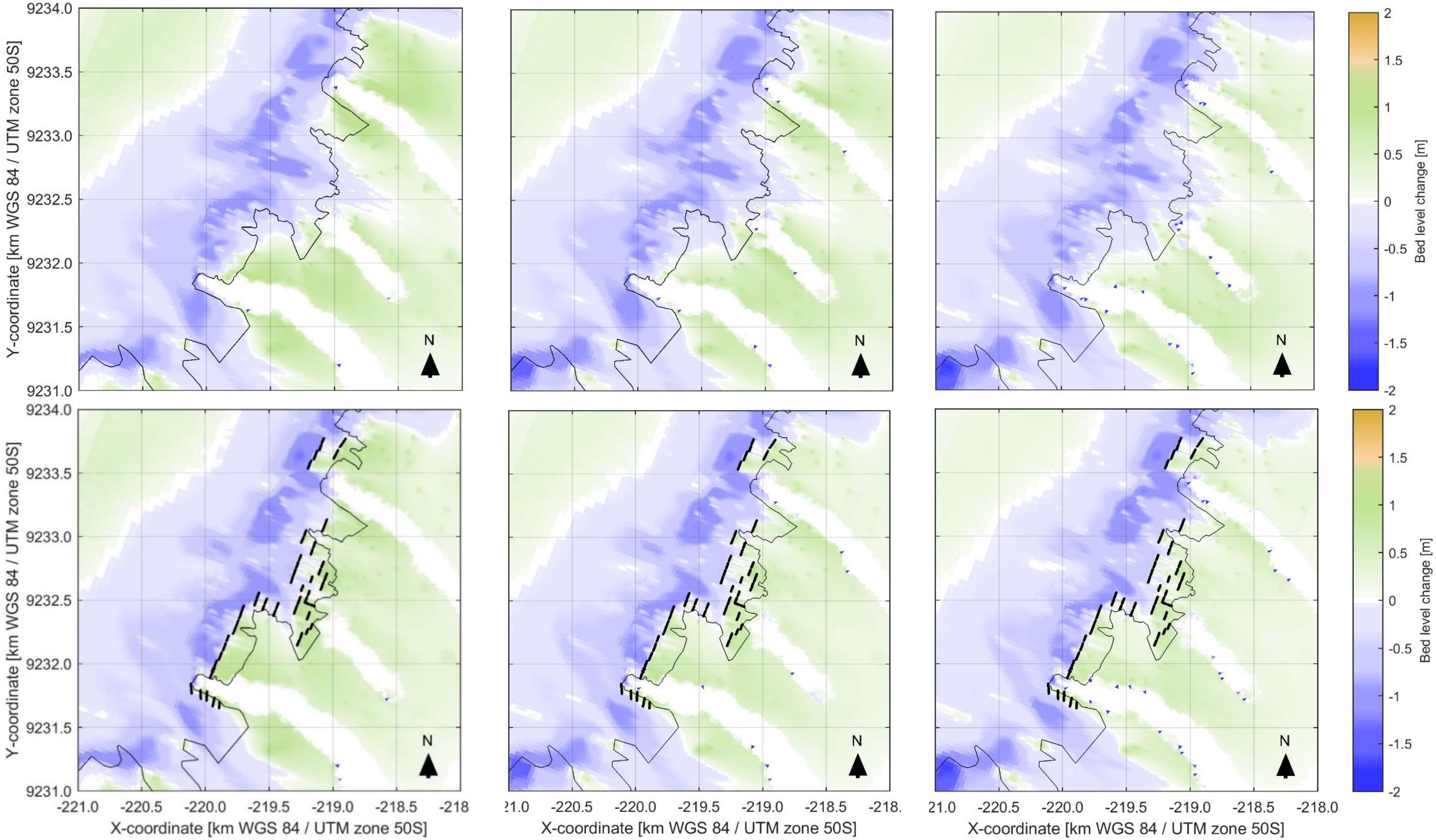

Figure 3.5 Total bed level change after 10 years for the best- (left), intermediate (centre) and worst-case (right) scenarios; upper panels show the autonomous development and lower panels simulations with permeable structures. Blue colours indicate erosive areas, green colours indicate partially drowning areas and brown colours indicate sedimentation rates that exceed the rate of rel. SLR. The thin black line indicating the coastline is included in these figures for reference only, but was not included in the model (flooding and drying is computed by the model). The small blue dots are likely plotting artefacts that do not (significantly) affect the results.

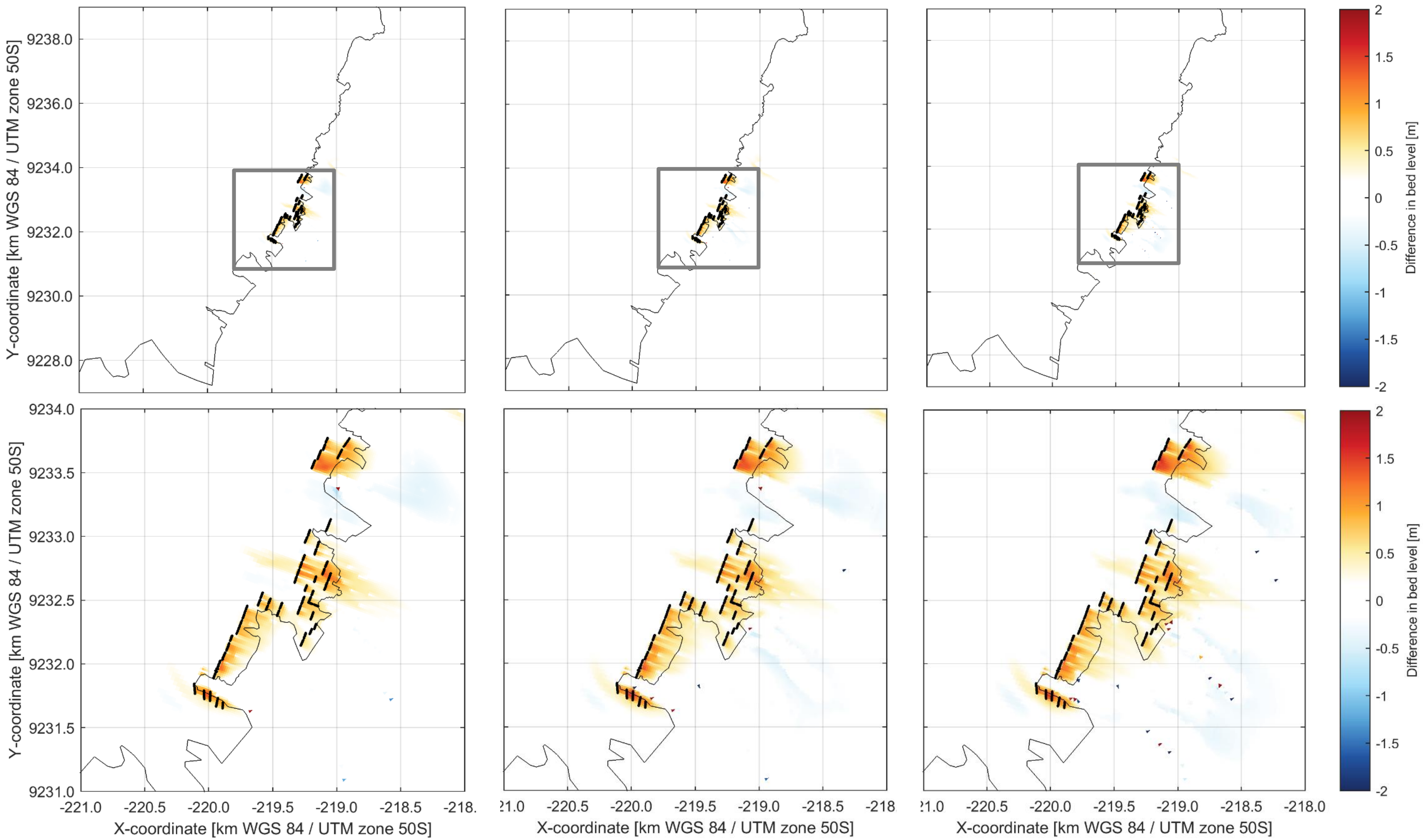

Figure 3.6 Difference plots between final bed level with permeable structures and autonomous development for best- (left), intermediate (centre) and worst-case (right) scenarios; upper panels show the extent of the project area, lower panels a zoom around the area of the structures. Red colours indicate higher bed levels in the simulation with permeable structures, blue colours indicate lower levels. The thin black line indicating the coastline is included in these figures for reference only, but was not included in the model (flooding and drying is computed by the model).

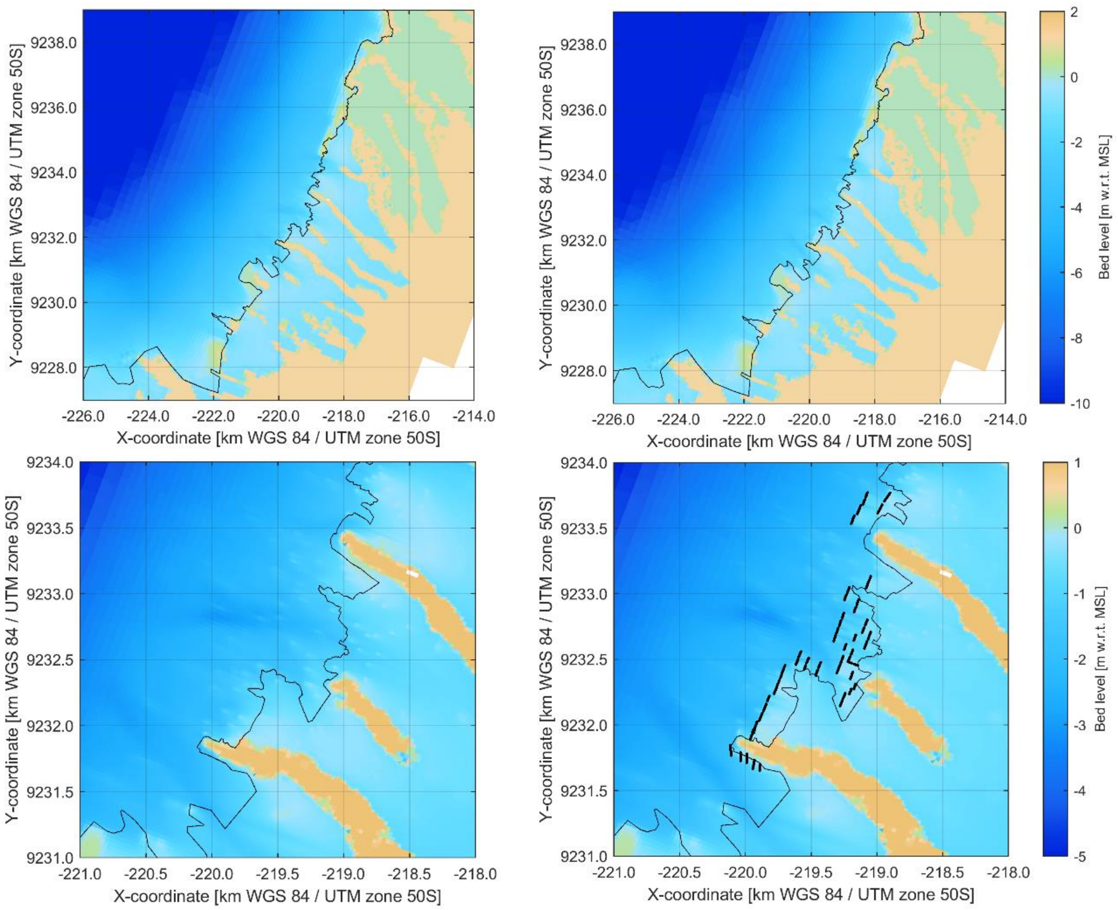

Figure 3.7 Final bed level relative to the new mean sea level (including sea level rise) after 10 years for the best-case scenario simulations. The results of the autonomous development (panels on the left) and simulations with permeable structures (panels on the right, structures indicated by black lines). Upper panels show the extent of the project area, lower panels a zoom around the area of the structures. Note the different colour scales used for both spatial scales. The thin black line indicates the old coastline that is included in these figures for reference only.

.

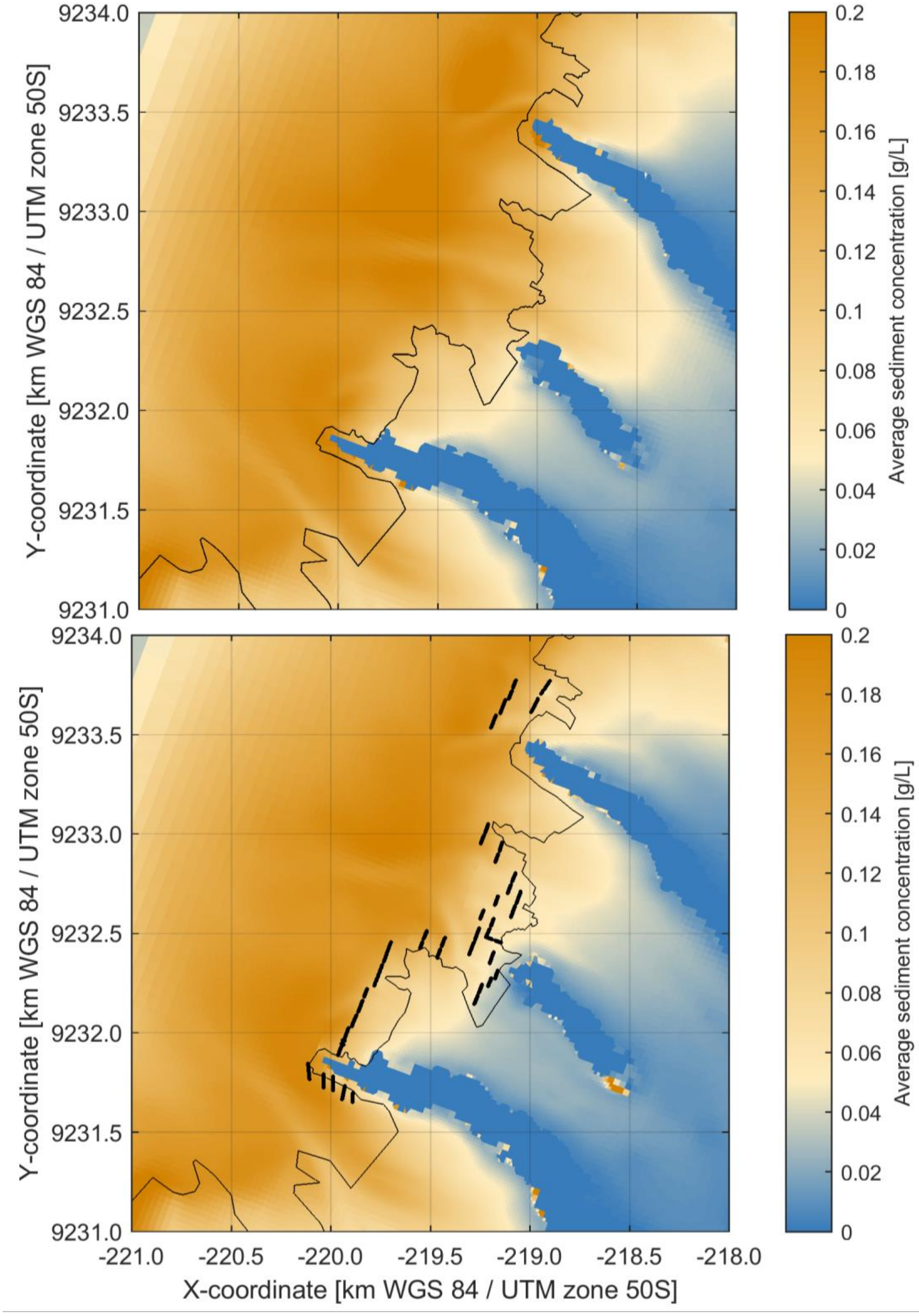

Figure 3.8 Sediment concentration averaged over 10 years for the best-case scenario simulations (upper panel autonomous development; lower panel with permeable structures indicated by black lines). The thin black line indicating the land boundary is only added forreference in these figures, but are not included in the model (flooding and drying is computed by the model).

3.3 Timeseries of bed level changes near permeable structures

Figures of the bed level development over time throughout the simulation (similar to Figure 3.2, but for other locations) are included in appendix E (for the best-case scenario in Figure E.5 up to Figure E.13). The autonomous development of the bed (red lines) initially shows sediment deposition for some locations and a constant bed level for other locations. After a certain number of years (the number varying per location and per scenario), deposition reverts to erosion at most locations. This shift occurs after a threshold amount of relative sea level rise, which is different for each location, has been exceeded.

For the simulations with permeable structures, the bed level development (black lines) initially shows stronger deposition rates (in fact closely following relative SLR, which was not the case for the autonomous case), and deposition continues for a longer period. In general, structures closer to the coast remain depositional for a longer period, whereas for structures farther seaward the bed level becomes stable or erodes after some time. Based on a comparison between the autonomous bed level development and the development behind permeable structures, the structures favour sedimentation and protect the bed against erosion. However, some structures at deeper locations cannot protect the bed anymore after a certain period of time (i.e. a critical relative sea level rise).

The total bed level change at the end of the best-case simulation for the autonomous development and for the development with permeable structures is provided in Table E.1 in the appendix. For most locations, the autonomous development of the bed level results in erosion (although net deposition occurs at six out of 53 locations). On average the bed level is eroded by 44 cm with a standard deviation of 34 cm. When including permeable structures, the bed level increases at most locations (although net erosion is predicted at five locations). The average deposition is 34 cm with a standard deviation of 23 cm. Note that for none of the observation points the bed level increases by 82 cm or more, so none of these locations can completely keep up with the rate of relative sea level rise.

For increasing rate of sea level rise, the bed level trends by autonomous development and when protected by permeable structures are very similar to the best-case scenario, although the shift from deposition to erosion occurs around one to two years earlier. The figures of the bed level development over time throughout the simulations for the intermediate and worst-case scenarios are included also in appendix E (respectively in Figure E.21 up to Figure E.29 and Figure E.37 up to Figure E.45). The final autonomous erosion was on average 45 cm (intermediate scenario) and 44 cm (worst-case scenario), whereas with permeable structures the average accretion was 38 cm (intermediate scenario) and 44 cm (worst-case scenario), as was already provided in Table 3.1. The variability between locations was not much affected (i.e. similar standard deviations). The total bed level changes with and without permeable structures at the end of the intermediate and worst-case scenarios are provided in Table E.2 and Table E.3 respectively. Note that for none of the observation points the bed level increase was more than or equal to the total amount of relative sea level rise, so none of these locations can fully keep up with the rate of relative sea level rise (for all scenarios).

Looking in more detail at the processes governing the threshold behaviour observed in the model results, while considering a larger spatial scale (i.e. not only focused on the permeable structures), two phases can be identified: in the first phase the bed level is increasing, though not keeping up with sea level rise; in the second phase the bed level is decreasing. The latter phase mainly occurred for the simulations without permeable structures. Initially the rising sea level causes the bed level to increase, as accommodation space increases and more suspended sediment can settle in these shallow areas. Due to inertia of the system (i.e. a response time before the profile is adjusted to the changes in forcing), the net accretion cannot keep pace with sea level rise and thus the water depth slowly increases. This allows for larger waves to penetrate shoreward, causing enhanced bed shear stresses. Once these bed shear stresses surpass the critical shear stress for erosion of the smallest sediment fraction (0.1 N/m²), the bed level in the autonomous development starts to deviate from results with structures, suggesting that the smallest sediment fraction already accretes less (or erodes). As long as the bed shear stress does not exceed the critical shear stress of the larger sediment fraction (0.5 N/m²) yet, no net erosion occurs (as was found for the simulations with permeable structures). After the bed shear stress exceeds 0.5 N/m² and the larger sediment fraction also starts eroding, the water depth increases more rapidly and the wave height increases, thereby further enhancing erosion. The net accretion reverts to net erosion, thus moving into the second phase of decreasing bed level (as was found for the simulations without permeable structures). This again leads to increased water depth, higher waves and more erosion, providing a positive feedback mechanism leading to rapid erosion. Note that the amount of sediment that is available is not limiting the increase the bed level, since the available mass of bed sediment in the foreshore has not been depleted for any of the simulations (not shown here). The threshold behavior is thus initiated by the changes in forcing (i.e. waves, shear stress and bed erosion), not by a lack of supply (i.e. sediment availability and concentration).

3.4 Comparison of structure clusters between scenarios

Permeable structures are clustered with neighbouring structures to obtain insights into spatial patterns (see Figure 2.6). By comparing the mean value and standard deviation of the bed level change per cluster, insight is gained into spatial variations between separate clusters (mean value) and spatial variations within clusters (standard deviation). The clusters consist of the following permeable structures:

- Cluster Wonorejo: KPP-9, KPP-10, TW1-1 and TW1-2
- Cluster Bogorame-North: KPP-1, KPP-2, KPP-4, KPP-5 and KPP-6
- Cluster Bogorame-South: 1, HE-1, HE-2, HE-3, KPP-3, KPP-7 and KPP-8
- Cluster Bedono-North: HE-3, 11-1, 11-2, 11-3, 11-4, 11-5 and 11-6
- Cluster Bedono-South: 12-1, 12-2, 12-3, 12-4 and 12-5

The final bed level change after 10 years of a cluster is determined by taking an average over all permeable structures within a cluster. In general, the cluster Wonorejo has largest autonomous erosion (about 70-80 cm), shown in Figure 3.9. The cluster Bedono-South captures most sediment behind the permeable structures (about 40-60 cm). Variations between the locations within a cluster are larger for the autonomous development (standard deviation of 15-40 cm), than behind the permeable structures (standard deviation of 15-25 cm). Particularly the cluster of Bogorame-South has large spatial variations (standard deviation of 37 cm for autonomous development), likely due to the large variations in local water depth within this cluster.

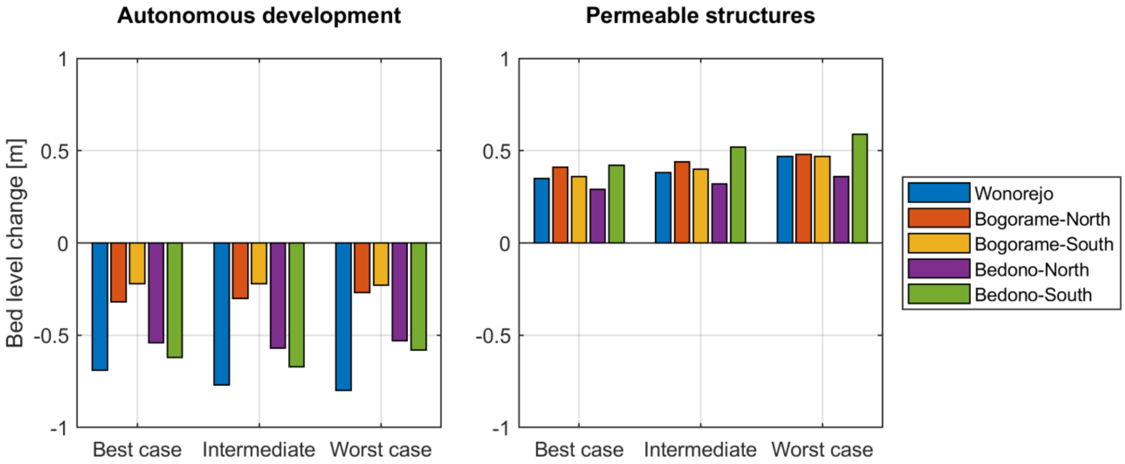

Figure 3.9: Average final bed level change after 10 years for all clusters per scenario for autonomous development (left panel) and behind permeable structures (right panel). Positive values indicate net accretion, negative values indicate net erosion.

For all areas, the amount of sediment captured behind the permeable structures increases with increasing rate of relative sea level rise. The autonomous development does not have a uniform response to increasing rate of relative sea level rise: in some areas the erosion exacerbates for increasing rate of relative sea level rise, whereas in other areas the amount of erosion reduces or remains roughly the same. This finding can be explained from the mechanisms behind the erosion process: when including permeable structures, the bed shear stresses behind these structures are reduced, thereby protecting the bed from erosion behind all the structures. With increasing rate of relative sea level rise, accommodation space becomes available that can be filled (e.g. increasing accretion rates). On the other hand, without permeable structures the bed is not protected from erosion. The rate of erosion, however, differs per location. Therefore, the autonomous bed level development does not respond so uniformly to increasing rate of relative sea level rise.

4 Discussion, recommendations & conclusions

This study aims to assess the effectiveness of the permeable structures implemented to restore eroding mangrove mud coastlines under various rates of relative sea level rise, using a modelling approach. Results show that without implementing permeable structures bed erosion will occur in the coastal area, drowning large parts of the Demak coastal zone for all investigated scenarios of relative sea level rise. The permeable structures reduce the erosion of the seabed by attenuating waves, and also trap sediments, thereby increasing the bed level. The permeable structures help to keep up with relative sea level rise until a threshold amount of sea level rise has been exceeded. The bed level can keep up for years even under the extreme subsidence rates considered in the modelled scenarios. After ten years, however, the Demak coastal zone will partially drown even for the best-case scenario when structures are implemented.

4.1 Reflection on method

Interpretation of the model results should be done with caution, as some important simplifications and underlying assumptions were made for the model setup. Firstly, processes that were not included in the model are 3D effects, interactions with mangroves (wave attenuation and sediment trapping) and chenier dynamics. In reality, sediments are often kept close to the coast due to freshwater stratification effects. The lack of 3D effects could lead to an underestimation of the amount of suspended sediments during the northwest monsoon. In the model sediments are mainly transported by the tide, i.e. landwards during flood and seaward during ebb. Moreover, the model may underestimate the capacity of the coastline to keep up with sea level rise, since mangroves were not included. The development of new cheniers and disappearing of old cheniers could affect the wave transformation in the coastal zone. Consequently, the model will also not give accurate predictions of spatially variations in flooding, erosion and sedimentation for situations where cheniers migrate. Chenier behaviour along this coast is poorly understood and very dynamic (Van Bijsterveldt *et al*, 2020). Chenier presence and movement can vary at multiple timescales, depending on availability of sand from rivers or on coastal erosion. Hence, considering the uncertainty, including the cheniers with more detail in the model applied in this study will sort little effect.

Secondly, the permeable structures are implemented as ‘thin dams’ in the Flow module. These thin dams completely close off one side of a cell and thus have the same length and orientation as the grid cells. Moreover, they are implemented as impermeable structures, thereby underestimating the flow and sediment transport through the structures. The flow and sediment transport through the structures are, however, expected to be very small, as most of the flow and sediment transport happens through the gaps between the structures (which are included in the model). In the wave module, the permeable structures are implemented as ‘obstacles’ that have more realistic properties with a structure height of MSL+2.0 m and a transmission coefficient that depends on the local conditions.

Thirdly, the bed friction parameter in the wave module accounts for smaller dissipation of wave energy by bed friction on muddy beds than on sandy beds. However, wave attenuation on the fluid mud layer by viscous energy dissipation, is not included in the model, although it was shown to be important at a similar mangrove-mud coast in Guyana (Winterwerp, *et al.*, 2007). Ruben Borsje (2019) concluded based on observations in Demak that damping of waves by fluid mud is relevant in this coastal system and that the attenuation can be computed sufficiently well with SWAN-Mud. However, such an approach requires an accurate determination of the relevant mud characteristics and it is not possible to include SWAN-Mud in a coupled Flow-Wave model with sediment transport yet. Consequently, an important wave dissipation term is missing. Moreover, Borsje speculates that a shoreward streaming effect of fluid mud may cause mud accumulation at the seaward side of the structure. This potential streaming effect is not included in the model used in this report, which could mean that a factor for large-scale sediment redistribution is missing. However, thus far this behaviour has not yet been observed in the area.

Finally, land subsidence was assumed linear over time and spatially uniform. However, subsidence can be a very local phenomenon. Consequently, the model will not give accurate indications of spatially-varying patterns in relative sea level rise at the scale of the entire project area.

Even though there are many considerations to be made when using the model, its results can be used to gain insight into the Demak coastal system and in general into the influence of the permeable structures under relative sea level rise.

4.2 Interpretation of model results

It is important to note that the process-based numerical model is used as a tool to gain more insight into the behaviour of the Demak coastal system under relative SLR and into the effectiveness of implementing permeable structures to restore the mangrove-mud coast. The model does not give exact predictions of flooding and bed level changes in the area, but when combined with interpretation by experts, the model results can help to give a rough indication of trends and developments. In this section, the model results are interpreted for further use.

Overall, the model results show sedimentation behind the permeable structures, whereas the autonomous development results in erosion at these same locations. So, under all scenarios of relative sea level rise, the permeable structures would help to capture sediments. Reflecting on the potential model responses (introduced in section 2.6.4) the model results suggest that without structures the coastal area would largely be ‘drowning’. If the structures are regularly maintained, the bed level behind the permeable structure can ‘keep up with relative sea level rise’ for a certain time (i.e. years) until a threshold amount of SLR has been exceeded. This indicates that while the bed level can keep up with relative SLR, the transport capacity is sufficient. The structures can prevent the intertidal areas from completely ‘drowning’, but eventually the bed accretion trend cannot keep pace with SLR anymore. This behaviour corresponds to the ‘partial drowning’ (or ‘catch-up’) response introduced in section 2.6.4.

For the threshold behaviour, explained in section 3.3, the onset of a feedback mechanism in the model is largely determined by the critical shear stress for erosion. Thus, the value of this key sediment parameter requires some justification. The value of 0.5 N/m^2 that was applied for the less mobile, weakly consolidated sediment fraction is commonly used (e.g. Van Maren *et al.*, 2015). Even if for example a value up to 0.8 N/m^2 would be used, the onset of the threshold behaviour would have been later, but the overall simulated trend would not have been very different.

A few final remarks can be made based on the model results:

- Under varying scenarios of sea level rise and land subsidence, the model results show the coast will retreat further and parts of the coastal area will flood due to the increase in water depth.
- The amount of relative sea level rise to which the coast is subjected, is for about 90% dependent on land subsidence.
- When comparing the simulation with permeable structures with the autonomous development, the autonomous development shows erosion in the intertidal area,

whereas the structures result in sediment accretion in their area of influence. The difference in bed level increases with increasing rate of relative sea level rise. The final bed level behind the permeable structures is on average 0.78 m higher in the best-case scenario and 0.88 m higher in the worst-case scenario.
- In the model the structures are assumed to remain in a good state throughout the entire simulation of ten years, whereas the quality of the structures deteriorates in the field. So, the model results are only representative for an ideal situation in which the structures are maintained regularly.

4.3 Recommendations

First recommendations aregiven to improve application of the permeable structures in the next phase of the project:

- The model results show that relative sea level rise can cause a lot of erosion and flooding. As about 90% of the relative sea level rise is caused by land subsidence, efforts should be undertaken to minimise the amount of land subsidence. The model results substantiate this statement.
- The improved model can also be used as a tool to assess the potential of new coastal interventions on the time scale of 5 to 10 years, such as additional structures along the entire coast or new interventions. The model could then be applied to optimise the spatial design of such interventions.

Next, recommendations are given to improve application of the current model results for utilisation within the project:

- In order to validate the morphological results, a more detailed comparison should be carried out with the observed bed level development of the monitoring task within this project. Now that the monitoring data analysis has been completed, the main findings of that analysis can be compared with the main findings based on the model results.
- The scope of the scenario study could be extended to include scenarios for sediment availability (i.e. limited sediment availability, unlimited sediment supply or spatially varying sediment supply, for example from river outflows). That way, the influence on sediment availability on the long-term morphological development of the Demak coastline could be researched. However, it is recommended to first investigate the effects of sediment availability in a simplified model (e.g. a 1D transect).

Finally, recommendations are given to substantially improve the results by implementing findings and results from other ongoing research projects. In order to do so, additional processes will have to be included in the model simulations:

- Include the effects of mangroves in the model. Since mangroves are able to trap sediments, thereby vertically increasing the bed level, they may help the intertidal zone to raise vertically with sea level rise provided that there is enough sediment influx. In order to properly capture the effect of mangroves, the complex interactions between the hydrodynamics, sediment transport and mangrove dynamics need to be reproduced by the model. This may be achieved by applying a new interactive modelling approach that combines D-Flow FM with a Python script for vegetation dynamics (still under development).
- Include the wave damping effect of the fluid mud layer by viscous energy dissipation. This process was studied within the MSc thesis of Ruben Borsje (2019). Moreover, based on the work of Borsje (2019), it is recommended to investigate whether mud streaming is causing mud accumulation seaward of the structures.

4.4 Conclusions

This study assessed the effectiveness of the permeable structures implemented to restore eroding mangrove mud coasts under influence of relative sea level rise. Scenarios for relative sea level rise ranged from 82 to 136 cm in ten years, due to extreme rates of land subsidence. An existing Delft3D Flexible Mesh model is utilised and improved to simulate the development of the coastal zone under these scenarios. Results show that structures can mitigate the impact of relative sea level rise. The bed level behind the structures can keep up with SLR for multiple years. However, even for the lower rates of sea level rise permeable structures will not be able to counteract submergence of large parts of the Demak coastal area over a period of ten years. Nevertheless, the structures postpone drowning of parts of the coastal zone, through wave attenuation and enhanced sedimentation. The results suggest a threshold amount of relative sea level rise beyond which the sedimentation rate behind the structures cannot keep pace with sea level rise, due to increased wave effects that initiate a positive feedback mechanism leading to rapid erosion. Two thresholds are identified, one where accretion stops and sediment levels become constant (initially for autonomous scenario and eventually for structures) and another one where erosion dominates (mainly found in absence of structures). This behaviour is observed at all data points behind structures.

To conclude, the permeable structures that are implemented to restore the sediment balance and stimulate regrowth of a healthy mangrove ecosystem help to trap sediments, thereby increasing the bed level. Assuming that the structures do not severely deteriorate over time, the bed level behind the permeable structures can to some extent keep up with relative sea level rise. However, under all the scenarios studied, the structures cannot prevent flooding nor capture enough sediment to keep up with the rate of relative sea level rise throughout the entire ten-year period. This behaviour corresponds to a ‘partial drowning’ response and is mainly caused by the large amount of land subsidence, which is responsible for 90% of the rate of relative sea level rise.

References

Alongi, D. M. (2008). Mangrove forests: resilience, protection from tsunamis, and responses to global climate change. Estuarine, Coastal and Shelf Science, 76(1), 1-13.

Arentz, L., & Van Wesenbeeck, B. (2013). Design for test with permeable dams near Timbul Sloko (Indonesia). *Memo*.

Ariathurai, C., & Arulanandan, K. (1978). Erosion rates of cohesive soils. ASCE, Journal of the Hydraulics Division, 104(2), 279–282.

Augustinus, P.G.E.F. (1999). Geomorphology and sedimentology of mangroves in estuaries and along the adjacent coastal areas. In STIUCA, R. and NICHERSU, I. (eds.), The Delta’s: State-of-the-art pro-tection and management.TULCEA, Rumania, pp. 13–18.

Borsje, R.M. (2019). Wave-Driven Set-Up of Fluid Mud. *MSc thesis*. Delft University of Technology.

Chaussard, E., Amelung, F., Abidin, H., & Hong, S. H. (2013). Sinking cities in Indonesia: ALOS PALSAR detects rapid subsidence due to groundwater and gas extraction. *Remote Sensing of Environment*, 128, 150-161.

De Goede, E. D. (2020). Historical overview of 2D and 3D hydrodynamic modelling of shallow water flows in the Netherlands. *Ocean Dynamics*, 70(4), 521-539.

Deltares (2015). D-Flow Flexible Mesh user manual. *Tech. Rep.* 1.1.148, Deltares.

Ecoshape (2015). Building with nature Indonesia (securing eroding delta coastlines): Design and engineering plan. *Tech. rep.*, Ecoshape.

Egbert, Gary D., and Svetlana Y. Erofeeva. Efficient inverse modeling of barotropic ocean tides. *Journal of Atmospheric and Oceanic Technology* 19.2 (2002): 183-204.

Fitzgerald, D. M., Fenster, M. S., Argow, B. A., & Buynevich, I. V. (2008). Coastal impacts due to sea-level rise. *Annual Review of Earth and Planetary Sciences*, 36.

Fredsøe, J. (1984). Turbulent boundary layer in wave-current interaction. *Journal of Hydraulic Engineering* 110: p. 1103–1120.

Hadi, S. P., & Buchori, I. (2018). The Population Growth and Carrying Capacity in Semarang City. In E3S Web of Conferences (Vol. 31, p. 07010). EDP Sciences.

IPCC, (2014): Climate Change 2014: Synthesis Report. Contribution of Working Groups I, II and III to the Fifth Assessment Report of the Intergovernmental Panel on Climate Change [Core Writing Team, R.K. Pachauri and L.A. Meyer (eds.)]. IPCC, Geneva, Switzerland, 151 pp. {WGI E.6, TS 5.7.1, 12.4.1, 13.4.1, 13.5.1, 13.6.5, 13.7.2, Table 13.5, section *2.2.3}*

Kernkamp, H. W. J., A. Van Dam, G. S. Stelling and E. D. de Goede (2011). "Efficient scheme for the shallow water equations on unstructured grids with application to the Continental Shelf." *Ocean Dynamics* 61(8): 1175-1188.

Koster, J. (2019). The effect of permeable structures on spatial sediment dynamics and mangrove reoccurrence: tackling spatial distribution of sediment variables in an intertidal mudflat Demak, Indonesia. Intership report. Deltares & Wageningen University and Research.

Kirwan, M.L. & Megonigal, J. P. (2013). Tidal wetland stability in the face of human impacts and sea-level rise. Nature 504, 53–60.

KOICA (2012). Coastal protection and management policy addressing climate change impactin Indonesia. *Tech. rep.*

Lovelock, C.E., Cahoon, D.R., Friess, D.A., Guntenspergen, G.R., Krauss, K.W., Reef, R., Rogers, K., Saunders, M.L., Sidik, F, Swales, A., Saintilan, N., Thuyen, L. X., and Triet, T. (2015). The vulnerability of Indo-Pacific mangrove forests to sea-level rise. USGS Staff -- Published Research. 988.

Lubis, A. M., Sato, T., Tomiyama, N., Isezaki, N., & Yamanokuchi, T. (2011). Ground subsidence in Semarang (Indonesia) investigated by ALOS–PALSAR satellite SAR interferometry. *Journal of Asian Earth Sciences*, *40(5)*, 1079–1088.

Marfai, M., & King, L. (2007). Monitoring land subsidence in Semarang, Indonesia. *Environmental Geology*, *53*, 651–659.MBSDMP (2019). Manila Bay Sustainable Development Master Plan –Final Master Plan Report. [online] May 2019. [Accessed on 14 February 2020] Available from: http://www.mbsdmp.com/resources

Minderhoud, P. S. J., Erkens, G., Pham, V. H., Bui, V. T., Erban, L., Kooi, H., & Stouthamer, E. (2017). Impacts of 25 years of groundwater extraction on subsidence in the Mekong delta, Vietnam. Environmental Research Letters, 12(6), 064006.

MMAF (2012). Oceanography condition in coastal of Sayung sub-district, district of Demak (province of Central Java). *Tech. rep.*, LGF team in Demak, Ministry of Marine Affairs and Fisheries, Republic of Indonesia.

Nicholls, R. J., & Cazenave, A. (2010). Sea-level rise and its impact on coastal zones. science, 328(5985), 1517-1520.Phien-Wej, N., Giao, P. H., & Nutalaya, P. (2006). Land subsidence in Bangkok, Thailand. Engineering geology, 82(4), 187-201.

Rodolfo, K. S., & Siringan, F. P. (2006). Global sea-level rise is recognised, but flooding from anthropogenic land subsidence is ignored around northern Manila Bay, Philippines. Disasters, 30(1), 118-139.

Roelvink, J.A. (2006) Coastal morphodynamics evolution techniques. *Coastal Engineering,* 53: p. 277-287.Saengsupavanich, C. (2013). Erosion protection options of a muddy coastline in Thailand: stakeholders' shared responsibilities. Ocean & Coastal Management, 83 , 81–90.

Schmitt, K., Albers, T., Pham, T., & Dinh, S. (2013). Site-specific and integrated adaptation to climate change in the coastal mangrove zone of Soc Trang province, Vietnam. J. Coast Conserv.

Smits, B.P. (2016). Morphodynamic optimisation of the design of semi-permeable dams for rehabilitation of a mangrove-mud coast. A case study of Demak, Indonesia. *MSc thesis*. Delft University of Technology.

Slangen, A. B. A., Katsman, C. A., Van de Wal, R. S. W., Vermeersen, L. L. A., & Riva, R. E. M. (2012). Towards regional projections of twenty-first century sea-level change based on IPCC SRES scenarios. *Climate dynamics*, 38(5-6), 1191-1209.

SWAN (2000). Swan cycle iii version 40.11 user manual. *Tech. rep.*, Delft University of Technology.

Van Bijsterveldt, C. E., Van Wesenbeeck, B. K., Van der Wal, D., Afiati, N., Pribadi, R., Brown, B., & Bouma, T. J. (2020). How to restore mangroves for greenbelt creation along eroding coasts with abandoned aquaculture ponds. *Estuarine, Coastal and Shelf Science*, 106576.

Van Cuong, C., Brown, S., To, H., & Hockings, M. (2015). Using melaleuca fences as soft coastal engineering for mangrove restoration in Kien Giang (Vietnam). *Ecological Engineering*, 81, 256–265.

Van Maren, D. S., Winterwerp, J. C., & Vroom, J. (2015). Fine sediment transport into the hyper-turbid lower Ems River: the role of channel deepening and sediment-induced drag reduction. *Ocean Dynamics*, 65(4), 589-605.

Van Wesenbeeck, B.K., Balke, T., Van Eijk, P., Tonneijck, F., Siry, H., Rudianto, M., & Winterwerp, J. (2015). Aquaculture induced erosion of tropical coastlines throws coastal communities back into poverty. *Ocean & Coastal Management*, *116* , 466–469.

Van der Wulp, S. A., Dsikowitzky, L., Hesse, K. J., & Schwarzbauer, J. (2016). Master Plan Jakarta, Indonesia: The Giant Seawall and the need for structural treatment of municipal waste water. *Marine pollution bulletin*, 110(2), 686-693.

Winterwerp, J. C., De Graaff, R. F., Groeneweg, J., & Luijendijk, A. P. (2007). Modelling of wave damping at Guyana mud coast. *Coastal Engineering*, 54(3), 249-261.

Winterwerp, J., Erftemeijer, P., Suryadiputra, N., Van Eijk, P., & Zhang, L. (2013). Defining eco-morphodynamic requirements for rehabilitating eroding mangrove-mud coasts. *Wetlands*, *33* , 515–526.

Winterwerp, J., Van Wesenbeeck, B., Van Dalfsen, J., Tonneijck, F., Astra, A., Verschure, S., & Van Eijk, P. (2014). Sustainable solution massive erosion central java. *Tech. rep.*, Deltares & Wetlands International.

Woodruff, J. D., Irish, J. L., & Camargo, S. J. (2013). Coastal flooding by tropical cyclones and sea-level rise. Nature, 504(7478), 44-52.

Wyrtki, K. (1961). Physical oceanography of the Southeast Asian water, naga report. *Tech. rep.*, Scripps Institute of Oceanography, University of California.

Appendices

A Wind data

hydronamic *Offshore Wind roses and Workability* Boskalis

Offshore wind roses and workability

Coordinate: *6.0°S 110.50°E*
Depth: *56m*
Samples: *24836 samples (1997.1.1−2013.12.31)*
Database: *WorldWaves offshore database (February 2015)*

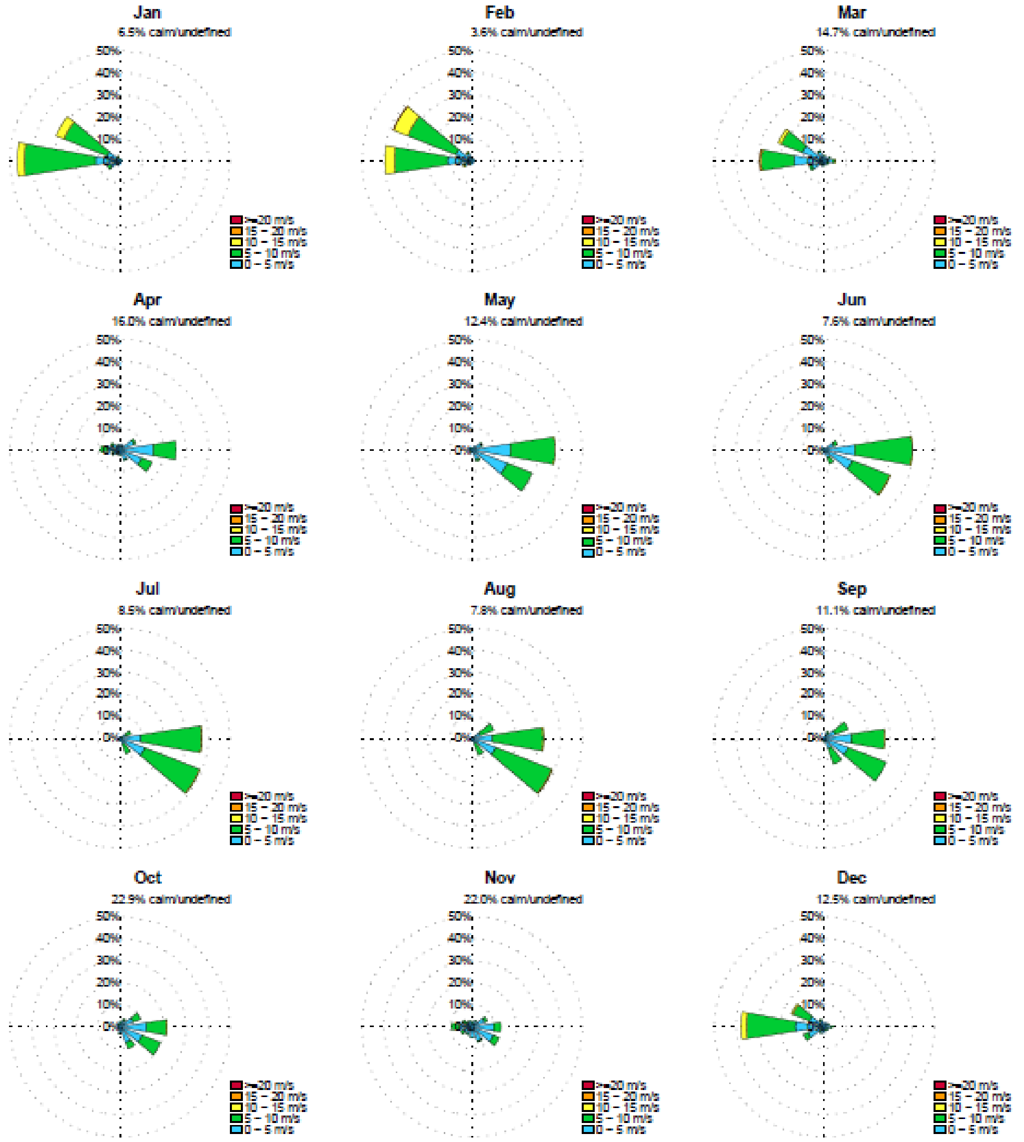

Workability [%]

	Jan	Feb	Mar	Apr.	May	Jun	Jul	Aug	Sep	Oct	Nov	Dec	year
U<1.6m/s (<=Bft.1)	10	9	24	28	20	11	10	9	14	30	35	22	18
U<3.4m/s (<=Bft.2)	20	23	48	55	38	23	17	16	25	49	63	45	35
U<5.5m/s (<=Bft.3)	44	44	74	86	74	60	48	46	62	81	90	67	65
U<8.0m/s (<=Bft.4)	76	70	92	98	98	95	92	93	96	99	99	89	91
U<10.8m/s (<=Bft.5)	96	93	99	100	100	100	100	100	100	100	100	98	99
U<13.9m/s (<=Bft.6)	100	99	100	100	100	100	100	100	100	100	100	100	100
U<17.2m/s (<=Bft.7)	100	100	100	100	100	100	100	100	100	100	100	100	100
U<20.8m/s (<=Bft.8)	100	100	100	100	100	100	100	100	100	100	100	100	100

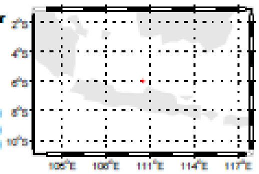

− **Input time series:** *g:\WERKBAARHEID\Worldwaves\data\offshore_points\2015\wave\world\Dat_files\ww15_offshore_06.0S_110.5E.dat*
− **m-file:** *G:\matlab\GSAL\Matlab\MetOcean_MATLAB_20150422\Plot_wave_wind_roses\plot_wave_wind_roses_2014_v2.m*
− **print date:** *29−Apr−2015 16:07:36*

B Wave data

hydronamic — *Offshore wave roses and workability* — Boskalis

Offshore wave roses and workability for total wave height (sea and swell)

Coordinate: *6.0°S 110.50°E*
Depth: *56m*
Samples: *24836 samples (1997.1.1–2013.12.31)*
Database: *WorldWaves offshore database (February 2015)*

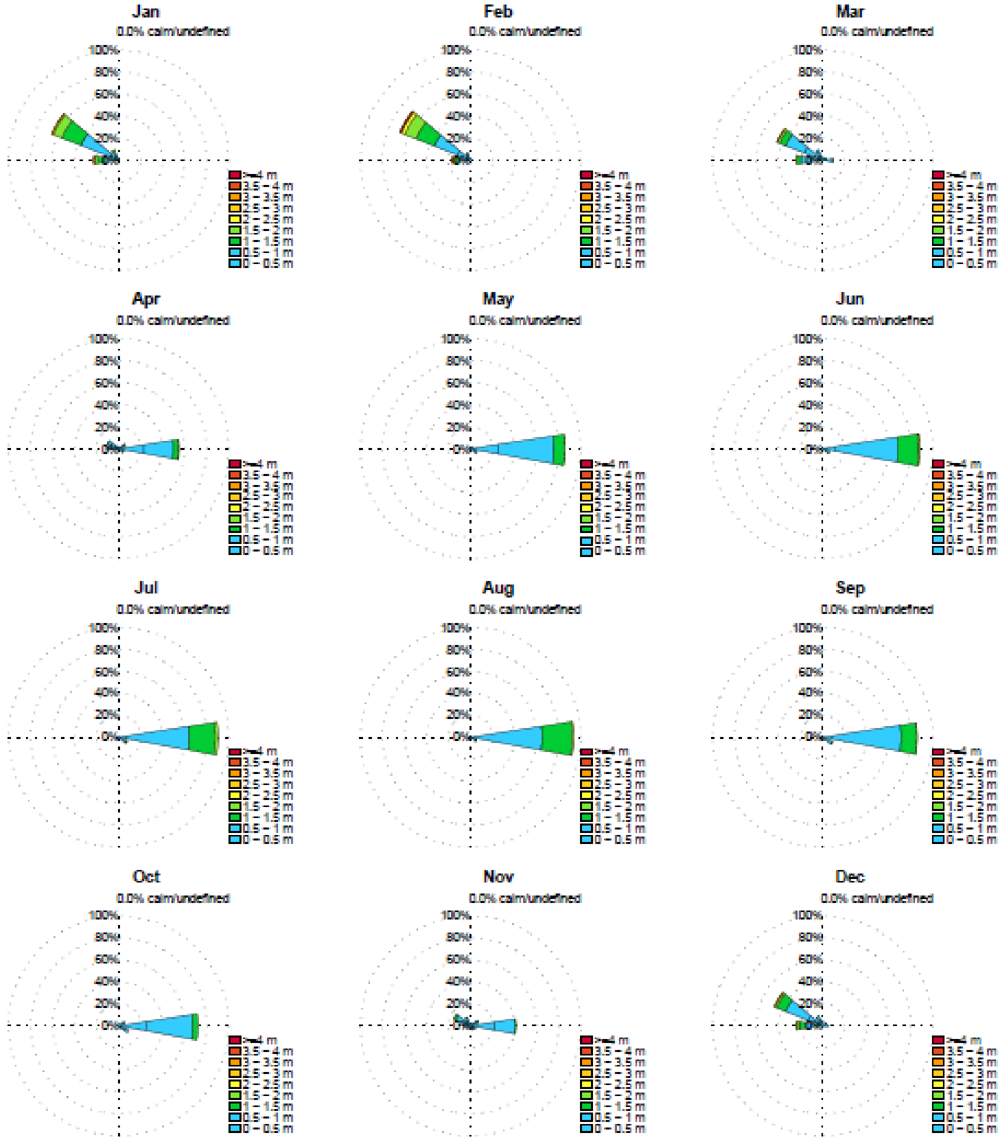

Workability [%]

	Jan	Feb	Mar	Apr.	May	Jun	Jul	Aug	Sep	Oct	Nov	Dec	year
H_s≤0.50m	19	29	54	58	38	16	8	5	14	45	62	44	33
H_s≤0.75m	41	45	75	84	69	50	37	32	53	80	88	65	60
H_s≤1.00m	62	60	87	94	90	80	73	72	85	95	96	80	81
H_s≤1.50m	86	82	97	99	100	99	98	99	100	100	100	95	96
H_s≤2.00m	97	95	100	100	100	100	100	100	100	100	100	99	99
H_s≤2.50m	99	98	100	100	100	100	100	100	100	100	100	100	100
H_s≤3.00m	100	99	100	100	100	100	100	100	100	100	100	100	100
H_s≤3.50m	100	100	100	100	100	100	100	100	100	100	100	100	100

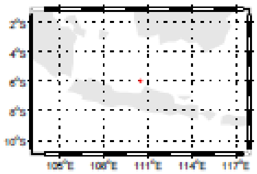

– input time series: *g:\WERKBAARHEID\Worldwaves\data\offshore_points\2015\wave\world\extracted\Dat_files\ww15_offshore_06.0S_110.5E.dat*
– m-file: *G:\matlab\GSAL\Matlab\MetOcean_MATLAB_20150422\Plot_wave_wind_roses\plot_wave_wind_roses_2014_v2.m*
– print date: *24-Apr-2015 16:54:11*

C Bathymetry data

In this appendix the bathymetry sets are described. GEBCO data was used for the offshore bathymetry in the model. Some background information about GEBCO is given in section C.1. Moreover, section C.2 describes two sets of bathymetry data that were available from depth measurements.

C.1 GEBCO database

The offshore bathymetry was taken from General Bathymetric Chart of the Oceans (GEBCO), which was founded by an international group of experts. Their work amounts to a range of bathymetric data sets and data products, including gridded bathymetric data sets. The dataset that was used was GEBCO'08, a global bathymetric grid with one arc-minute spacing (about 1 km) that was originally based on the bathymetric contours contained within the Centenary Edition of the GEBCO Digital Atlas, in many regions (particularly shallow water areas and semi-enclosed seas) extended with additional control contours and sounding point data. It is a continuous digital terrain model for ocean and land, with land elevations derived from the Global Land One-km Base Elevation (GLOBE) database. For more information about the development and limitations of the grid, please see the data set documentation hosted on the British Oceanographic Data Centre (BODC) website.

C.2 Depth measurements

Stefan Verschure performed depth measurements around the cheniers near Timbulsloko and in the area behind them, where the coast has eroded. The locations where Stefan took the depth measurements are indicated in Figure C.1. In Figure C.2 the location of the depth measurements by Pak Sugeng are indicated with green markers. The locations of the measurements by Stefan Verschure are also indicated for reference.

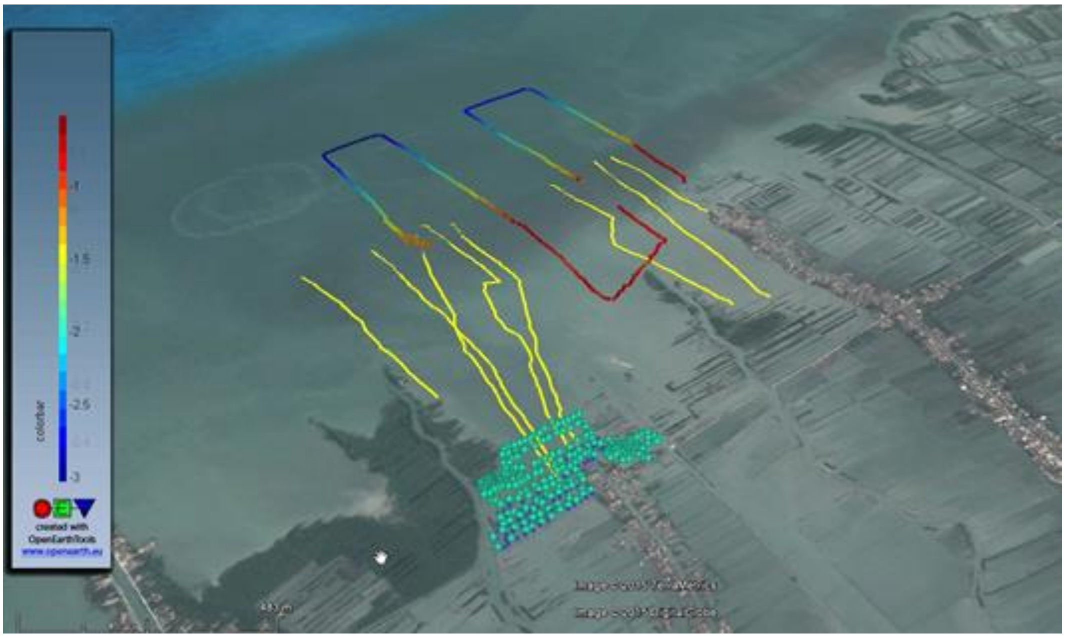

Figure C.1: Locations of depth measurements performed by Stefan Verschure

Figure C.2: Locations of depth measurements performed by Pak Sugeng (Google Earth)

As can be seen from the figures, the depth measurements give quite a detailed local bathymetry set. However, in the rest of the modeled area, only GEBCO information was available with relatively low resolution. As the bottom profile has a very gentle slope, depth contours will be mostly parallel. Therefore, the local nearshore bathymetry data is assumed to be representative for the entire coastline. Depth samples were manually added to reproduce the parallel depth contours.

D Additional model description and setup

D.1 Model description

In this appendix the flow module (D-Flow FM), the wave module (D-Waves) and the sediment & morphology module (D-Morphology) are described in more detail. These descriptions are primarily based on the D-Flow FM user manual (Deltares, 2015).

D.1.1 Flow module

D-Flow Flexible Mesh (D-Flow FM) is the hydrodynamic module of the Delft3D Flexible Mesh suite. It can perform simulations of non-steady flow and transport phenomena that result from tidal and meteorological forcing on structured and unstructured grids. The governing model equations of D-Flow FM are, equivalent to its predecessor Delft3D, the shallow water equations. These are derived from the Navier-Stokes equations for an incompressible fluid under the shallow water assumption (i.e. hydrostatic pressure) and the Boussinesq approximation (i.e. constant density in inertia terms).

The main improvement in D-Flow Flexible Mesh relative to its predecessors is the use of unstructured grids, as opposed to the structured curvilinear grids that were previously required. This offers more flexibility in the grid resolution by combining curvilinear grids with unstructured grids composed of triangles, in order to increase the resolution locally. D-Flow FM implements a finite volume solver on a staggered grid. The continuity equation is solved implicitly for all points in a single combined system. Time integration is done explicitly for part of the advection term, resulting in a stability criterion for the time step. Based on the CFL condition (Courant number), a dynamic computational time step is applied, thereby ensuring numerical stability.

D.1.2 Wave module

Delft3D Flexible Mesh uses the SWAN wave model to simulate the evolution of random, short-crested, wind-generated waves. A brief model description of the SWAN model is given here. A more detailed, conceptual description is documented in SWAN (2000). SWAN is a third-generation numerical model that computes wave transformation from deep water to nearshore values based on a wave action balance. The model does not solve for individual waves but transforms an offshore wave spectrum to a wave spectrum nearshore. These spectra are defined by a spectral shape, wave height, peak period and frequencies. Other input parameters that should be defined are the bottom level, initial water level, wind speed and wind direction.

The physical phenomena that are included in the SWAN simulation are generation of waves, shoaling, refraction, quadruplet wave-wave interactions, whitecapping, depth-induced breaking, bed friction and wave-setup. Wave setup is accounted for in the flow module. Triad wave-wave interactions are not taken into account. Based on algorithms, SWAN iterates the wave conditions for each grid cell, thereby generating output in any desired point within the grid.

For the SWAN wave module, a structured grid is used. The flow and wave modules are dynamically coupled, interpolating the results between the grids. This means data is continuously exchanged between the flow and wave simulations at a user-defined interval, usually every hour. This ensures a direct feedback between the hydrodynamics and wave-induced effects, such as radiation stress and bed shear stresses.

D.1.3 Sediment module

The sediment transport and morphology module computes both bed load and suspended load transport of non-cohesive sediments, and suspended load of cohesive sediments. For this study only cohesive sediments were modelled.

Suspended sediment transport is computed by solving the advection-diffusion equation. The exchange of material at the bed is included as source and sink terms based on the Partheniades-Krone formulations (Ariathurai *et* al,1978). The calculated water-bed fluxes are used to update the bed level. This morphological update is performed for each computational time step, thus ensuring that the hydrodynamic computations are carried out using the correct bathymetry. The input for the sediment module consists of initial and boundary conditions, as well as some physical parameters. The initial concentration can be prescribed as a uniform value or as a spatially-varying concentration field.

D.2 Model setup

D.2.1 Layout of flow and wave grids

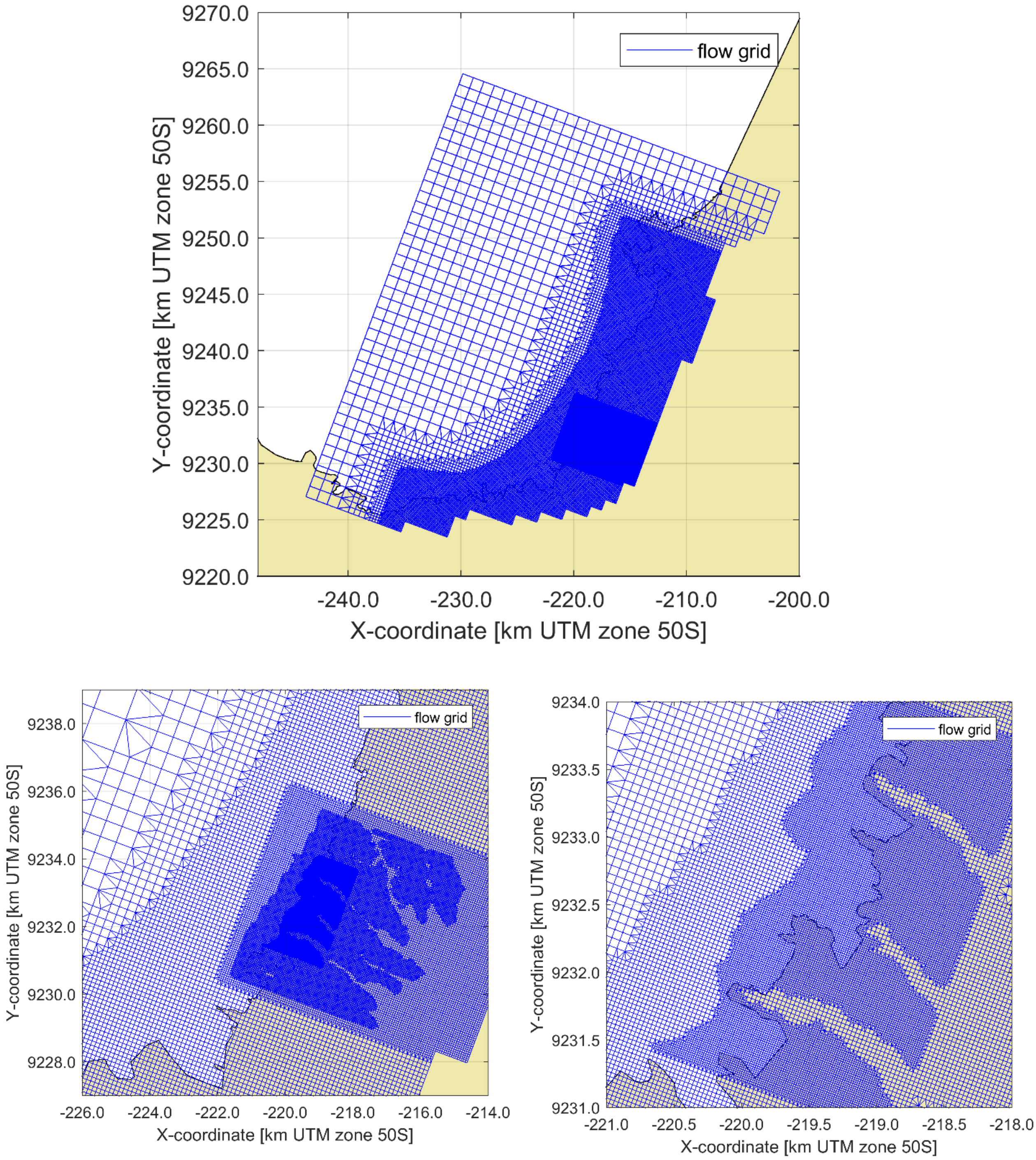

Figure D.1: Layout of flow grid for the whole domain (top panel), zoom at the coastline (lower left panel) and zoom around the project area (lower right panel). The grid cell size varies between roughly 1 km offshore and 16 m in the area of interest.

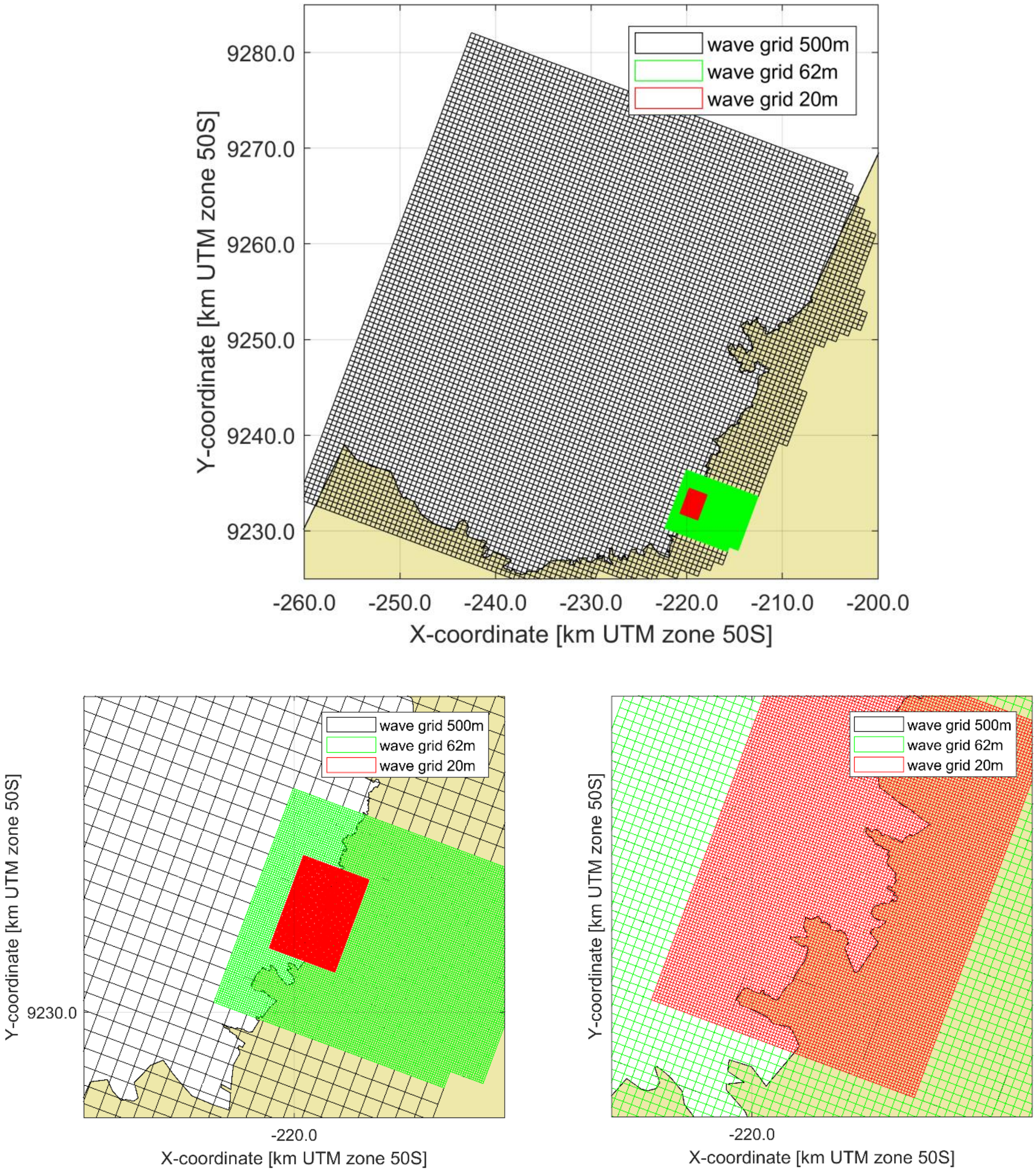

Figure D.2: Layout of three wave grids for the whole domain (top panel), zoom at the coastline (lower left panel) and zoom around the project area (lower right panel). The black mesh indicates the largest wave grid with cell size of 500 m, the green mesh indicates the middle wave grid with cell size of 62 m and the red mesh indicates the smallest wave grid with cell size of 20 m.

D.2.2 Bed shear stress statistics

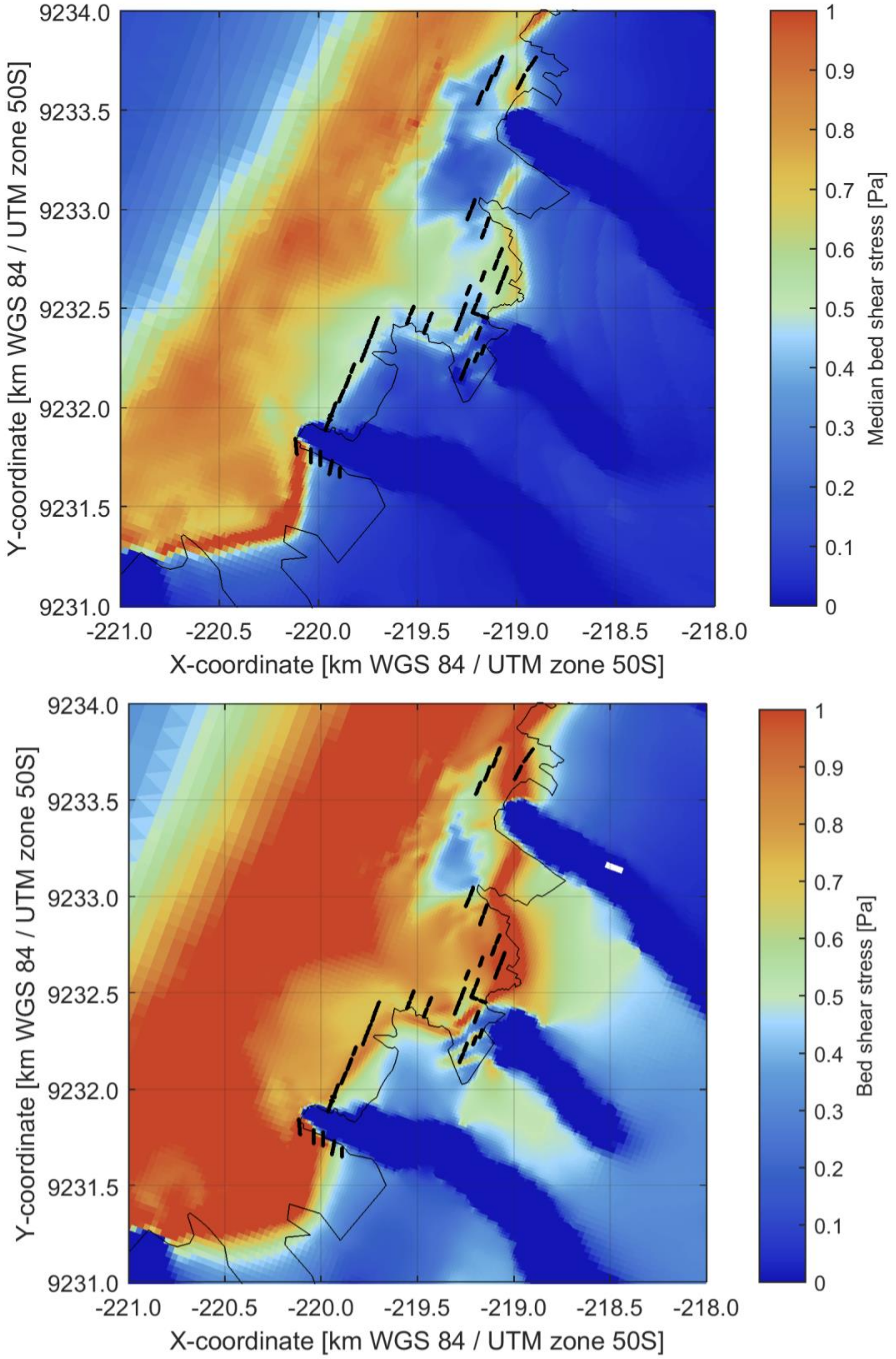

Figure D.3: Bed shear stress statistics of a morphostatic simulation. The upper panel shows the median value and the lower panel shows the 90th percentile value of the bed shear stress.

D.2.3 Circulation pattern

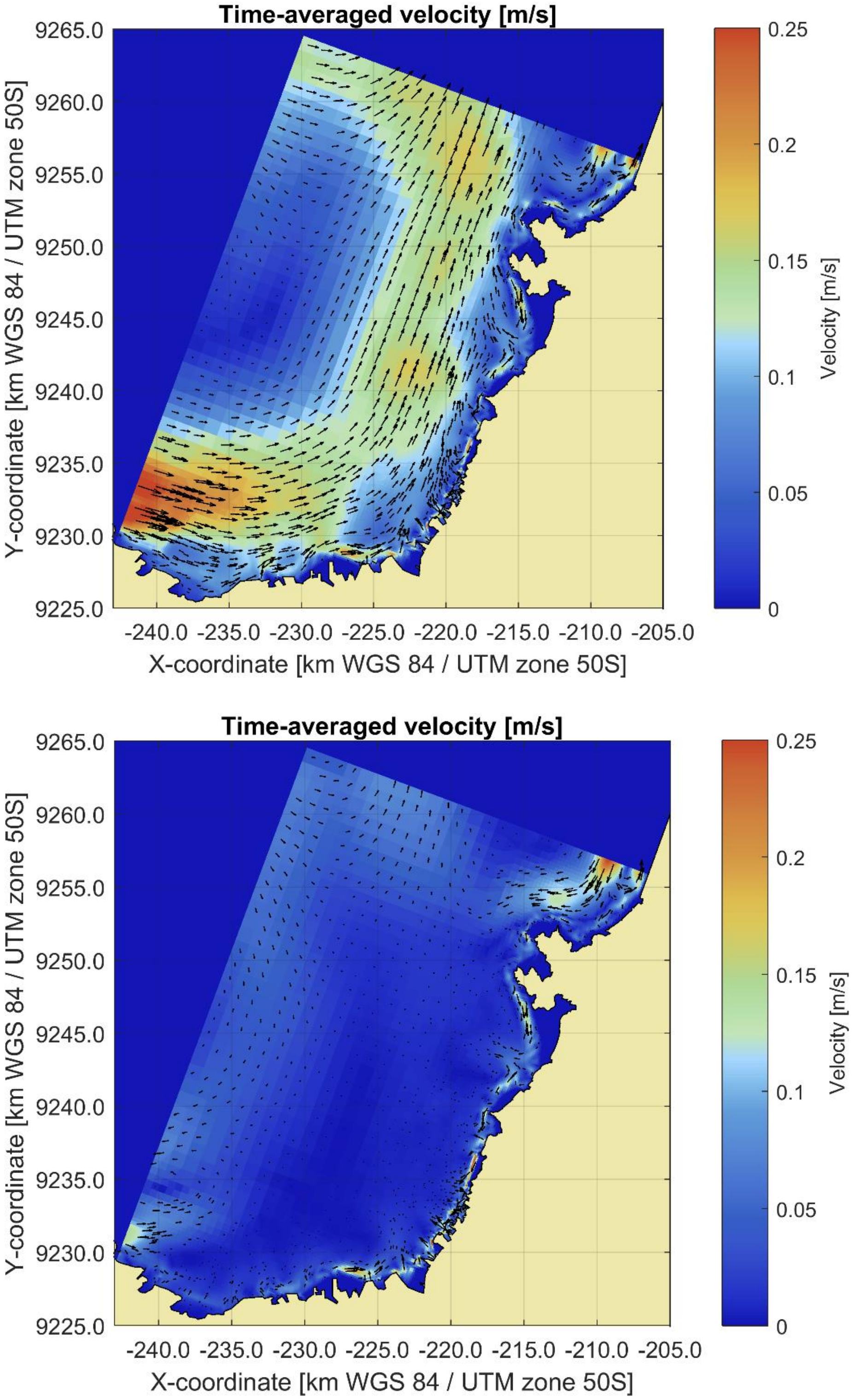

Figure D.4: The circulation pattern at the scale of the model domain with wind effects (upper panel) and without wind effects (lower panel).

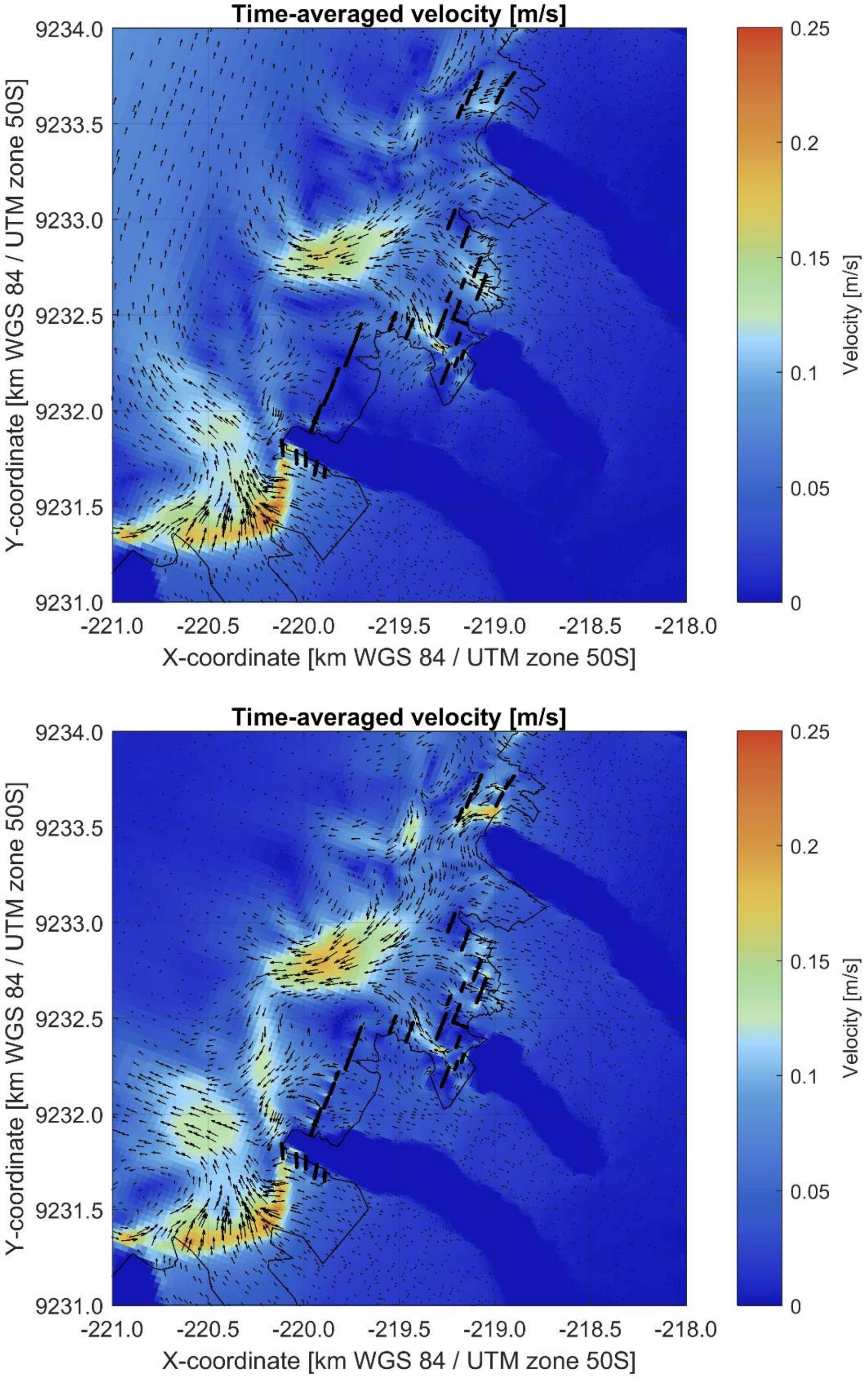

Figure D.5: The circulation pattern at the scale of the permeable structures with wind effects (upper panel) and without wind effects (lower panel).

E Additional results of scenario study

In this appendix, additional results of the scenario study are shown. First, the results of the best-case scenario are given in section E.1. Then, in section E.2, the results of the intermediate scenario are shown. Lastly, the results of the worst-case scenario are given in section E.3.

For each scenario two model simulations were performed: a simulation without permeable structures, indicating the autonomous development of the coast, and a simulation with the permeable structures. Results for each of these model simulations are shown in this appendix separately, as well as comparisons between the two simulations per scenario.

E.1 Best-case scenario

This section shows the results of simulations for the best-case scenario with a total relative sea level rise of 0.82 m after 10 years. The following additional figures are included:

- Bed level change (sedimentation & erosion)
- Bed level change (colour scale for relative Sea Level Rise) at the scale of the intertidal zone
- Bed level change (colour scale for relative Sea Level Rise) at the scale of the entire project area
- Timeseries of bed level at the locations of permeable structures

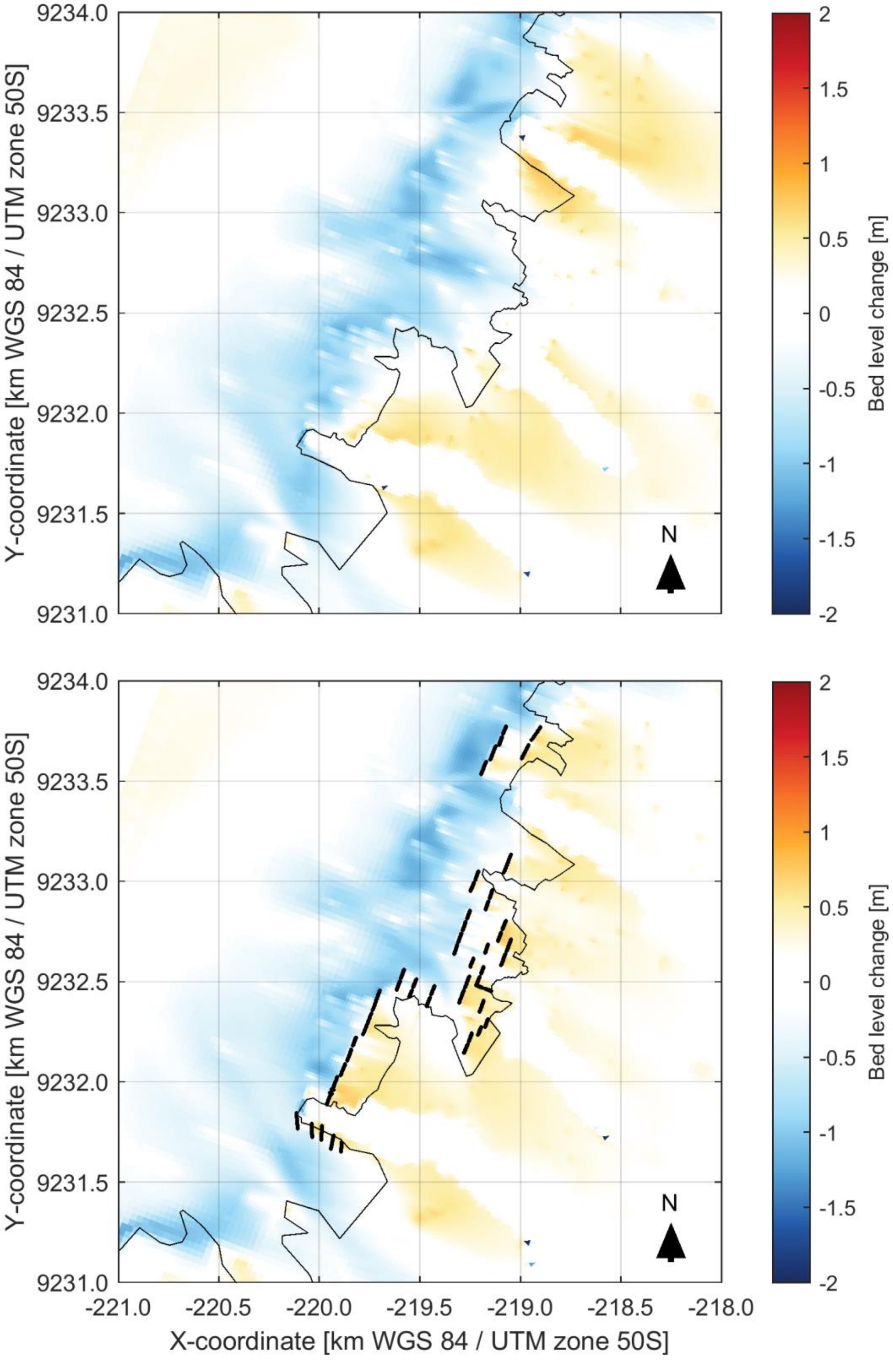

Figure E.1 Total bed level change after 10 years for the best-case scenario simulations. The upper panel shows the autonomous development and the lower panel shows the results of a simulation with permeable structures. Red colours indicate sedimentation areas and blue colours indicate erosion areas.

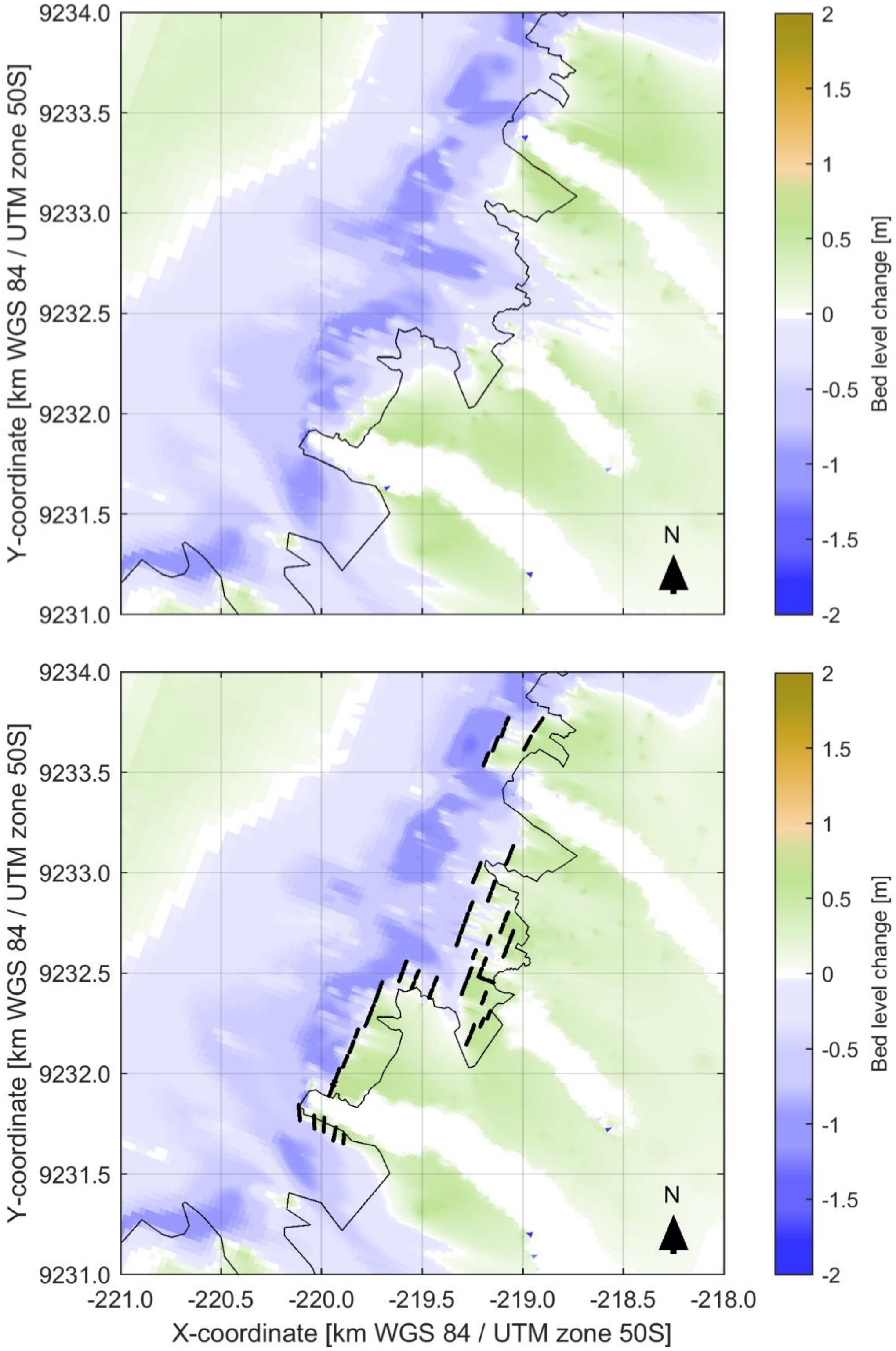

Figure E.2: Total bed level change after 10 years for the best-case scenario simulations (upper panel autonomous development; lower panel with permeable structures). Blue colours indicate erosive areas, green colours indicate partially drowning areas and brown colours indicate sedimentation rates that exceed the rate of relative sea level rise.

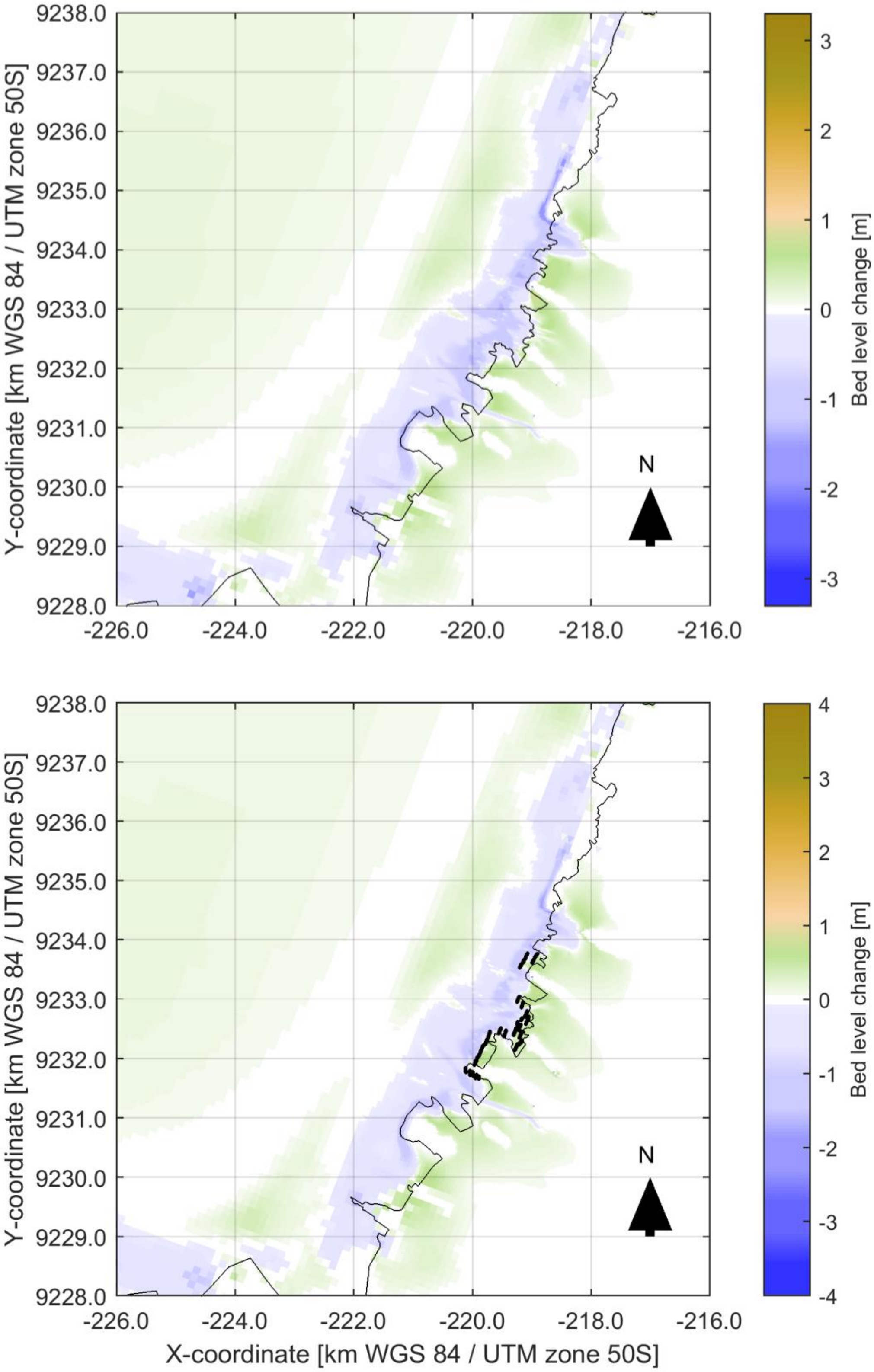

Figure E.3: Total bed level change after 10 years at the scale of the entire project area for the best-case scenario simulations (upper panel autonomous development; lower panel with permeable structures indicated by black lines). Blue colours indicate erosive areas, green colours indicate sedimentation areas where the sedimentation rate is smaller than the rate of relative sea level rise and brown colours indicate sedimentation rates that exceed the rate of relative sea level rise.

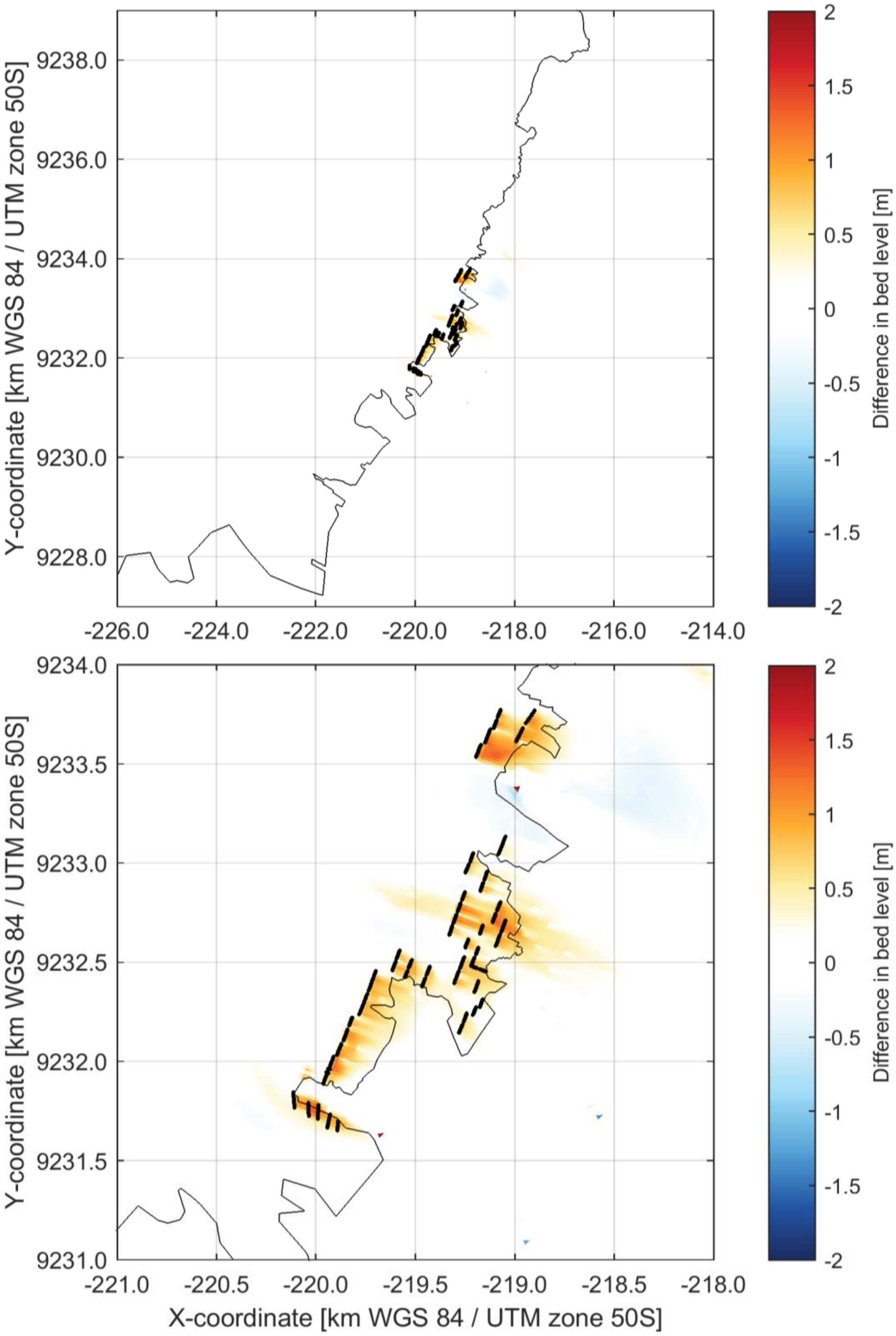

Figure E.4: Difference plot between final bed level with permeable structures and the autonomous development for the best-case scenario simulations (upper panel shows the extent of the project area; lower panel a zoom around the area of permeable structures). Red colours indicate higher bed levels in the simulation with permeable structures, whereas blue colours indicate lower bed levels.

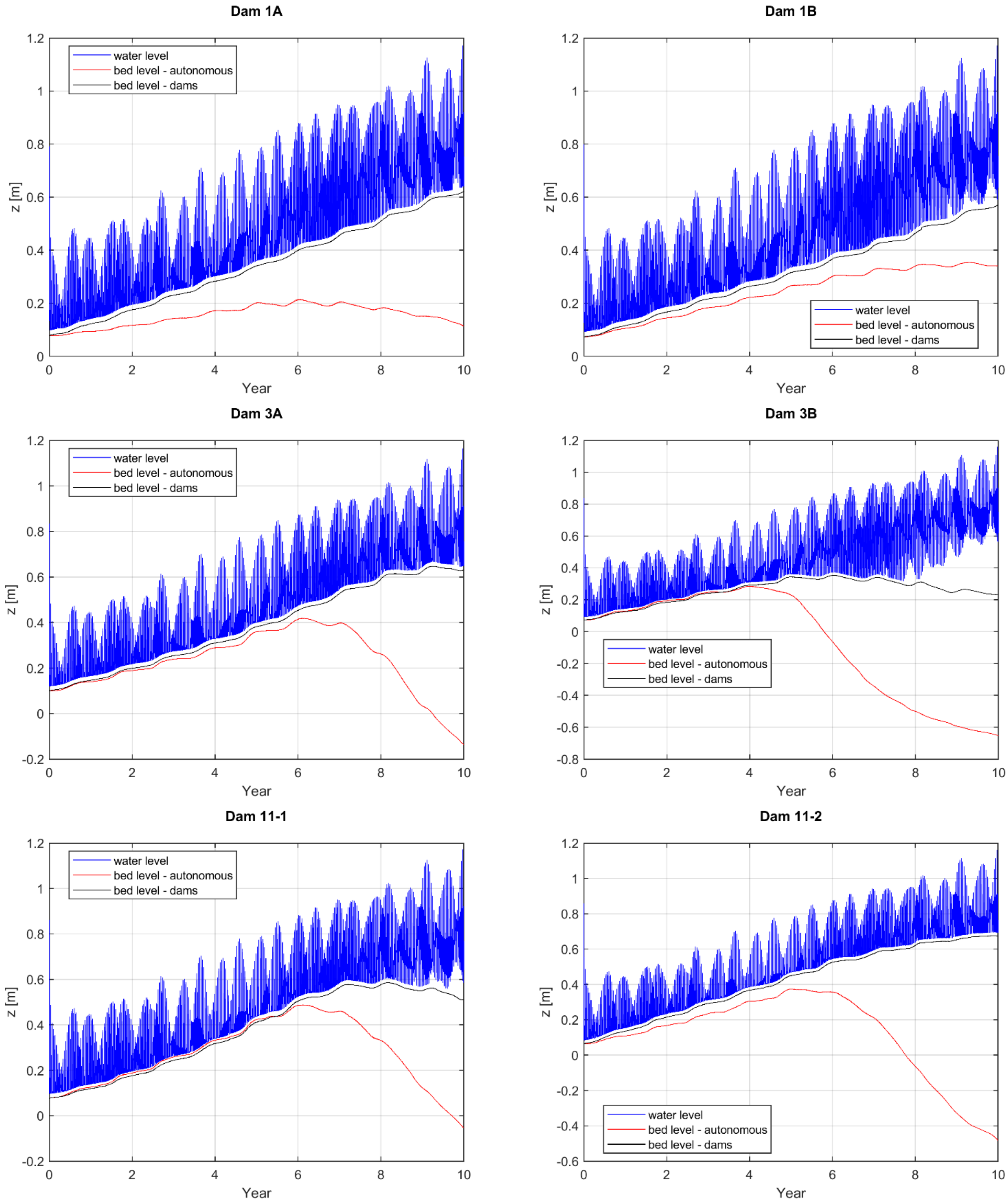

Figure E.5: Bed level development over time throughout the simulation for the best-case scenario at observation points behind the permeable structures. The blue line gives the tidal water level including relative sea level rise (on hydrodynamic timescale), the red line shows the bed level of the autonomous development and the black line shows the bed level with permeable structures. The subpanels show structures 1A (top left), 1B (top right), 3A (middle left), 3B (middle right), 11-1 (bottom left) and 11-2 (bottom right).

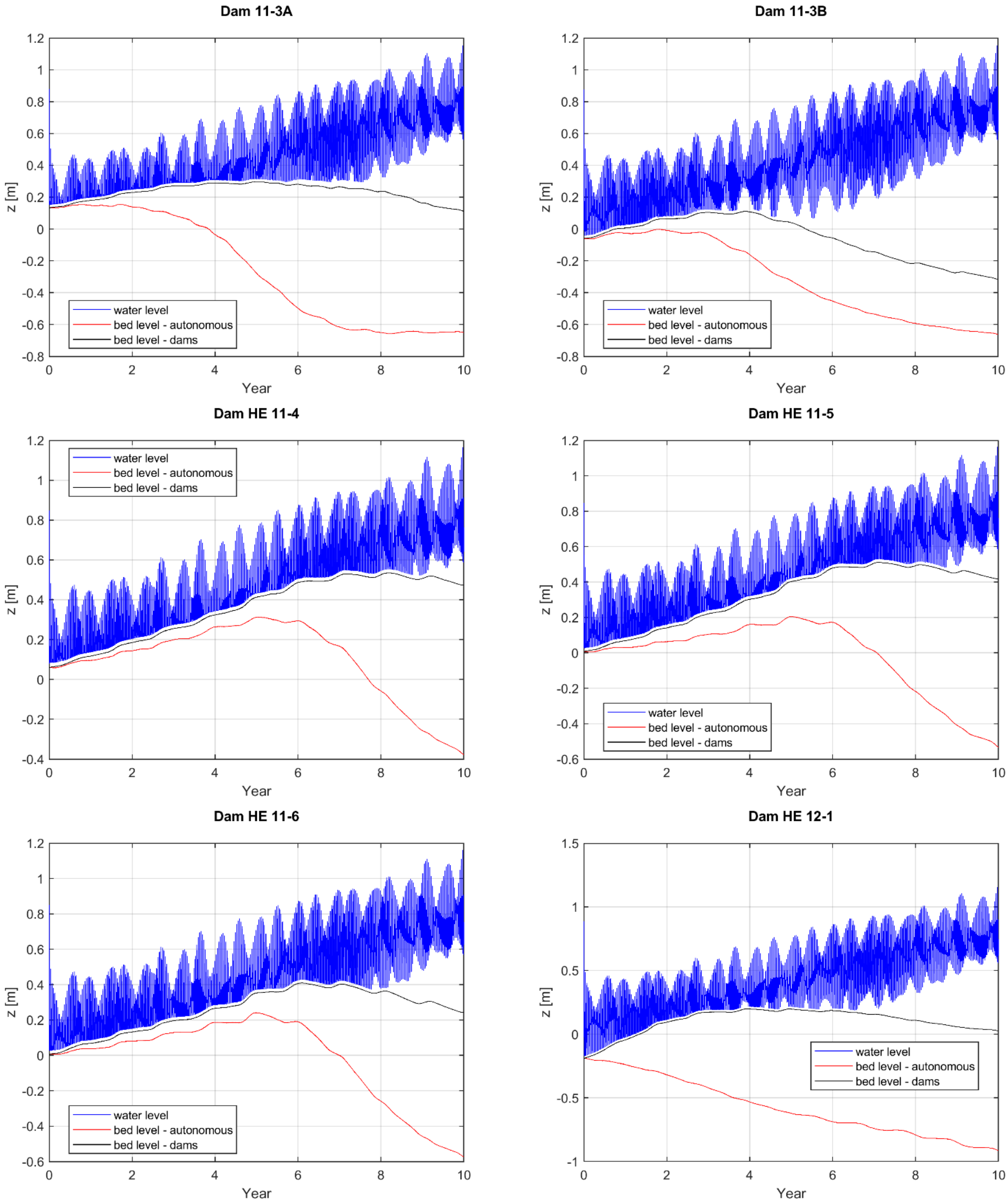

Figure E.6: Bed level development over time throughout the simulation for the best-case scenario at observation points behind the permeable structures. The blue line gives the tidal water level including relative sea level rise (on hydrodynamic timescale), the red line shows the bed level of the autonomous development and the black line shows the bed level with permeable structures. The subpanels show structures 11-3A (top left), 11-3B (top right), 11-4 (middle left), 11-5 (middle right), 11-6 (bottom left) and 12-1 (bottom right).

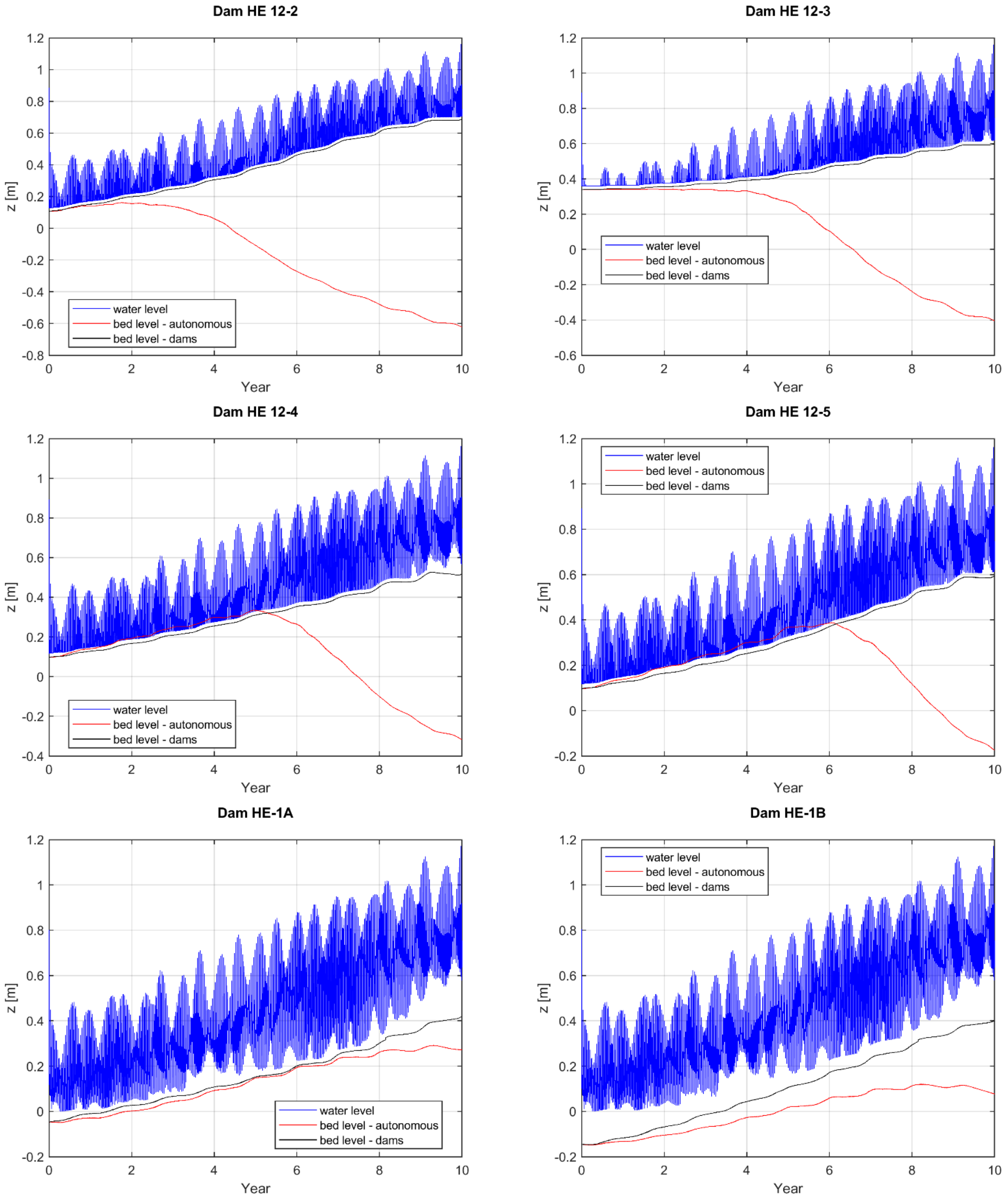

Figure E.7: Bed level development over time throughout the simulation for the best-case scenario at observation points behind the permeable structures. The blue line gives the tidal water level including relative sea level rise (on hydrodynamic timescale), the red line shows the bed level of the autonomous development and the black line shows the bed level with permeable structures. The subpanels show structures 12-2 (top left), 12-3 (top right), 12-4 (middle left), 12-5 (middle right), HE-1A (bottom left) and HE-1B (bottom right).

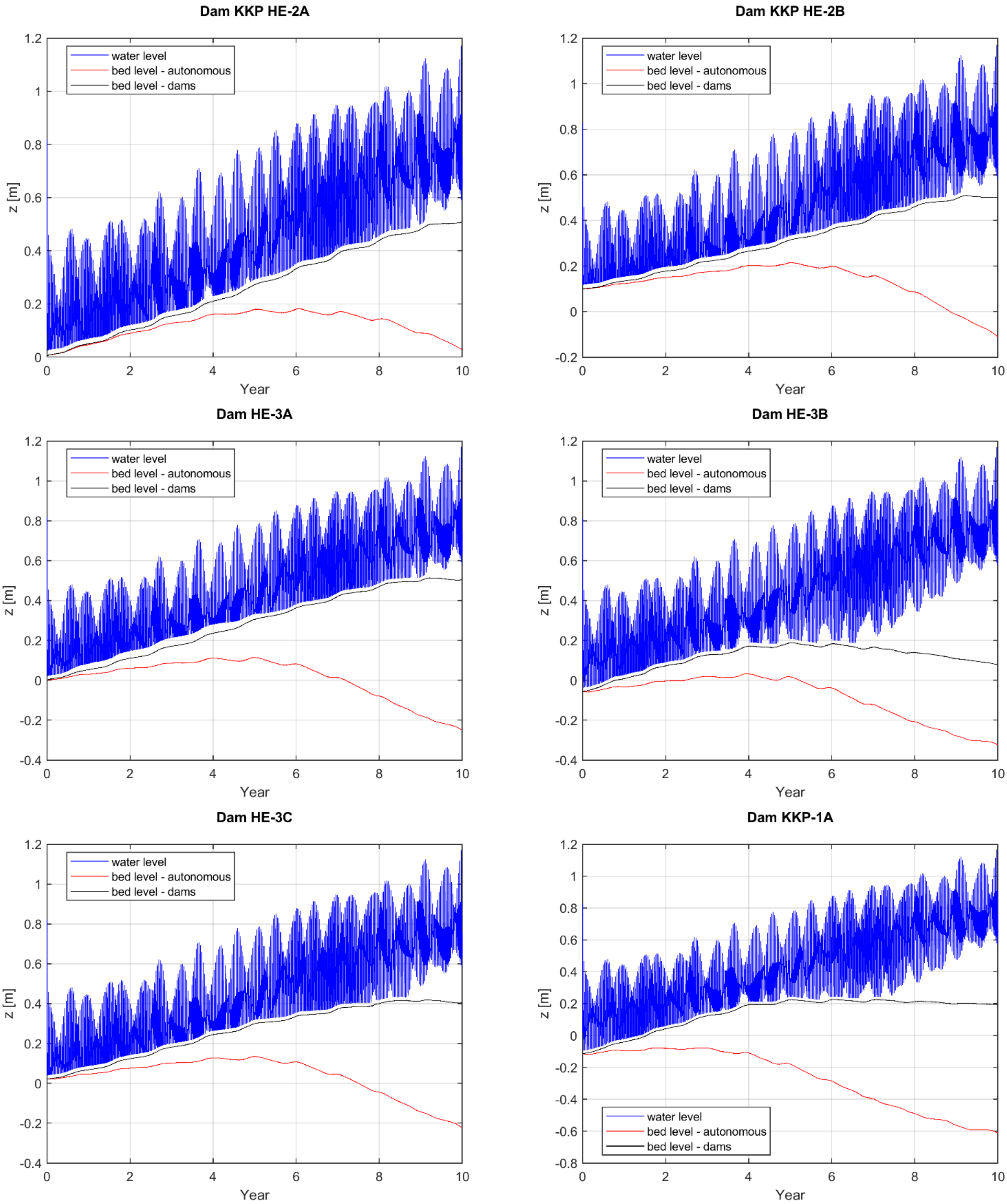

Figure E.8: Bed level development over time throughout the simulation for the best-case scenario at observation points behind the permeable structures. The blue line gives the tidal water level including relative sea level rise (on hydrodynamic timescale), the red line shows the bed level of the autonomous development and the black line shows the bed level with permeable structures. The subpanels show structures KKP HE-2A (top left), KKP HE-2B (top right), HE-3A (middle left), HE-3B (middle right), HE-3C (bottom left) and KKP-1A (bottom right).

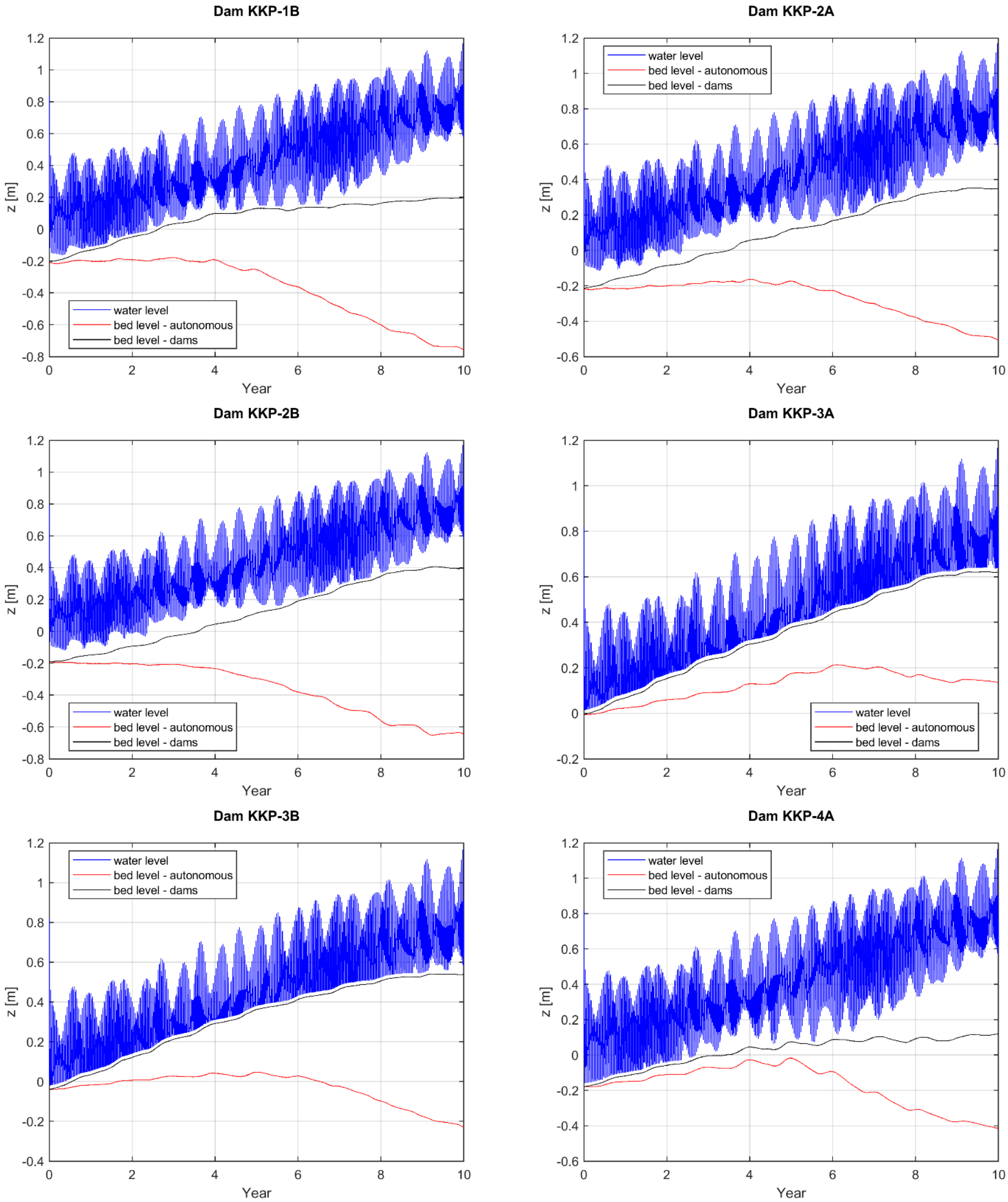

Figure E.9: Bed level development over time throughout the simulation for the best-case scenario at observation points behind the permeable structures. The blue line gives the tidal water level including relative sea level rise (on hydrodynamic timescale), the red line shows the bed level of the autonomous development and the black line shows the bed level with permeable structures. The subpanels show structures KKP-1B (top left), KKP-2A (top right), KKP-2B (middle left), KKP-3A (middle right), KKP-3B (bottom left) and KKP-4A (bottom right).

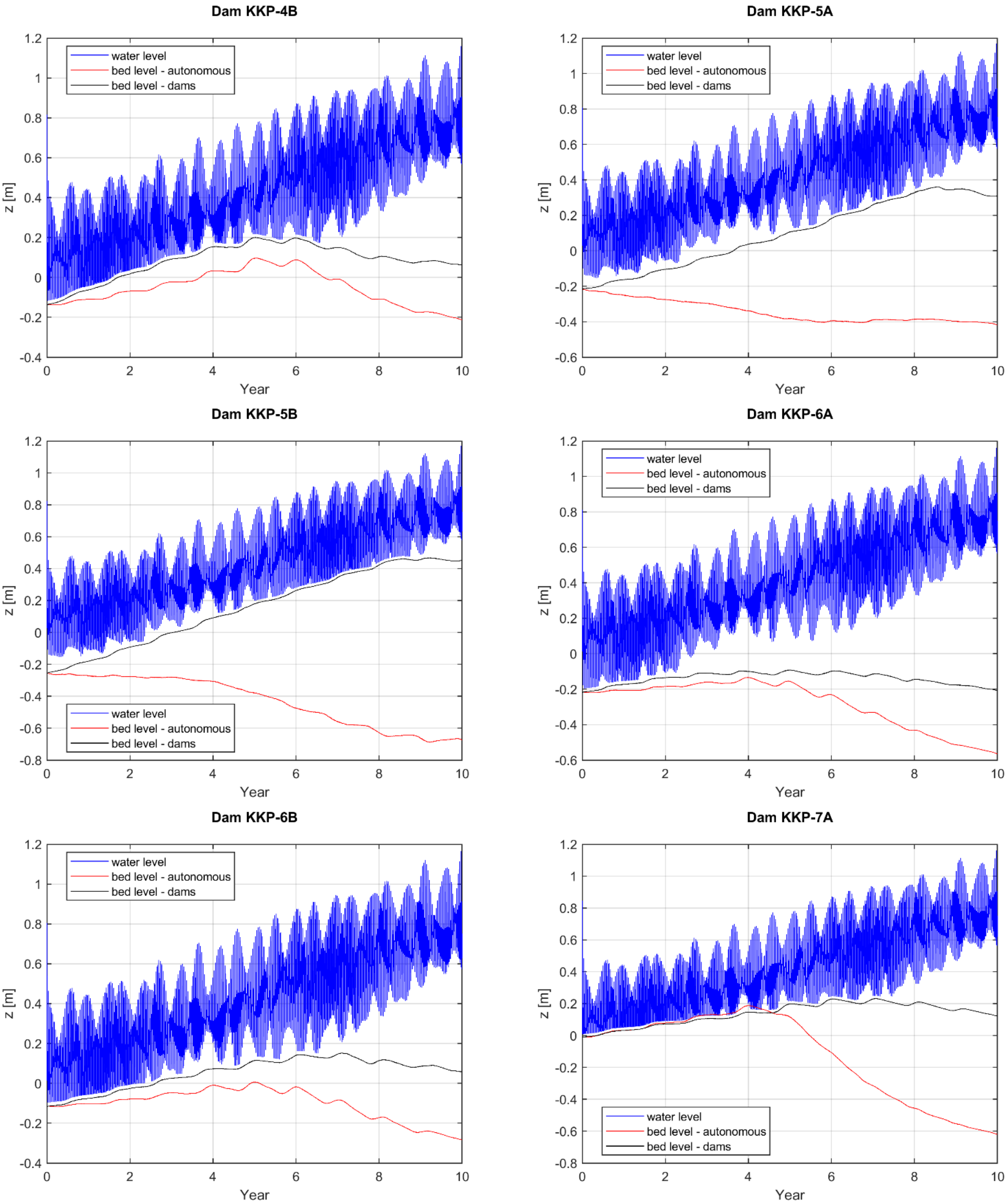

Figure E.10: Bed level development over time throughout the simulation for the best-case scenario at observation points behind the permeable structures. The blue line gives the tidal water level including relative sea level rise (on hydrodynamic timescale), the red line shows the bed level of the autonomous development and the black line shows the bed level with permeable structures. The subpanels show structures KKP-4B (top left), KKP-5A (top right), KKP-5B (middle left), KKP-6A (middle right), KKP-6B (bottom left) and KKP-7A (bottom right).

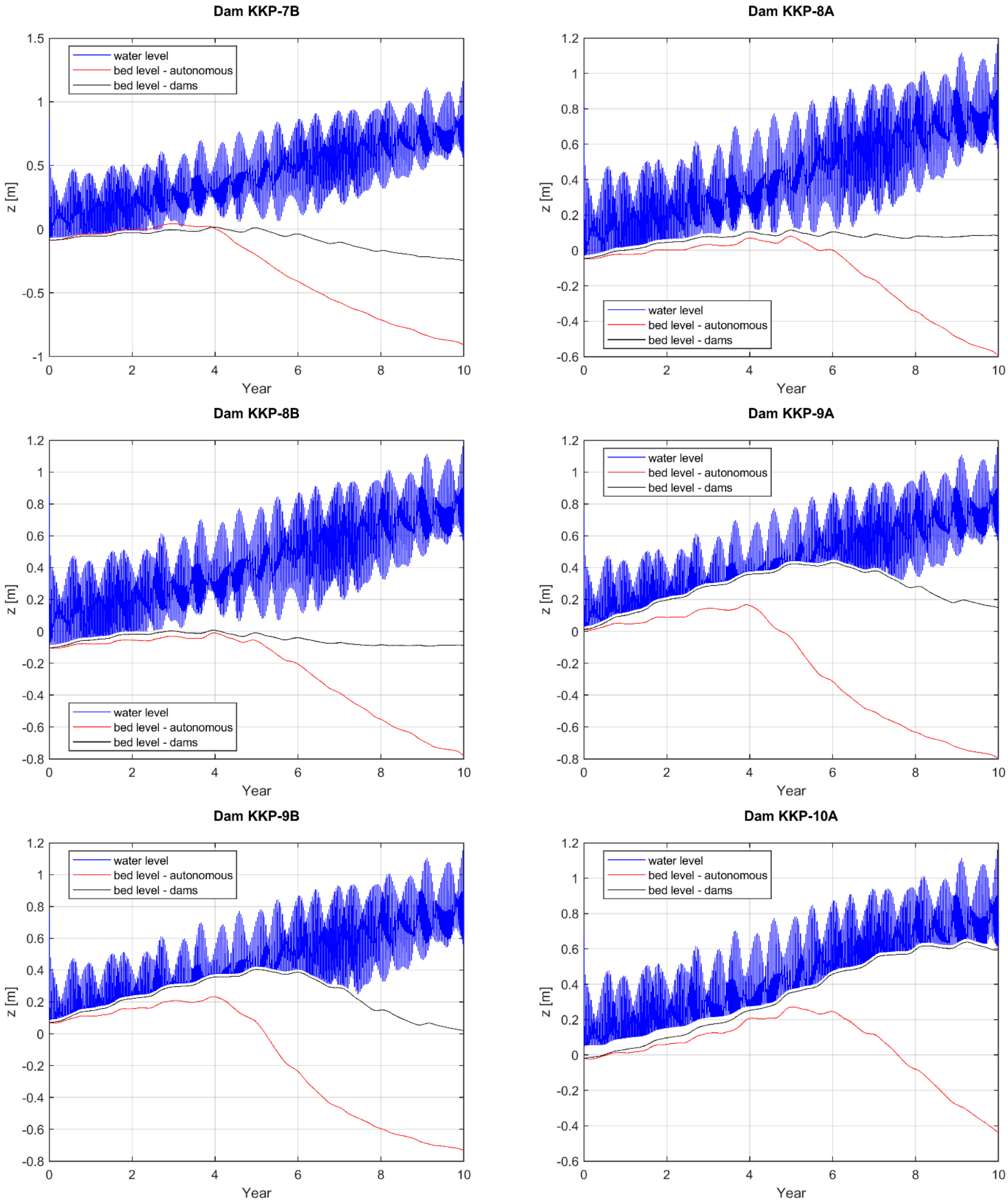

Figure E.11: Bed level development over time throughout the simulation for the best-case scenario at observation points behind the permeable structures. The blue line gives the tidal water level including relative sea level rise (on hydrodynamic timescale), the red line shows the bed level of the autonomous development and the black line shows the bed level with permeable structures. The subpanels show structures KKP-7B (top left), KKP-8A (top right), KKP-8B (middle left), KKP-9A (middle right), KKP-9B (bottom left) and KKP-10A (bottom right).

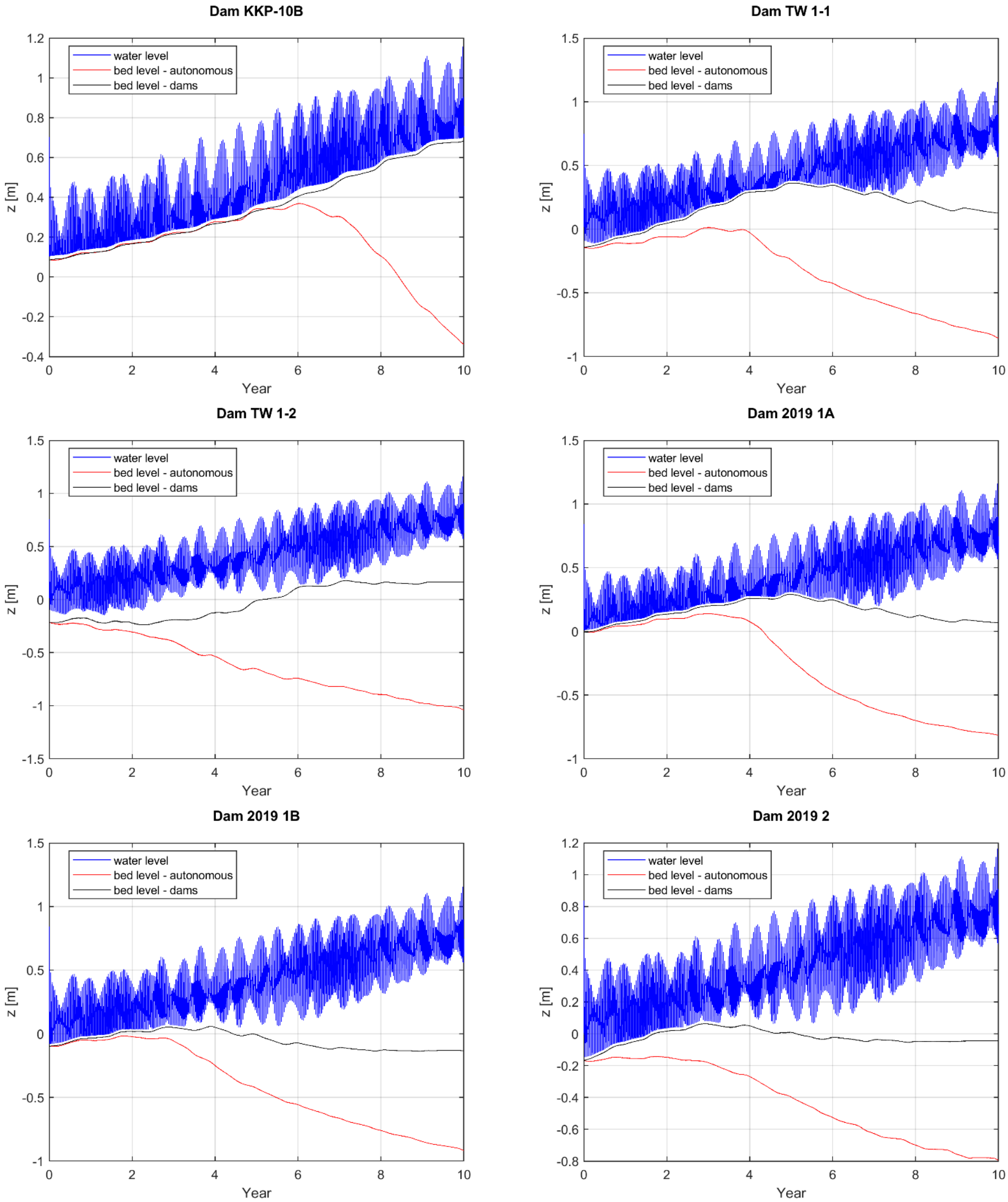

Figure E.12: Bed level development over time throughout the simulation for the best-case scenario at observation points behind the permeable structures. The blue line gives the tidal water level including relative sea level rise (on hydrodynamic timescale), the red line shows the bed level of the autonomous development and the black line shows the bed level with permeable structures. The subpanels show structures KKP-10B (top left), TW 1-1 (top right), TW 1-2 (middle left), 2019-1A (middle right), 2019-1B (bottom left) and 2019-2 (bottom right).

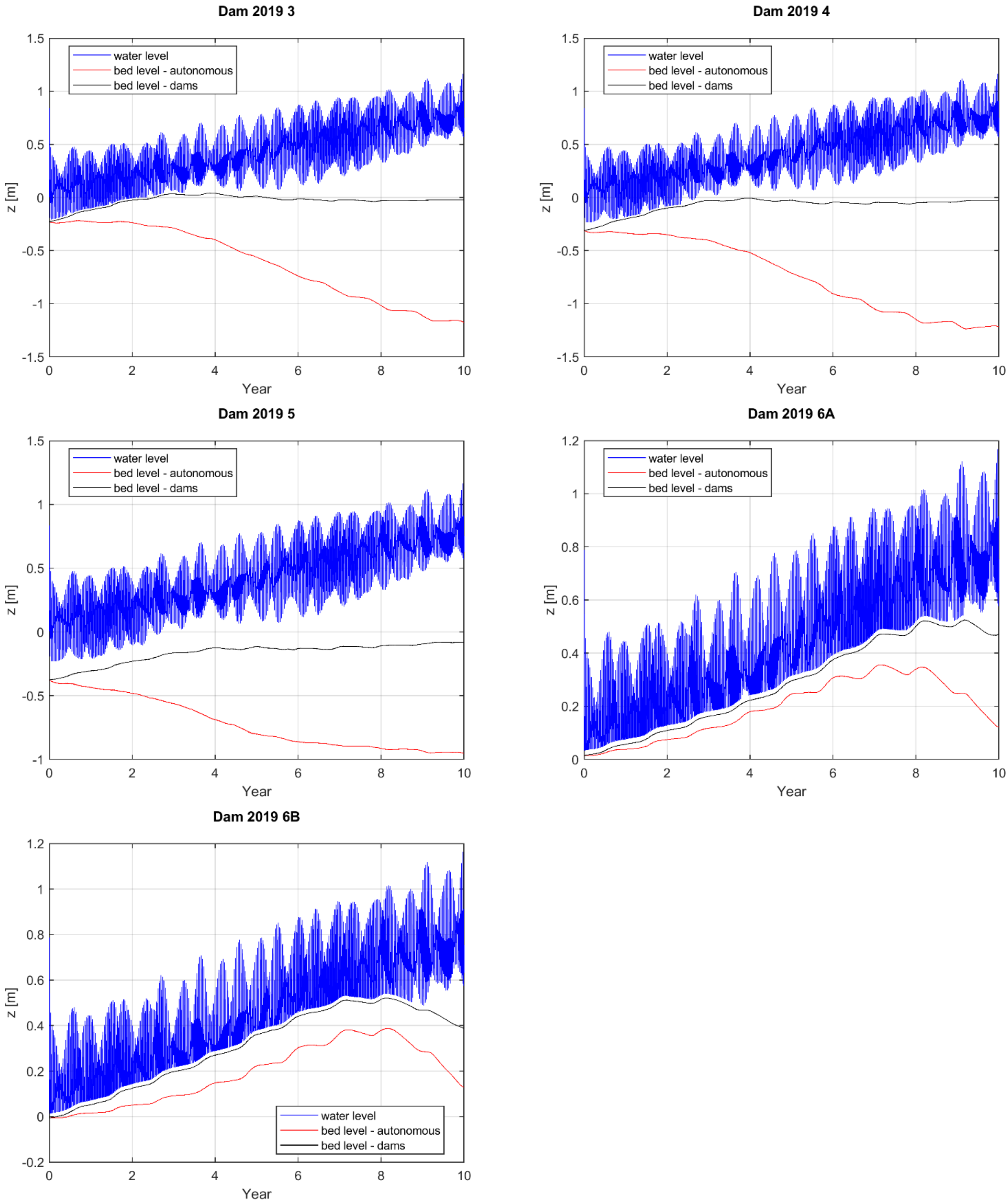

Figure E.13: Bed level development over time throughout the simulation for the best-case scenario at observation points behind the permeable structures. The blue line gives the tidal water level including relative sea level rise (on hydrodynamic timescale), the red line shows the bed level of the autonomous development and the black line shows the bed level with permeable structures. The subpanels show structures 2019-3 (top left), 2019-4 (top right), 2019-5 (middle left), 2019-6A (middle right) and 2019-6B (bottom left).

Table E.1: Total bed level change at the observation points behind the permeable structures at the end of the best-case scenario simulation.

Observation point	Autono-mous	Permeable structures	Difference	Observation point	Autono-mous	Permeable structures	Difference
1A	0,04	0,58	0,54	KKP-9A	-0,83	0,16	0,98
1B	0,29	0,53	0,24	KKP-9B	-0,82	-0,04	0,78
3A	-0,27	0,55	0,82	KKP-10A	-0,45	0,64	1,09
3B	-0,74	0,19	0,92	KKP-10B	-0,46	0,63	1,09
HE-1A	0,34	0,50	0,15	11-1	-0,17	0,43	0,60
HE-1B	0,22	0,57	0,34	11-2	-0,60	0,61	1,22
KKP HE-2A	0,02	0,51	0,50	11-3A	-0,79	-0,03	0,76
KKP HE-2B	-0,23	0,41	0,64	11-3B	-0,61	-0,25	0,36
HE-3A	-0,27	0,52	0,79	HE 11-4	-0,47	0,43	0,90
HE-3B	-0,28	0,13	0,41	HE 11-5	-0,59	0,43	1,02
HE-3C	-0,26	0,39	0,66	HE 11-6	-0,62	0,25	0,87
KKP-1A	-0,53	0,31	0,84	HE 12-1	-0,77	0,21	0,98
KKP-1B	-0,60	0,41	1,01	HE 12-2	-0,78	0,61	1,38
KKP-2A	-0,33	0,59	0,92	HE 12-3	-0,78	0,28	1,06
KKP-2B	-0,50	0,61	1,11	HE 12-4	-0,46	0,45	0,91
KKP-3A	0,16	0,64	0,47	HE 12-5	-0,31	0,54	0,85
KKP-3B	-0,21	0,59	0,80	TW 1-2	-0,85	0,40	1,25
KKP-4A	-0,23	0,34	0,57	TW 1-1	-0,73	0,29	1,02
KKP-4B	-0,07	0,22	0,29	2019 1A	-0,82	0,10	0,92
KKP-5A	-0,20	0,55	0,75	2019 1B	-0,84	-0,03	0,81
KKP-5B	-0,45	0,74	1,19	2019 2	-0,65	0,12	0,77
KKP-6A	-0,35	0,01	0,36	2019 3	-1,01	0,21	1,22
KKP-6B	-0,16	0,19	0,35	2019 4	-0,96	0,30	1,25
KKP-7A	-0,62	0,14	0,77	2019 5	-0,59	0,32	0,90
KKP-7B	-0,85	-0,17	0,68	2019 6A	0,09	0,50	0,40
KKP-8A	-0,58	0,14	0,72	2019 6B	0,11	0,38	0,28
KKP-8B	-0,72	0,02	0,74	**average**	**-0,44**	**0,34**	**0,78**

E.2 Intermediate scenario

This section shows the results of simulations for the intermediate scenario with a total relative sea level rise of 1.05 m after 10 years. The following figures are included:

- Wave field (wave height and direction) and influence of sea level rise
- Bed level change (sedimentation & erosion)
- Bed level change (colour scale for relative Sea Level Rise) at the scale of the intertidal zone
- Bed level change (colour scale for relative Sea Level Rise) at the scale of the entire project area
- Difference plot of the final bed level between simulations with and without permeable structures
- Sediment concentration statistics
- Timeseries of bed level at the locations of permeable structures

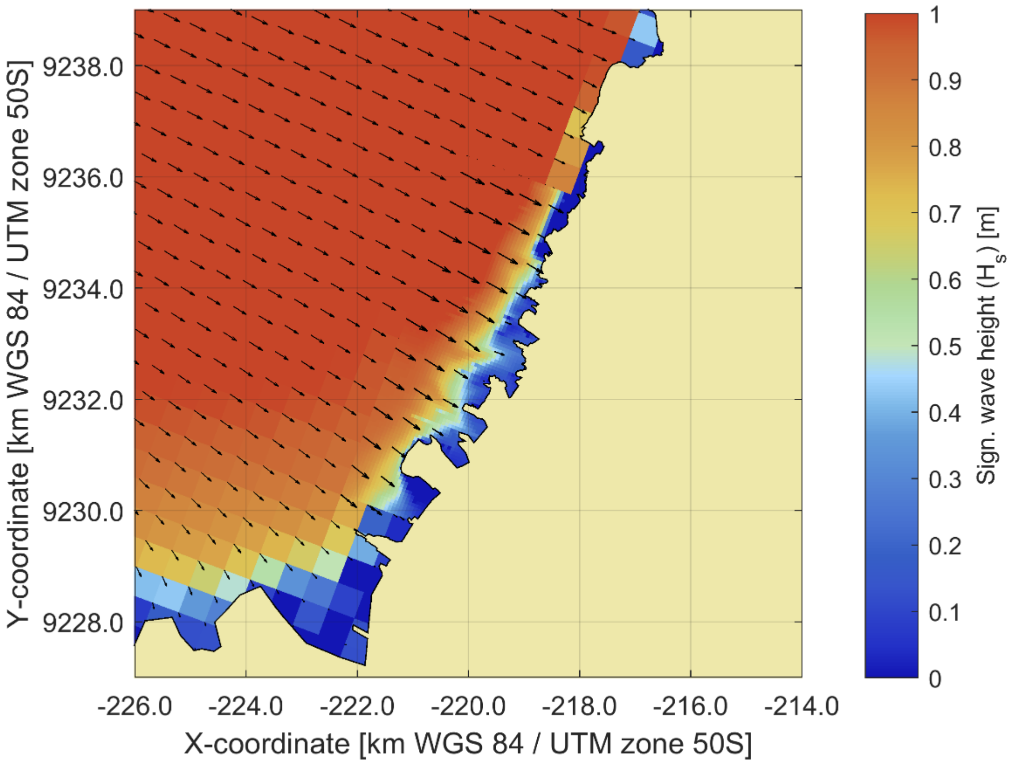

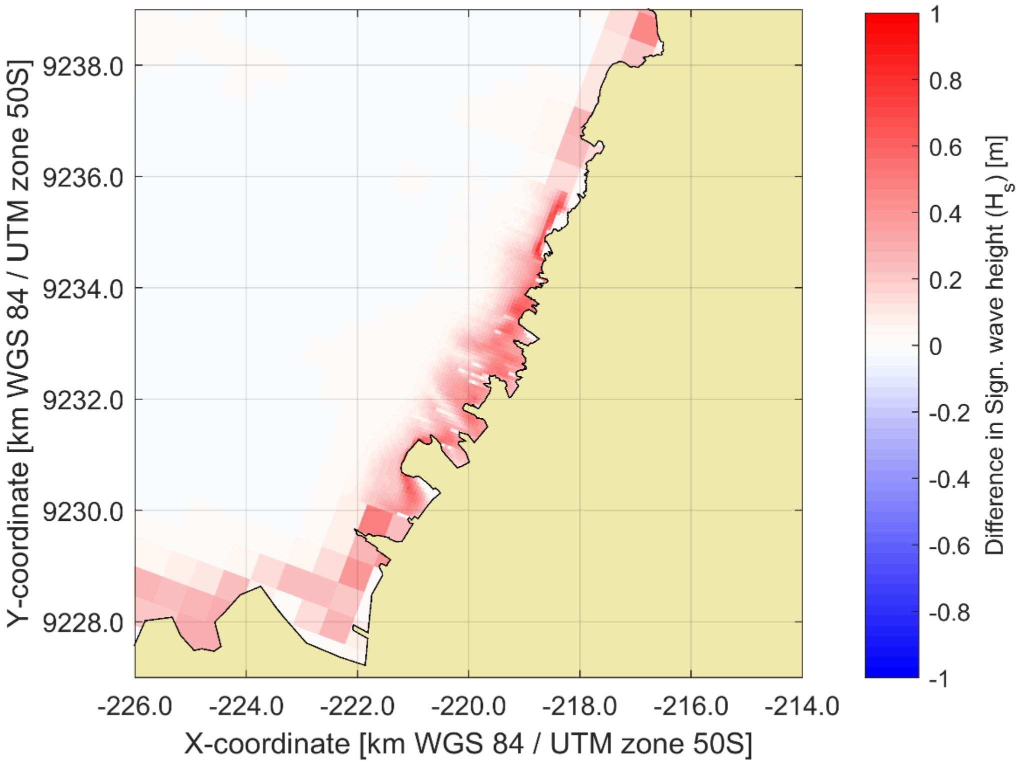

Figure E.14: Significant wave height during the peak of the monsoon for the intermediate scenario (upper panel) and differences in significant wave height between the start and the end of the simulation (lower panel)

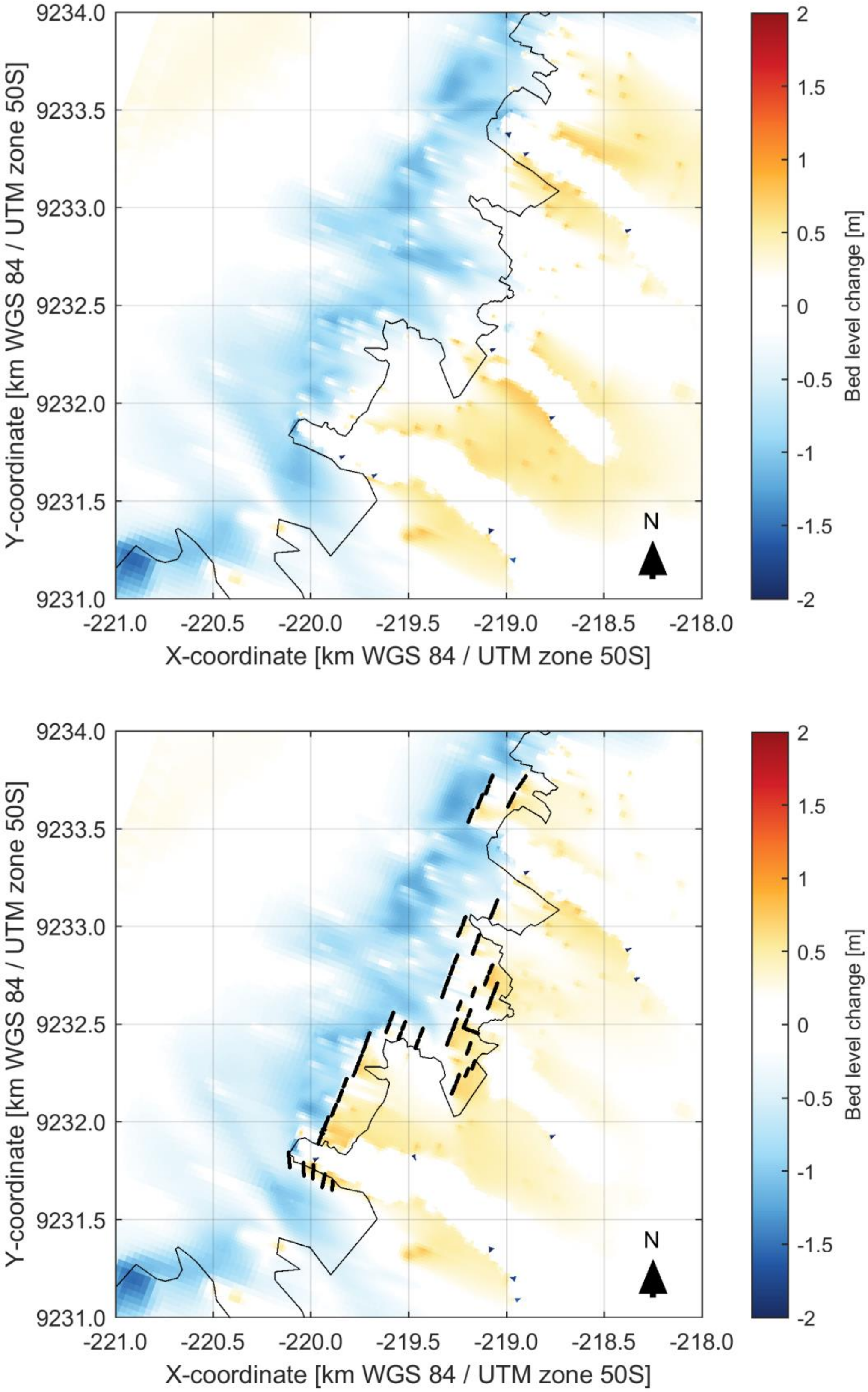

Figure E.15: Total bed level change after 10 years for the intermediate scenario simulations. The upper panel shows the autonomous development and the lower panel shows the results of a simulation with permeable structures. Red colours indicate sedimentation areas and blue colours indicate erosion areas.

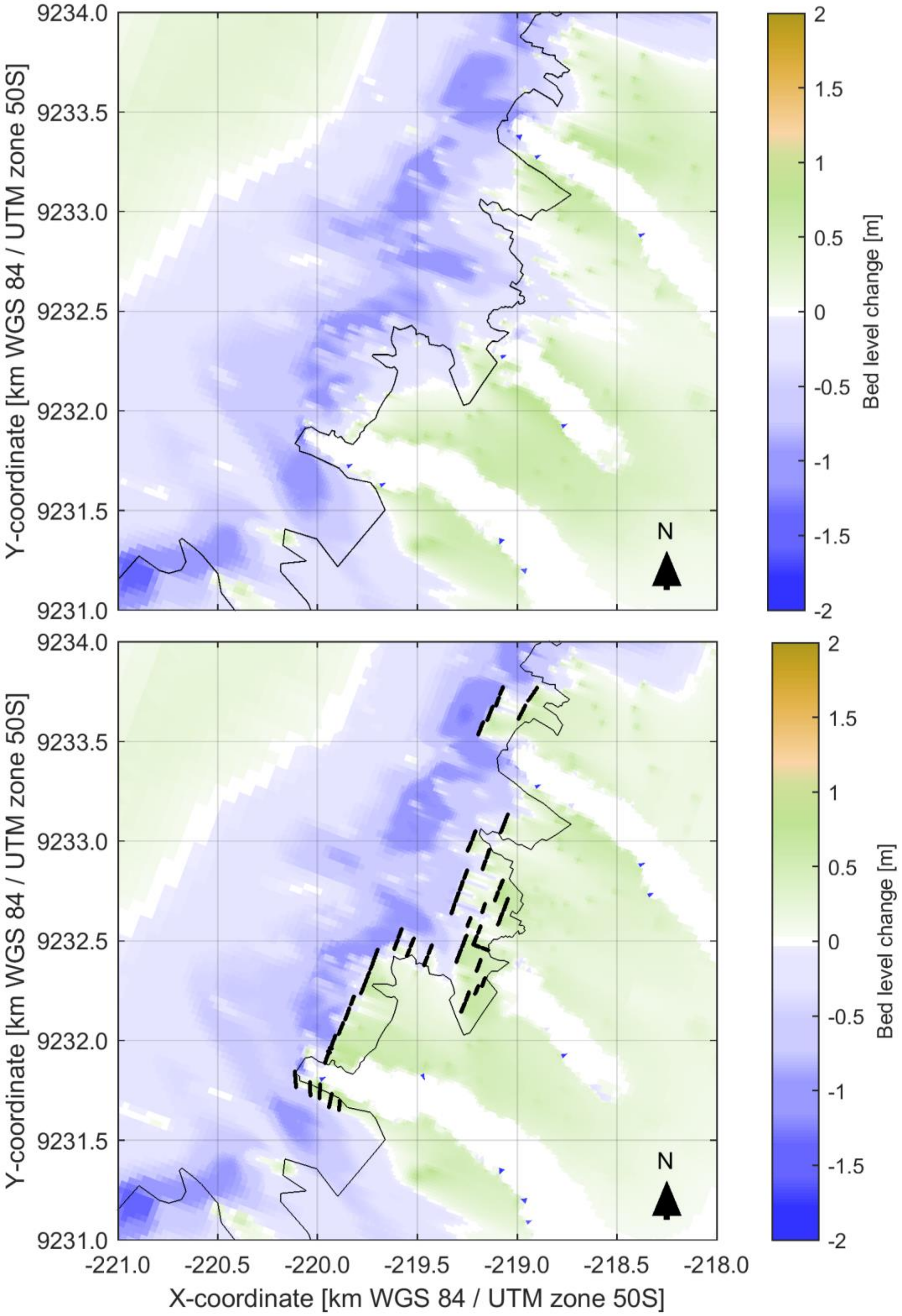

Figure E.16: Total bed level change after 10 years for the intermediate scenario simulations (upper panel autonomous development; lower panel with permeable structures). Blue colours indicate erosive areas, green colours indicate partially drowning areas and brown colours indicate sedimentation rates that exceed the rate of relative sea level rise.

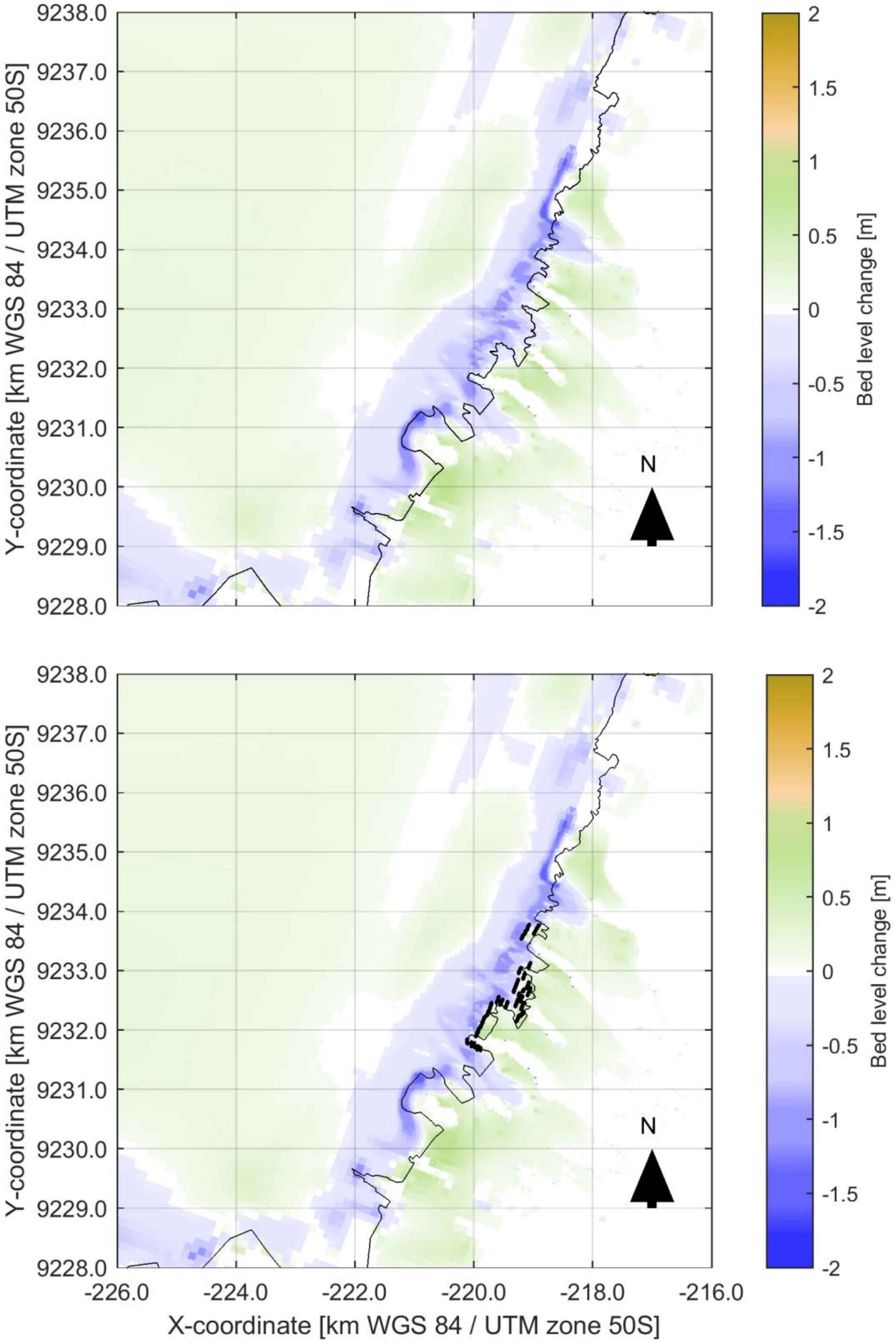

Figure E.17: Total bed level change after 10 years at the scale of the entire project area for the intermediate scenario simulations (upper panel autonomous development; lower panel with permeable structures). Blue colours indicate erosive areas, green colours indicate sedimentation areas where the sedimentation rate is smaller than the rate of relative sea level rise and brown colours indicate sedimentation rates that exceed the rate of relative sea level rise.

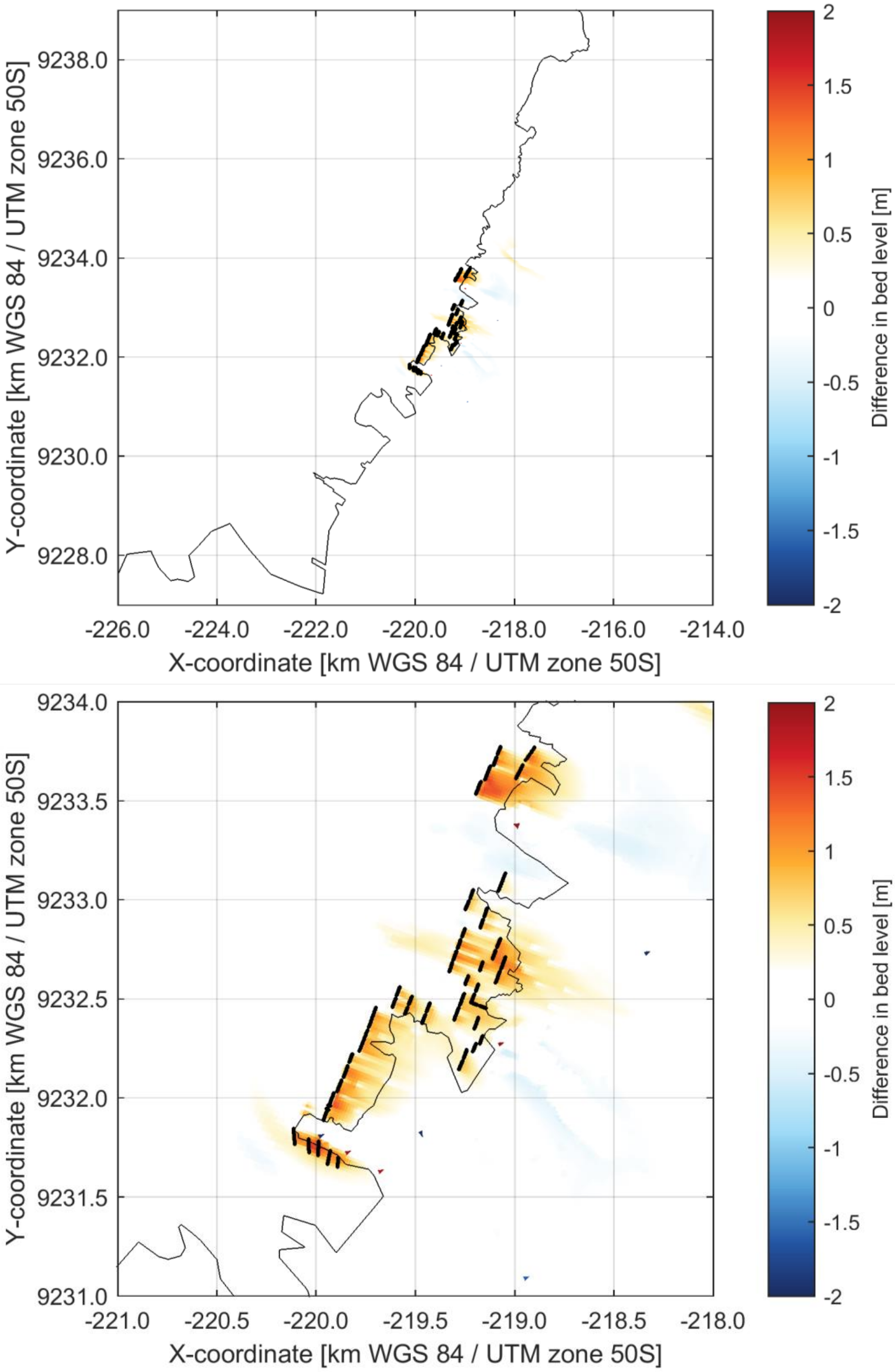

Figure E.18: Difference plot between final bed level with permeable structures and the autonomous development for the intermediate scenario simulations (upper panel shows the extent of the project area; lower panel a zoom around the area of permeable structures). Red colours indicate higher bed levels in the simulation with permeable structures, whereas blue colours indicate lower bed levels in the simulation with permeable structures.

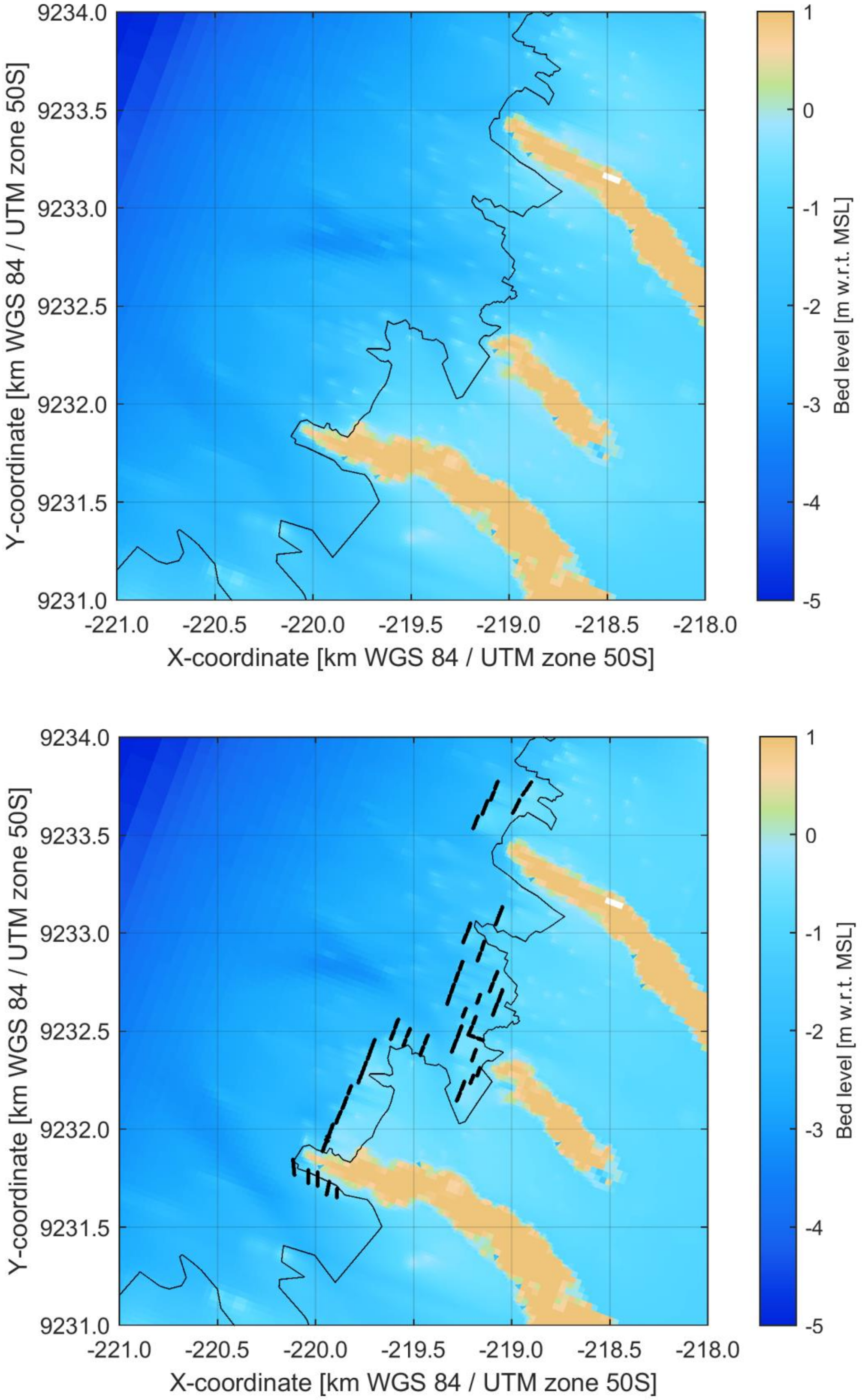

Figure E.19: Final bed level relative to the new mean sea level (including sea level rise) after 10 years for the intermediate scenario simulations. The upper panel shows the autonomous development and the lower panel shows the final bed level when permeable structures are applied. The old coastline is included for reference.

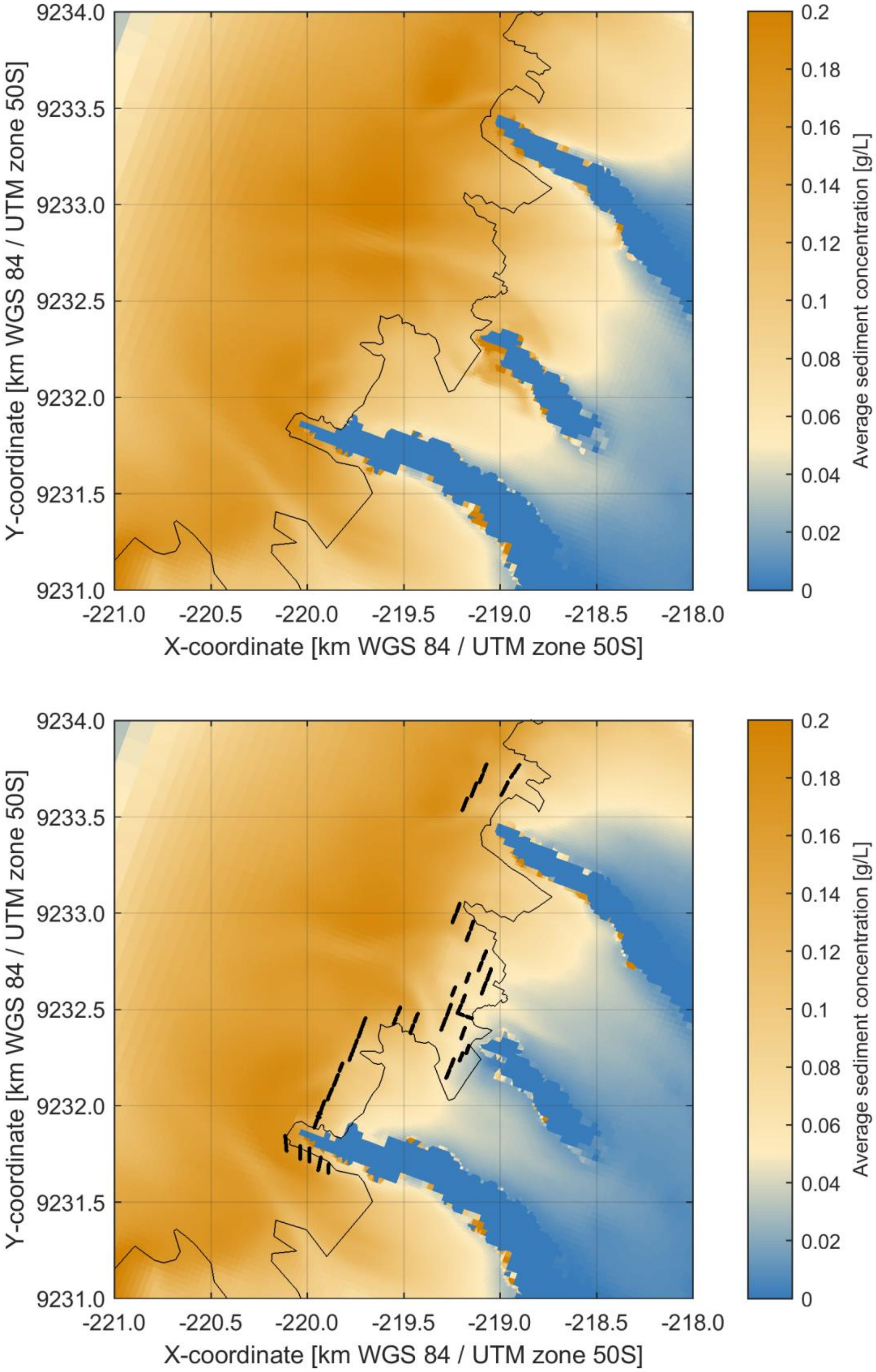

Figure E.20: Sediment concentration averaged over 10 years for the intermediate scenario simulations (upper panel autonomous development; lower panel with permeable structures).

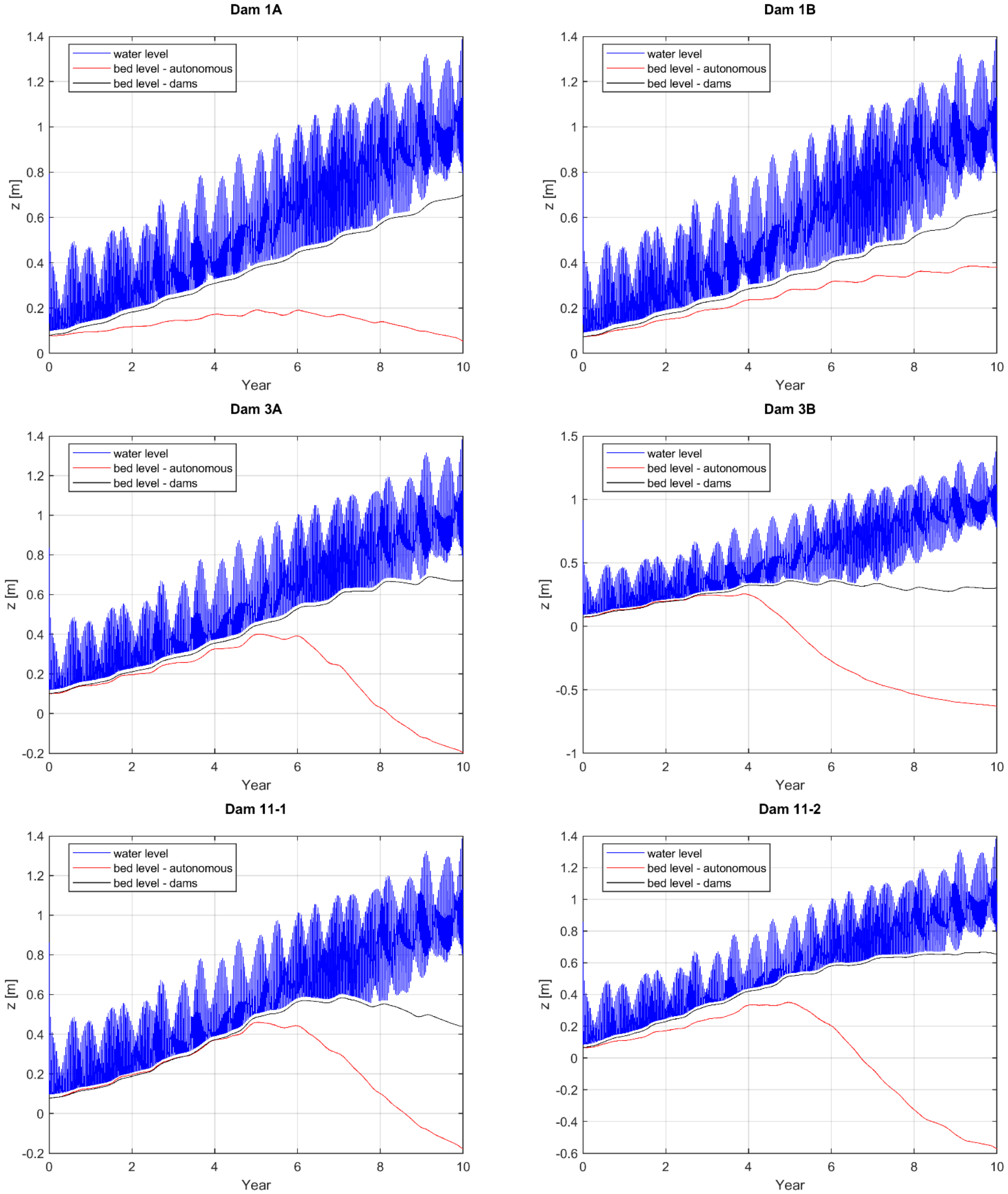

Figure E.21: Bed level development over time throughout the simulation for the intermediate scenario at observation points behind the permeable structures. The blue line gives the tidal water level including relative sea level rise (on hydrodynamic timescale), the red line shows the bed level of the autonomous development and the black line shows the bed level with permeable structures. The subpanels show structures 1A (top left), 1B (top right), 3A (middle left), 3B (middle right), 11-1 (bottom left) and 11-2 (bottom right).

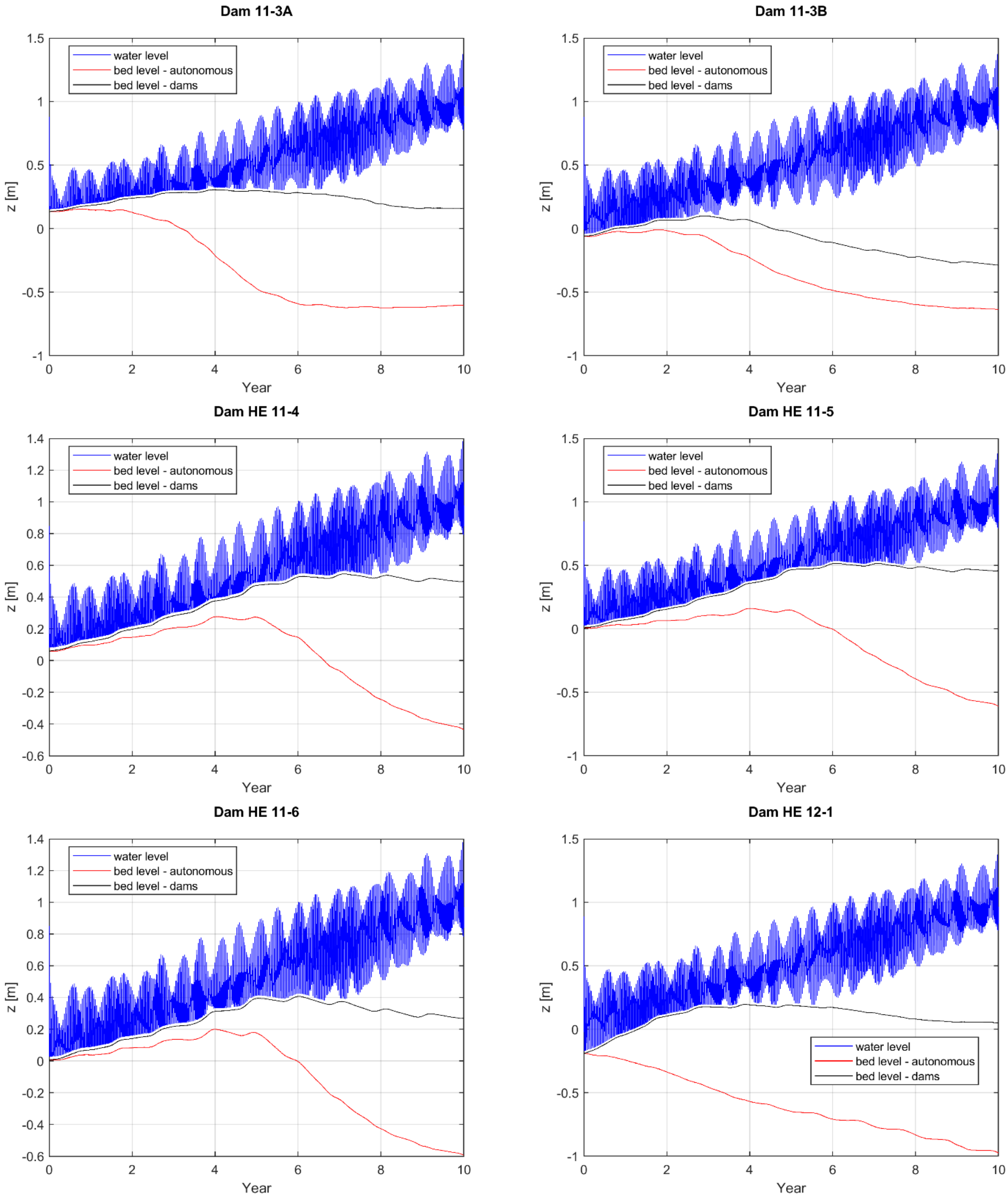

Figure E.22: Bed level development over time throughout the simulation for the intermediate scenario at observation points behind the permeable structures. The blue line gives the tidal water level including relative sea level rise (on hydrodynamic timescale), the red line shows the bed level of the autonomous development and the black line shows the bed level with permeable structures. The subpanels show structures 11-3A (top left), 11-3B (top right), 11-4 (middle left), 11-5 (middle right), 11-6 (bottom left) and 12-1 (bottom right).

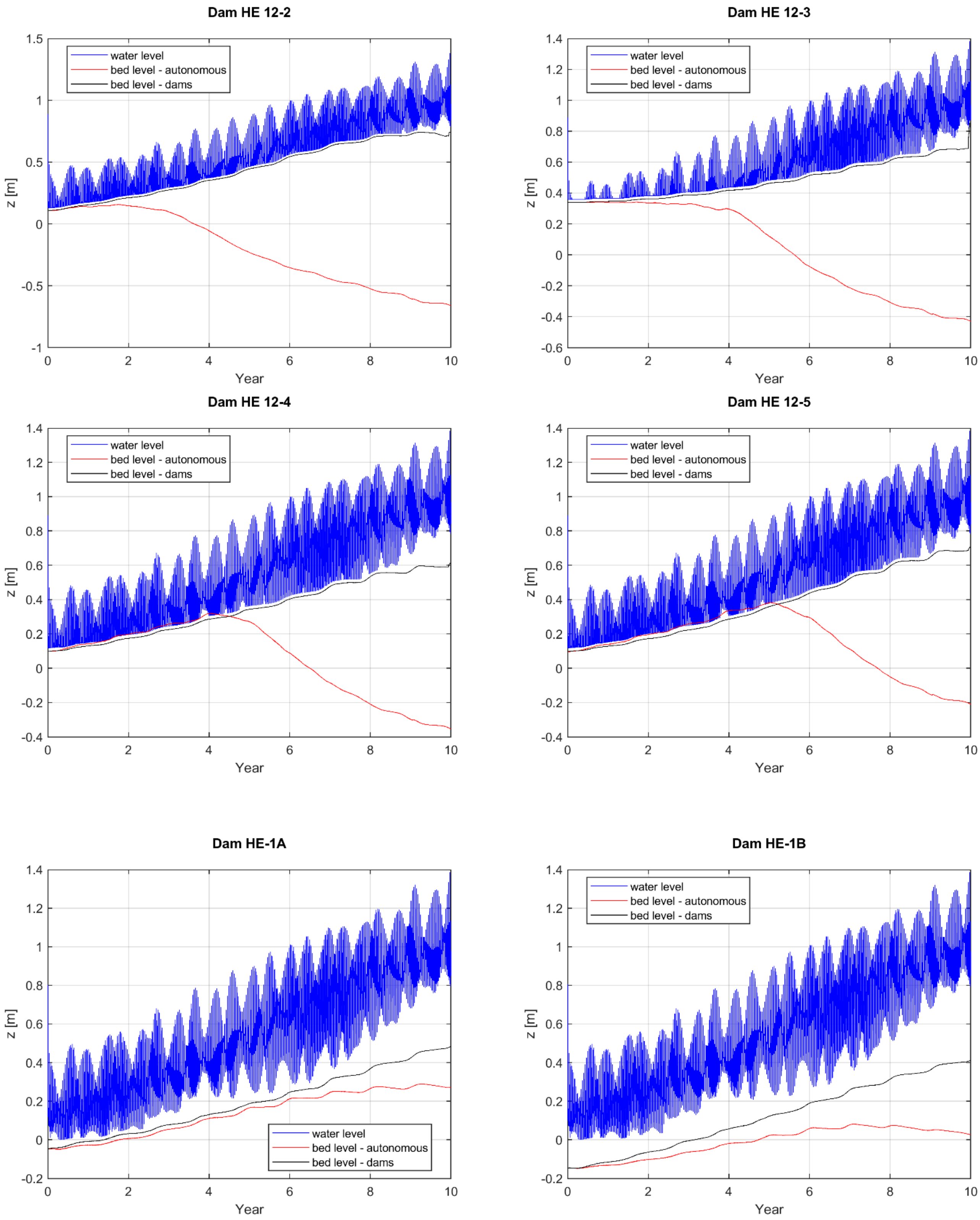

Figure E.23: Bed level development over time throughout the simulation for the intermediate scenario at observation points behind the permeable structures. The blue line gives the tidal water level including relative sea level rise (on hydrodynamic timescale), the red line shows the bed level of the autonomous development and the black line shows the bed level with permeable structures. The subpanels show structures 12-2 (top left), 12-3 (top right), 12-4 (middle left), 12-5 (middle right), HE-1A (bottom left) and HE-1B (bottom right).

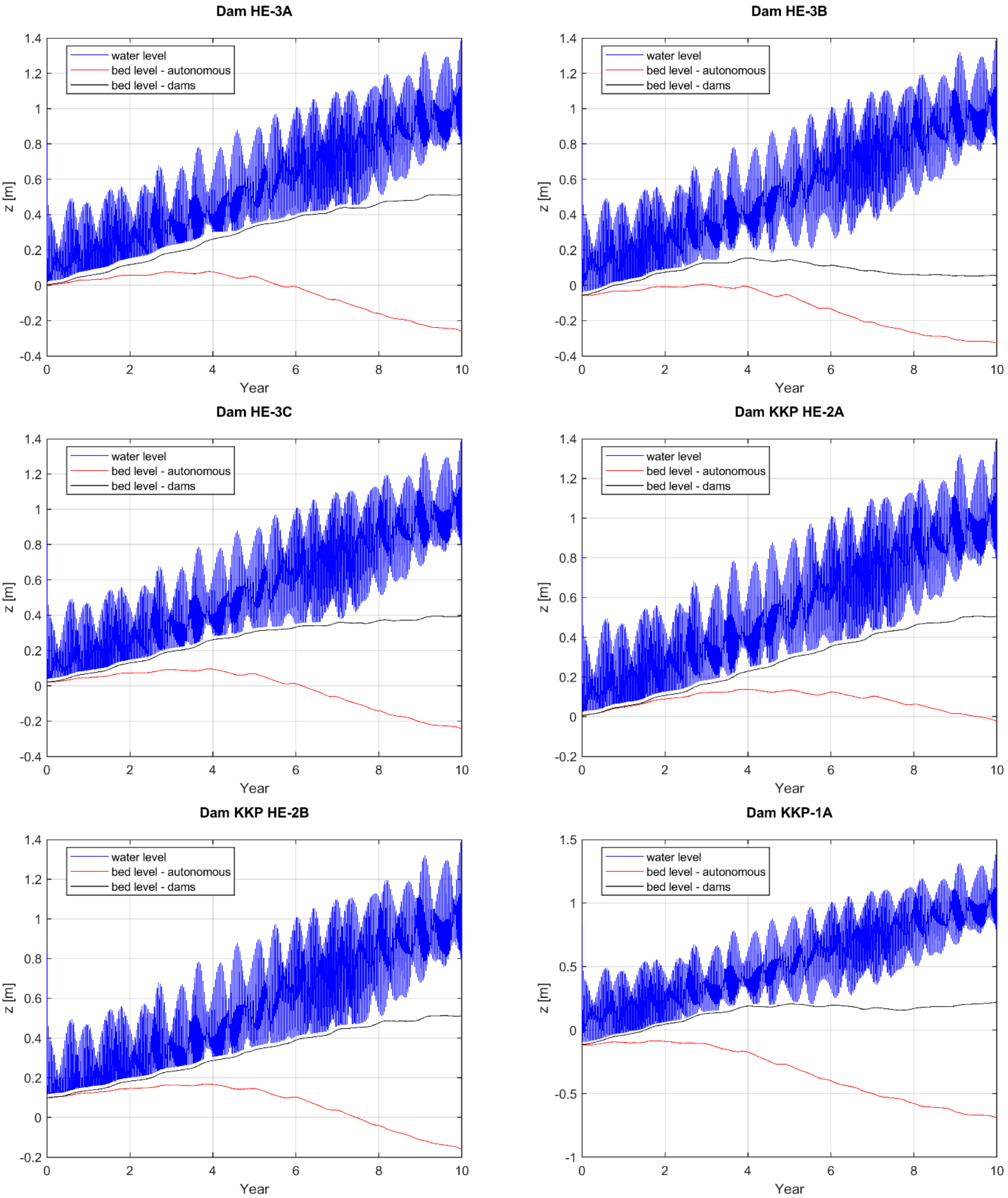

Figure E.24: Bed level development over time throughout the simulation for the intermediate scenario at observation points behind the permeable structures. The blue line gives the tidal water level including relative sea level rise (on hydrodynamic timescale), the red line shows the bed level of the autonomous development and the black line shows the bed level with permeable structures. The subpanels show structures KKP HE-2A (top left), KKP HE-2B (top right), HE-3A (middle left), HE-3B (middle right), HE-3C (bottom left) and KKP-1A (bottom right).

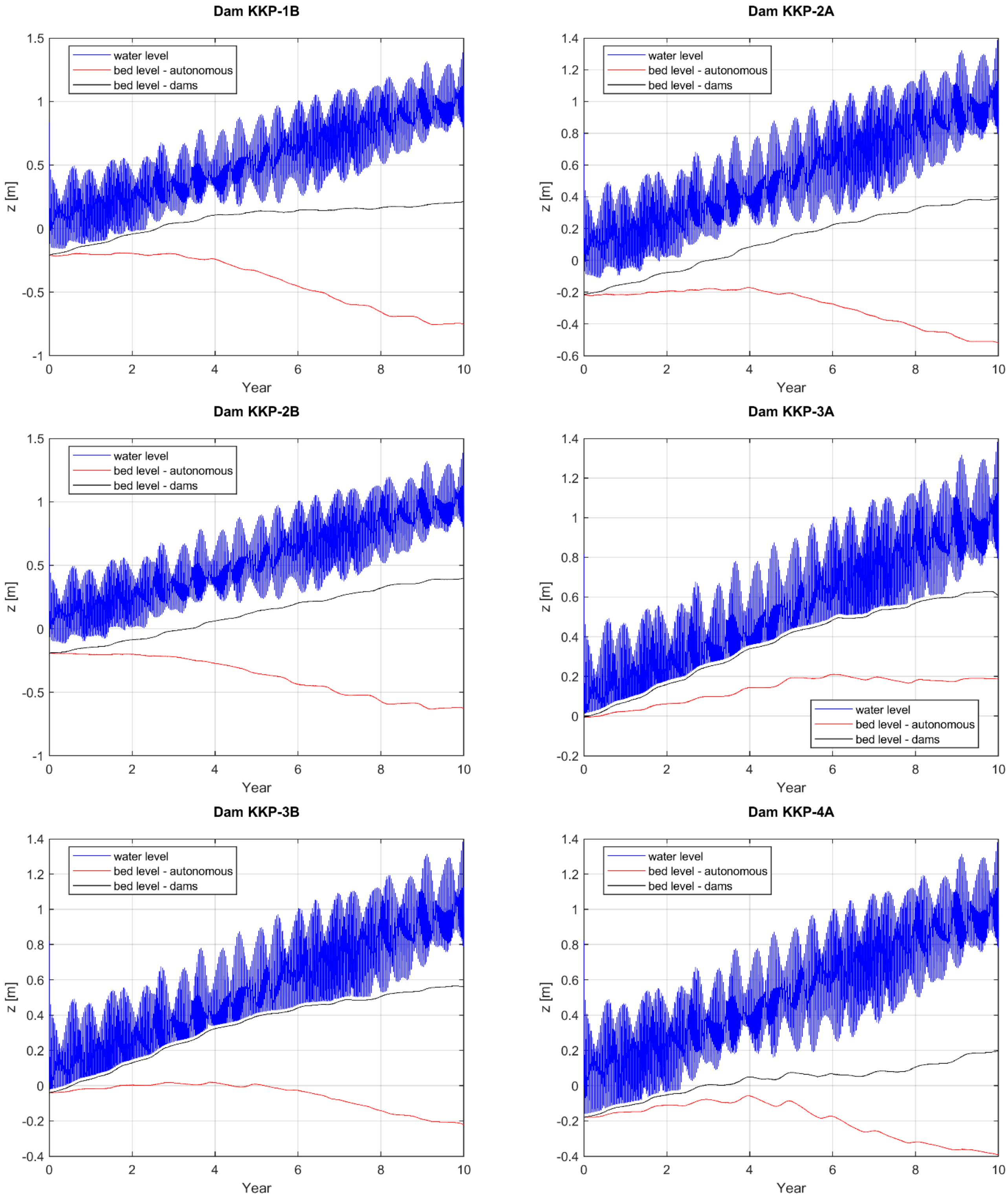

Figure E.25: Bed level development over time throughout the simulation for the intermediate scenario at observation points behind the permeable structures. The blue line gives the tidal water level including relative sea level rise (on hydrodynamic timescale), the red line shows the bed level of the autonomous development and the black line shows the bed level with permeable structures. The subpanels show structures KKP-1B (top left), KKP-2A (top right), KKP-2B (middle left), KKP-3A (middle right), KKP-3B (bottom left) and KKP-4A (bottom right).

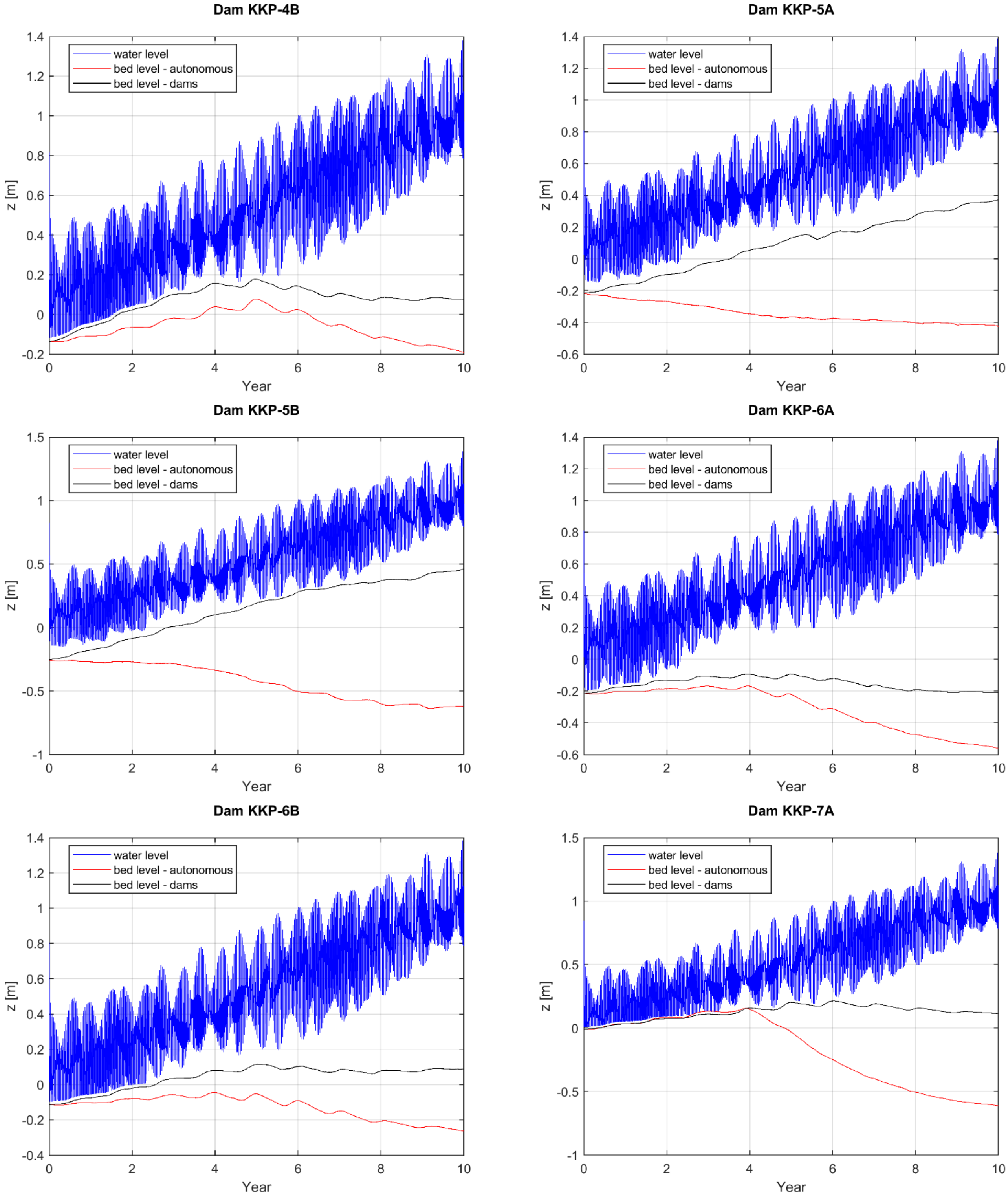

Figure E.26: Bed level development over time throughout the simulation for the intermediate scenario at observation points behind the permeable structures. The blue line gives the tidal water level including relative sea level rise (on hydrodynamic timescale), the red line shows the bed level of the autonomous development and the black line shows the bed level with permeable structures. The subpanels show structures KKP-4B (top left), KKP-5A (top right), KKP-5B (middle left), KKP-6A (middle right), KKP-6B (bottom left) and KKP-7A (bottom right).

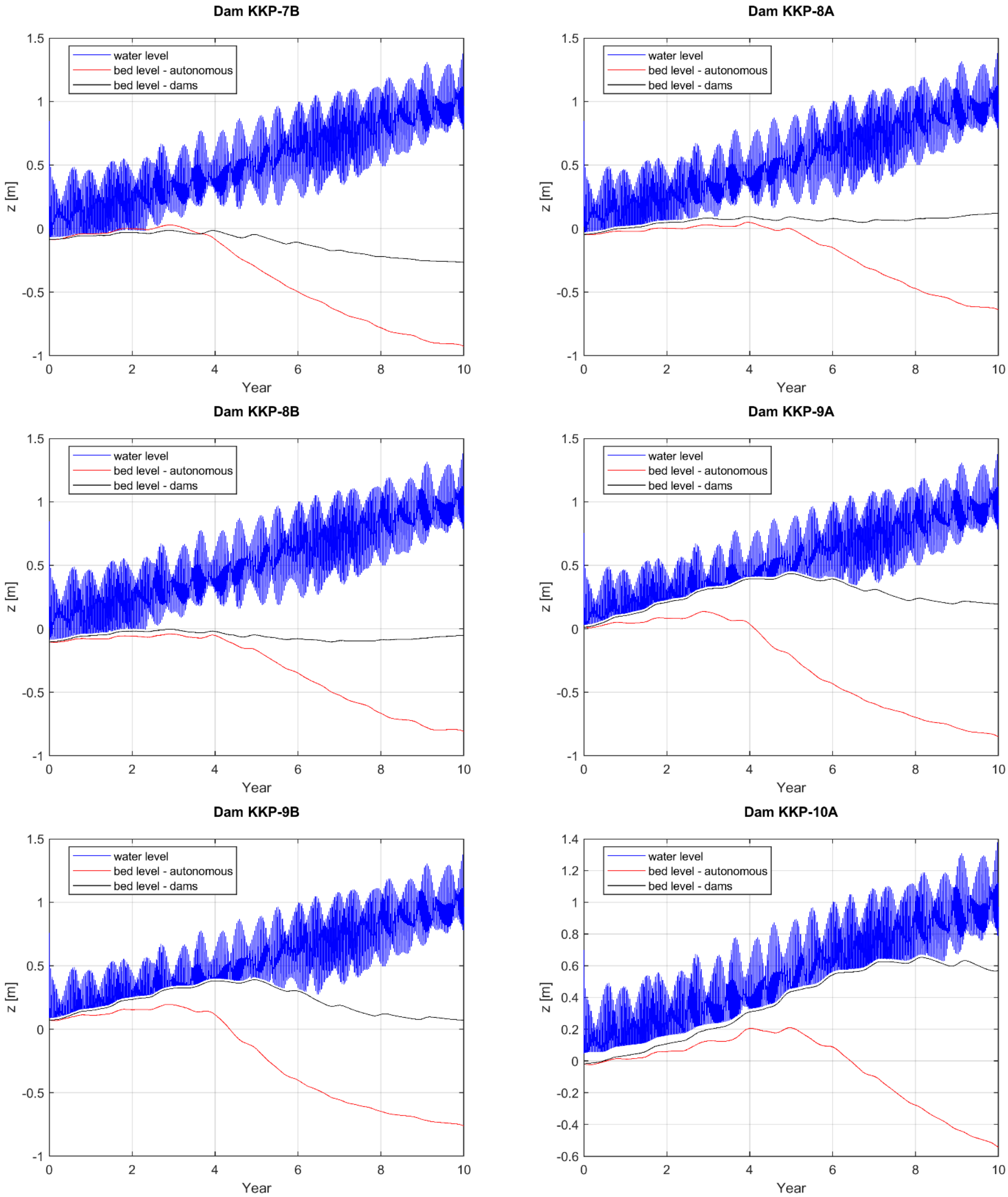

Figure E.27: Bed level development over time throughout the simulation for the intermediate scenario at observation points behind the permeable structures. The blue line gives the tidal water level including relative sea level rise (on hydrodynamic timescale), the red line shows the bed level of the autonomous development and the black line shows the bed level with permeable structures. The subpanels show structures KKP-7B (top left), KKP-8A (top right), KKP-8B (middle left), KKP-9A (middle right), KKP-9B (bottom left) and KKP-10A (bottom right).

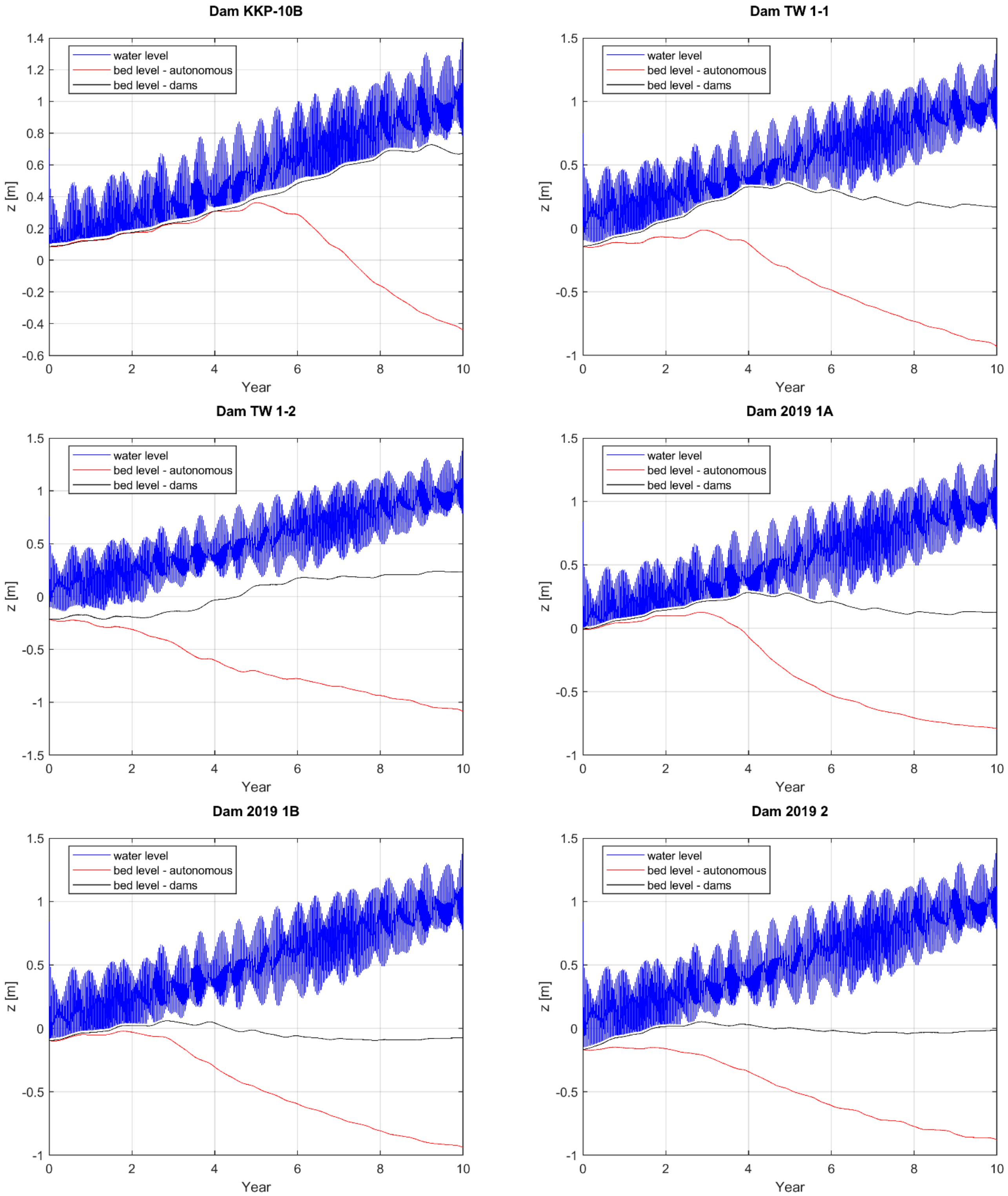

Figure E.28: Bed level development over time throughout the simulation for the intermediate scenario at observation points behind the permeable structures. The blue line gives the tidal water level including relative sea level rise (on hydrodynamic timescale), the red line shows the bed level of the autonomous development and the black line shows the bed level with permeable structures. The subpanels show structures KKP-10B (top left), TW 1-1 (top right), TW 1-2 (middle left), 2019-1A (middle right), 2019-1B (bottom left) and 2019-2 (bottom right).

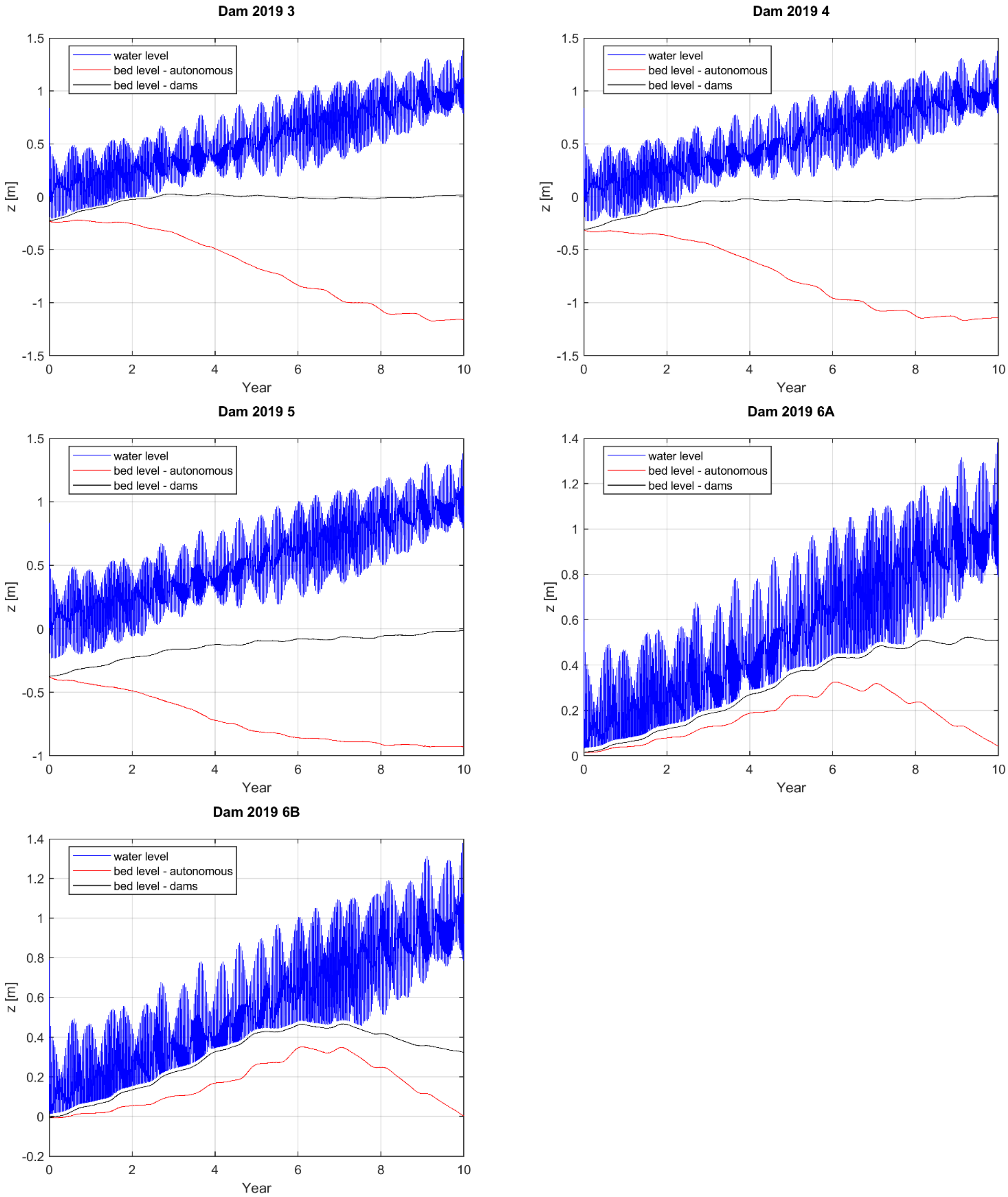

Figure E.29: Bed level development over time throughout the simulation for the intermediate scenario at observation points behind the permeable structures. The blue line gives the tidal water level including relative sea level rise (on hydrodynamic timescale), the red line shows the bed level of the autonomous development and the black line shows the bed level with permeable structures. The subpanels show structures 2019-3 (top left), 2019-4 (top right), 2019-5 (middle left), 2019-6A (middle right) and 2019-6B (bottom left).

Table E.2: Total bed level change at the observation points behind the permeable structures at the end of the intermediate scenario simulation

Observation point	Autono-mous	Permeable structures	Difference	Observation point	Autono-mous	Permeable structures	Difference
1A	-0,02	0,67	0,69	KKP-9A	-0,90	0,20	1,10
1B	0,39	0,61	0,22	KKP-9B	-0,85	0,02	0,88
3A	-0,31	0,61	0,92	KKP-10A	-0,56	0,63	1,19
3B	-0,70	0,26	0,97	KKP-10B	-0,56	0,64	1,20
HE-1A	0,39	0,58	0,19	11-1	-0,29	0,37	0,66
HE-1B	0,24	0,60	0,36	11-2	-0,68	0,58	1,26
KKP HE-2A	-0,02	0,54	0,56	11-3A	-0,73	0,04	0,77
KKP HE-2B	-0,27	0,45	0,72	11-3B	-0,57	-0,22	0,36
HE-3A	-0,28	0,54	0,82	HE 11-4	-0,52	0,46	0,98
HE-3B	-0,28	0,12	0,40	HE 11-5	-0,66	0,47	1,13
HE-3C	-0,28	0,40	0,68	HE 11-6	-0,62	0,29	0,91
KKP-1A	-0,61	0,36	0,96	HE 12-1	-0,85	0,25	1,09
KKP-1B	-0,57	0,44	1,01	HE 12-2	-0,83	0,65	1,47
KKP-2A	-0,32	0,63	0,95	HE 12-3	-0,81	0,53	1,34
KKP-2B	-0,47	0,61	1,08	HE 12-4	-0,50	0,54	1,04
KKP-3A	0,21	0,65	0,44	HE 12-5	-0,35	0,65	0,99
KKP-3B	-0,19	0,63	0,83	TW 1-2	-0,92	0,47	1,39
KKP-4A	-0,21	0,41	0,62	TW 1-1	-0,84	0,34	1,17
KKP-4B	-0,05	0,23	0,28	2019 1A	-0,79	0,16	0,95
KKP-5A	-0,23	0,62	0,85	2019 1B	-0,85	0,04	0,89
KKP-5B	-0,39	0,76	1,15	2019 2	-0,74	0,16	0,90
KKP-6A	-0,35	0,01	0,36	2019 3	-0,97	0,26	1,23
KKP-6B	-0,14	0,21	0,35	2019 4	-0,86	0,34	1,20
KKP-7A	-0,60	0,14	0,74	2019 5	-0,57	0,39	0,96
KKP-7B	-0,86	-0,18	0,68	2019 6A	0,02	0,51	0,50
KKP-8A	-0,62	0,19	0,81	2019 6B	-0,01	0,32	0,33
KKP-8B	-0,74	0,08	0,81	**average**	**-0,45**	**0,38**	**0,84**

E.3 Worst-case scenario

This section shows the results of simulations for the worst-case scenario with a total relative sea level rise of 1.36 m after 10 years. The following figures are included:

- Wave field (wave height and direction) and influence of sea level rise
- Bed level change (sedimentation & erosion)
- Bed level change (colour scale for relative Sea Level Rise) at the scale of the intertidal zone
- Bed level change (colour scale for relative Sea Level Rise) at the scale of the entire project area
- Difference plot of the final bed level between simulations with and without permeable structures
- Sediment concentration statistics
- Timeseries of bed level at the locations of permeable structures

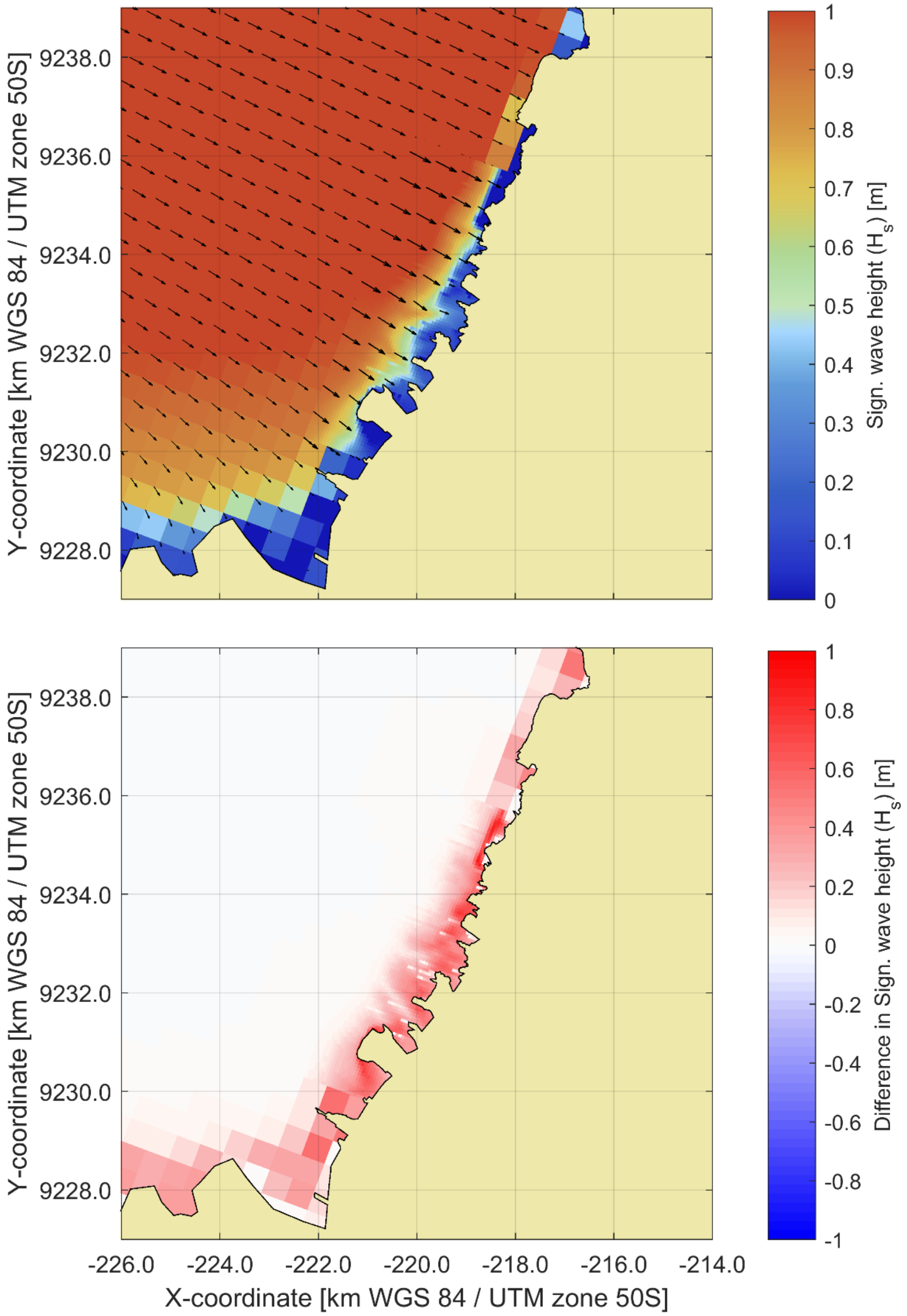

Figure E.30: Significant wave height during the peak of the monsoon for the worst-case scenario (upper panel) and differences in significant wave height between the start and the end of the simulation (lower panel)

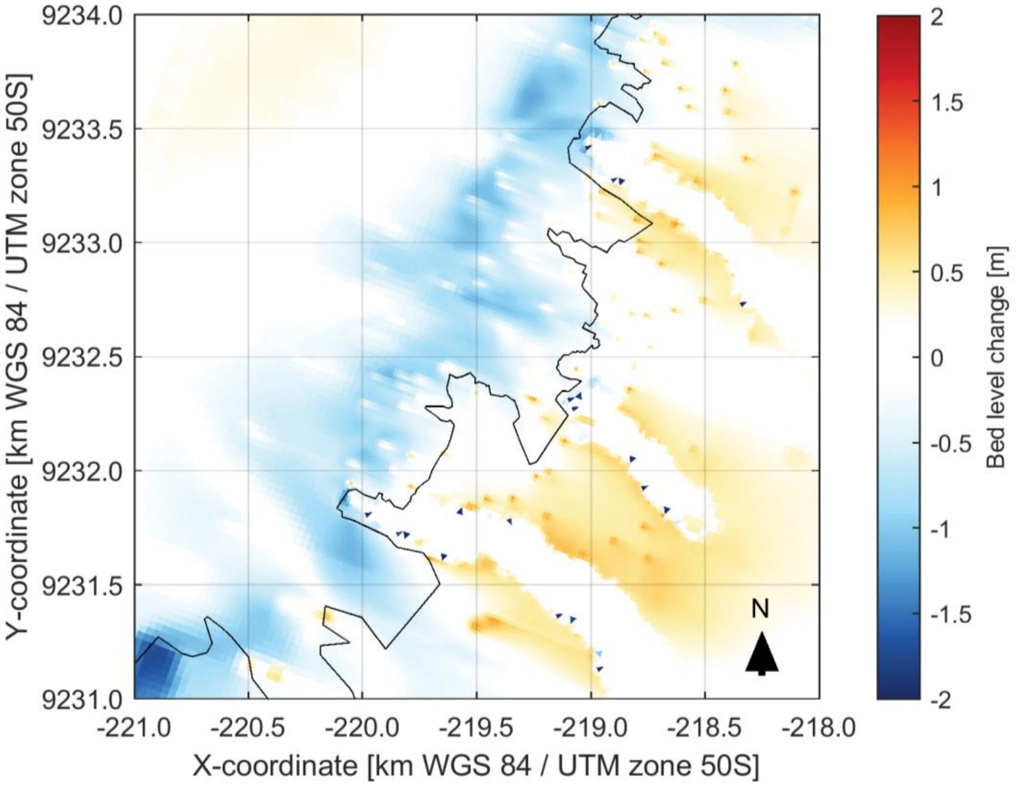

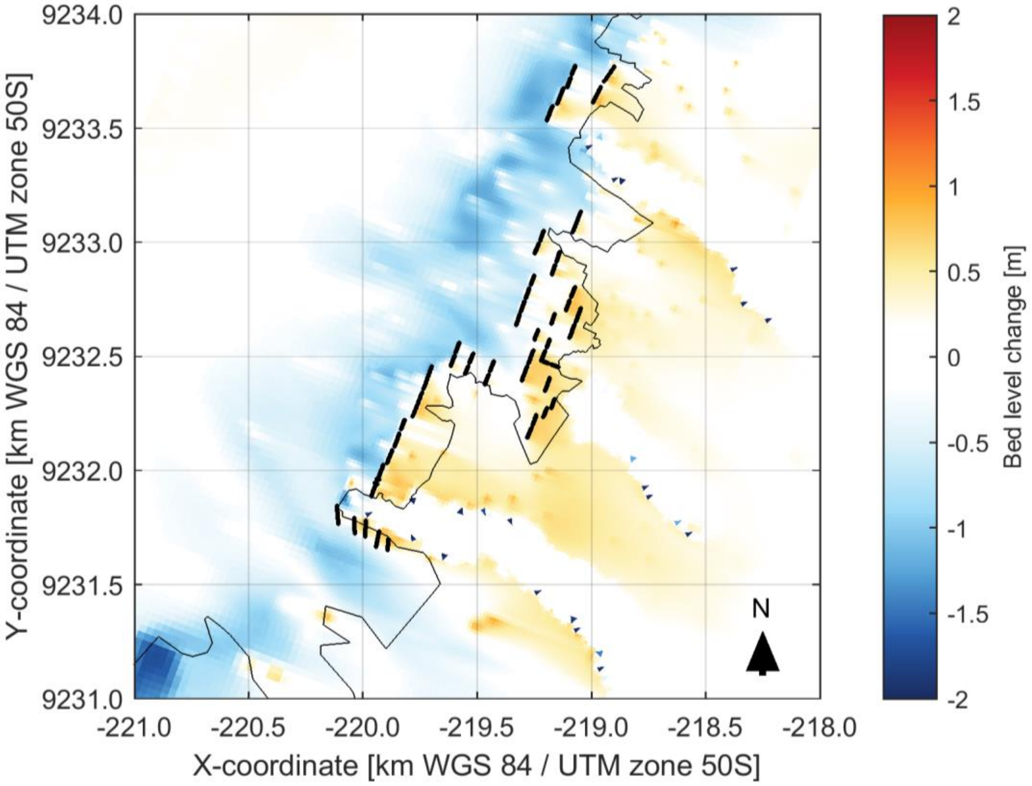

Figure E.31: Total bed level change after 10 years for the worst-case scenario. The upper panel shows the autonomous development and the lower panel shows the results of a simulation with permeable structures. Red colours indicate sedimentation areas

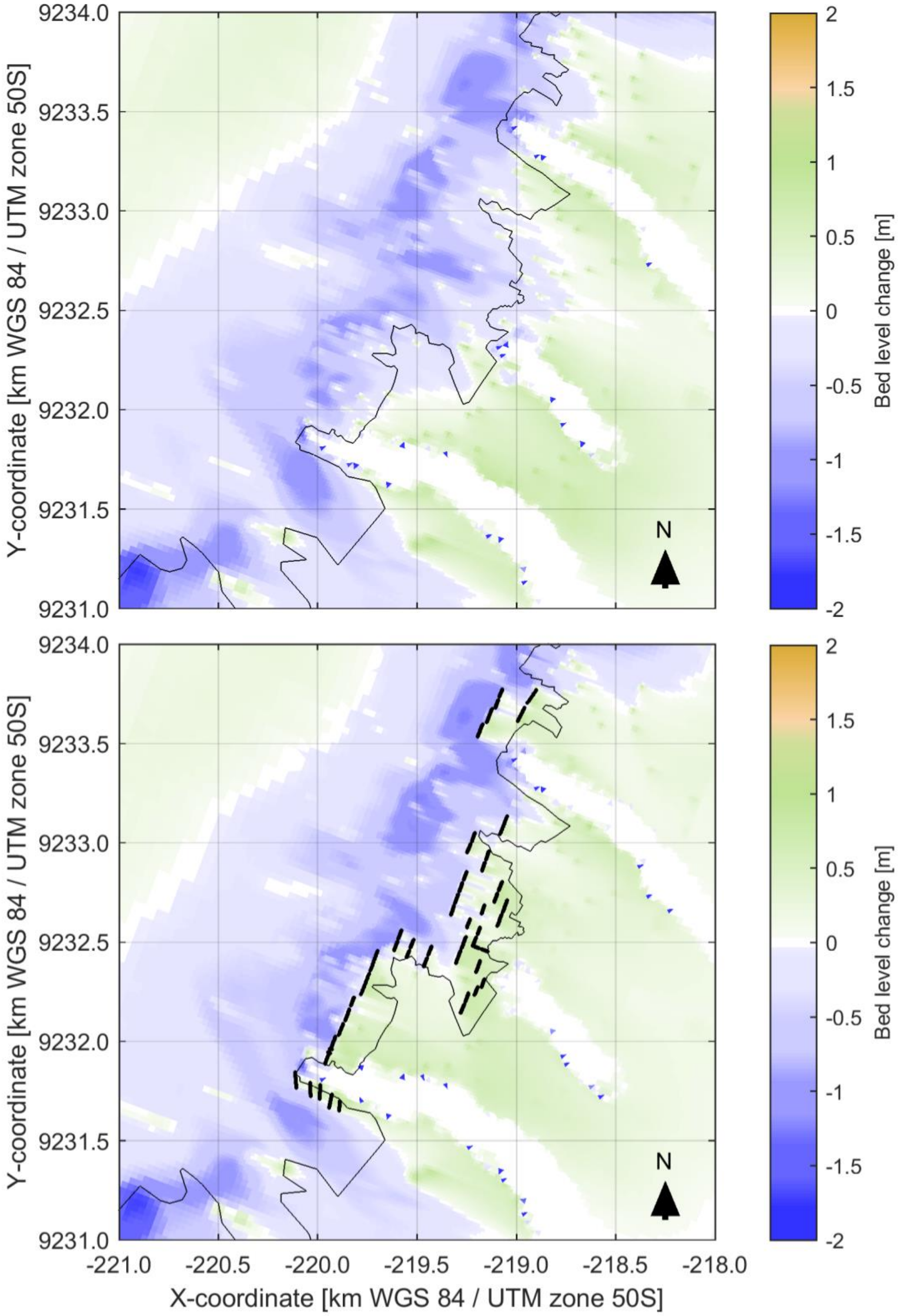

Figure E.32: Total bed level change after 10 years for the worst-case scenario (upper panel autonomous development; lower panel with permeable structures). Blue colours indicate erosive areas, green colours indicate partially drowning areas and brown colours indicate sedimentation rates that exceed the rate of relative sea level rise.

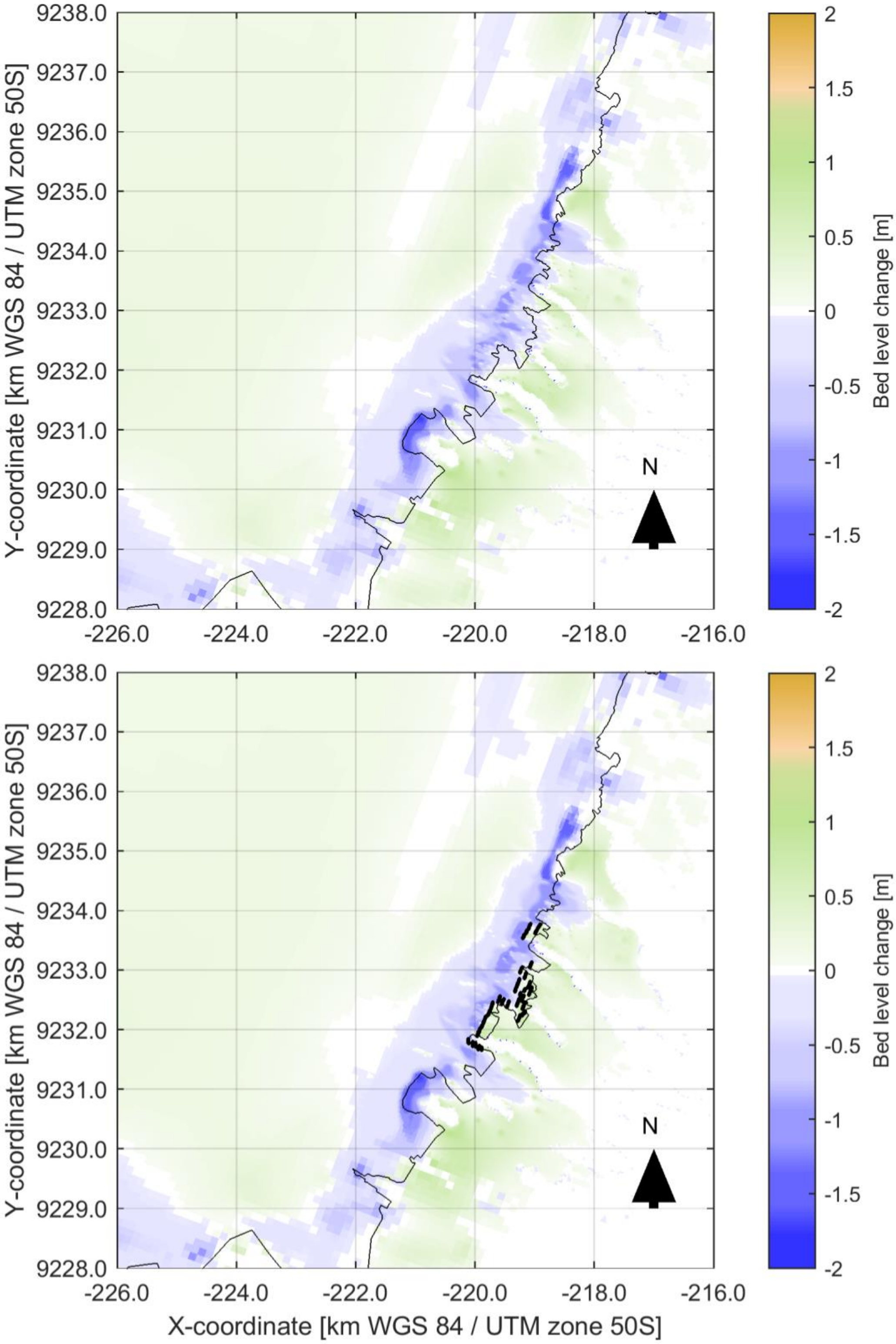

Figure E.33: Total bed level change after 10 years at the scale of the entire project area for the worst-case scenario simulations (upper panel autonomous development; lower panel with permeable structures). Blue colours indicate erosive areas, green colours indicate sedimentation areas where the sedimentation rate is smaller than the rate of relative sea level rise and brown colours indicate sedimentation rates that exceed the rate of relative sea level rise.

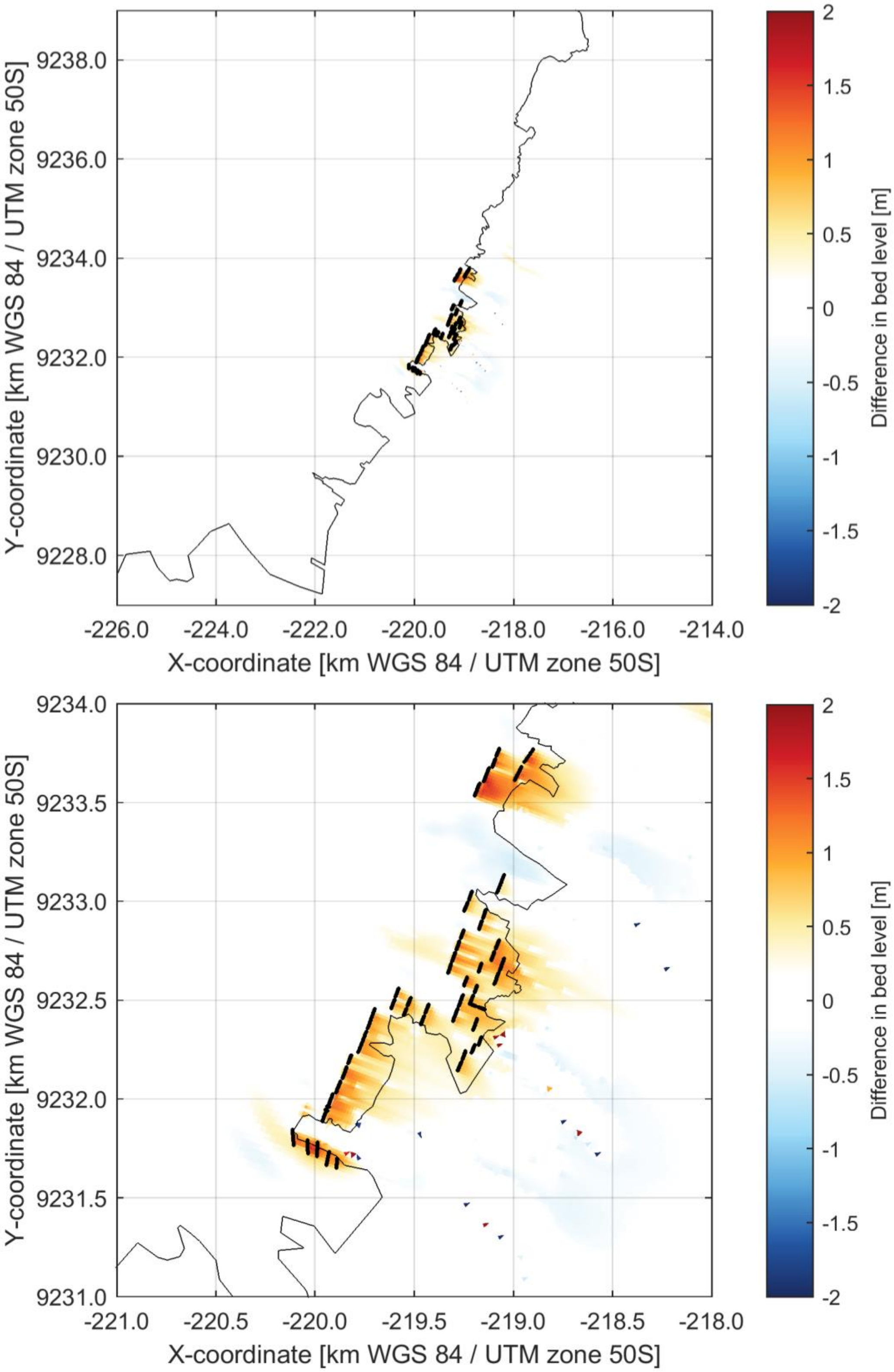

Figure E.34: Difference plot between final bed level with permeable structures and the autonomous development for the worst-case scenario (upper panel shows the extent of the project area; lower panel a zoom around the area of permeable structures). Red colours indicate higher bed levels in the simulation with permeable structures, whereas blue colours indicate lower bed levels in the simulation with permeable structures.

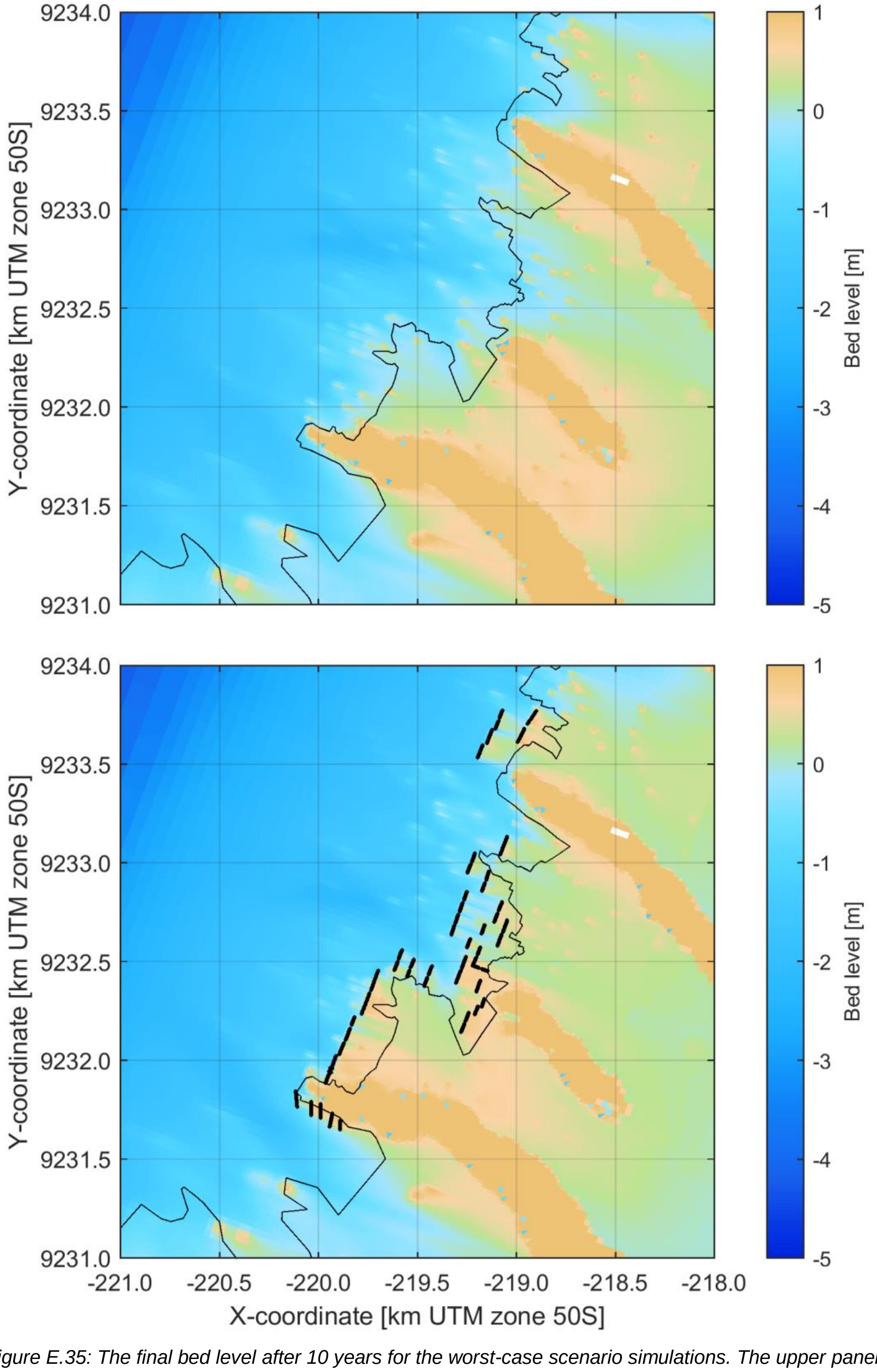

Figure E.35: The final bed level after 10 years for the worst-case scenario simulations. The upper panel shows the autonomous development and the lower panel shows the results of a simulation with permeable structures. Note that the vertical reference level z=0 has not changed, so the mean sea level is now located at z=+1.36 m.

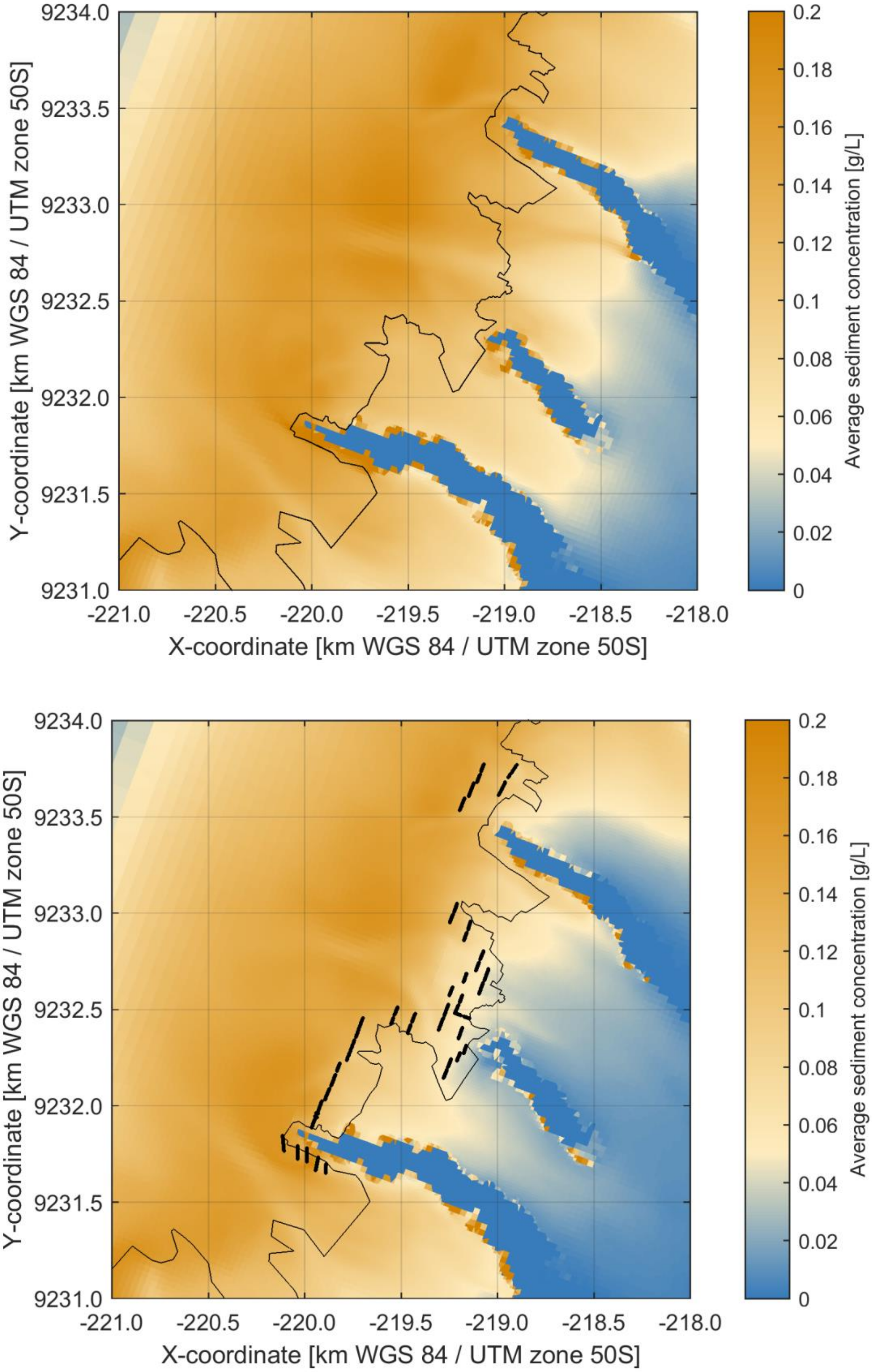

Figure E.36: Sediment concentration averaged over 10 years for the worst-case scenario simulations (upper panel autonomous development; lower panel with permeable structures).

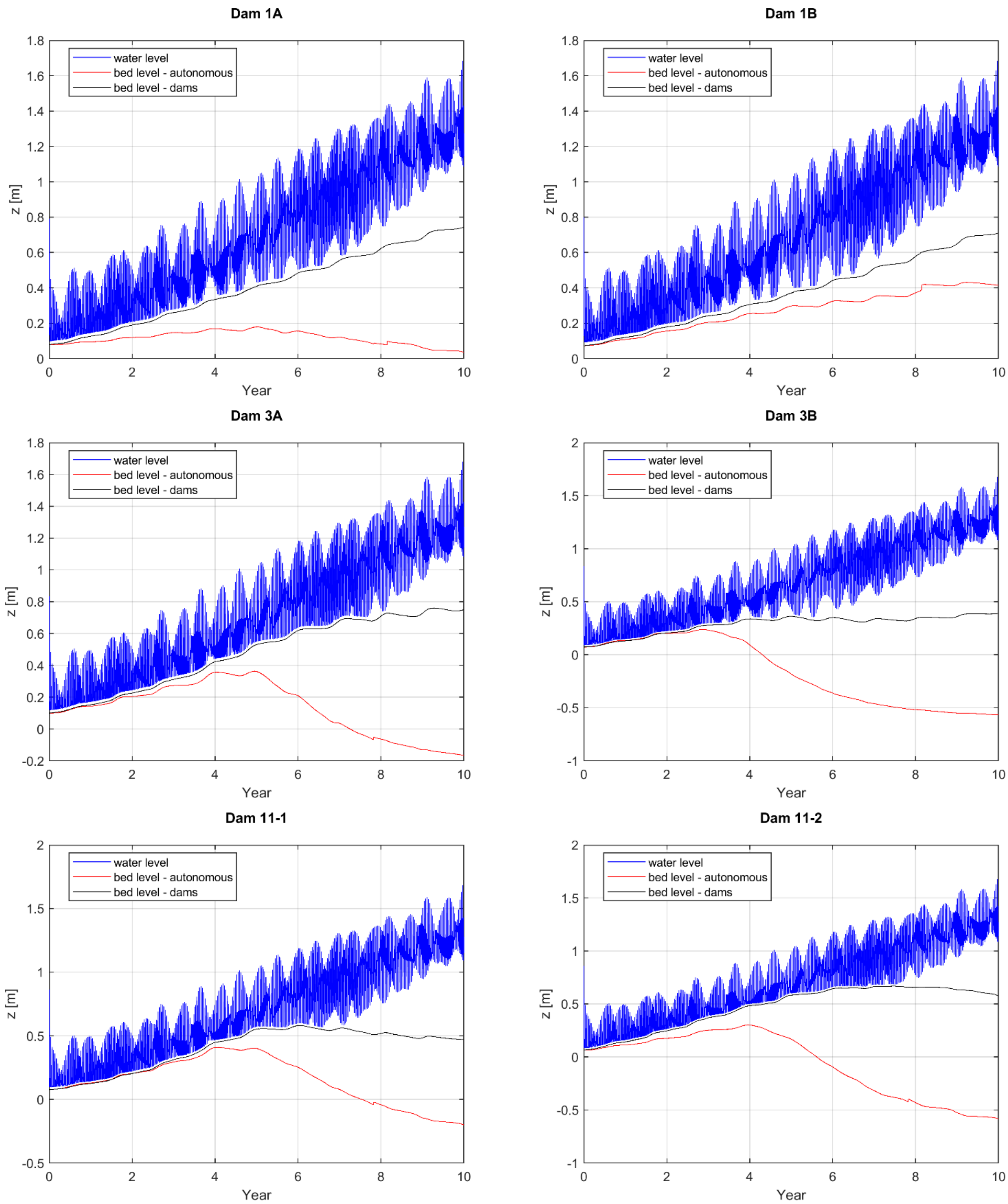

Figure E.37: Bed level development over time throughout the simulation for the worst-case scenario at observation points behind the permeable structures. The blue line gives the tidal water level including relative sea level rise (on hydrodynamic timescale), the red line shows the bed level of the autonomous development and the black line shows the bed level with permeable structures. The subpanels show structures 1A (top left), 1B (top right), 3A (middle left), 3B (middle right), 11-1 (bottom left) and 11-2 (bottom right).

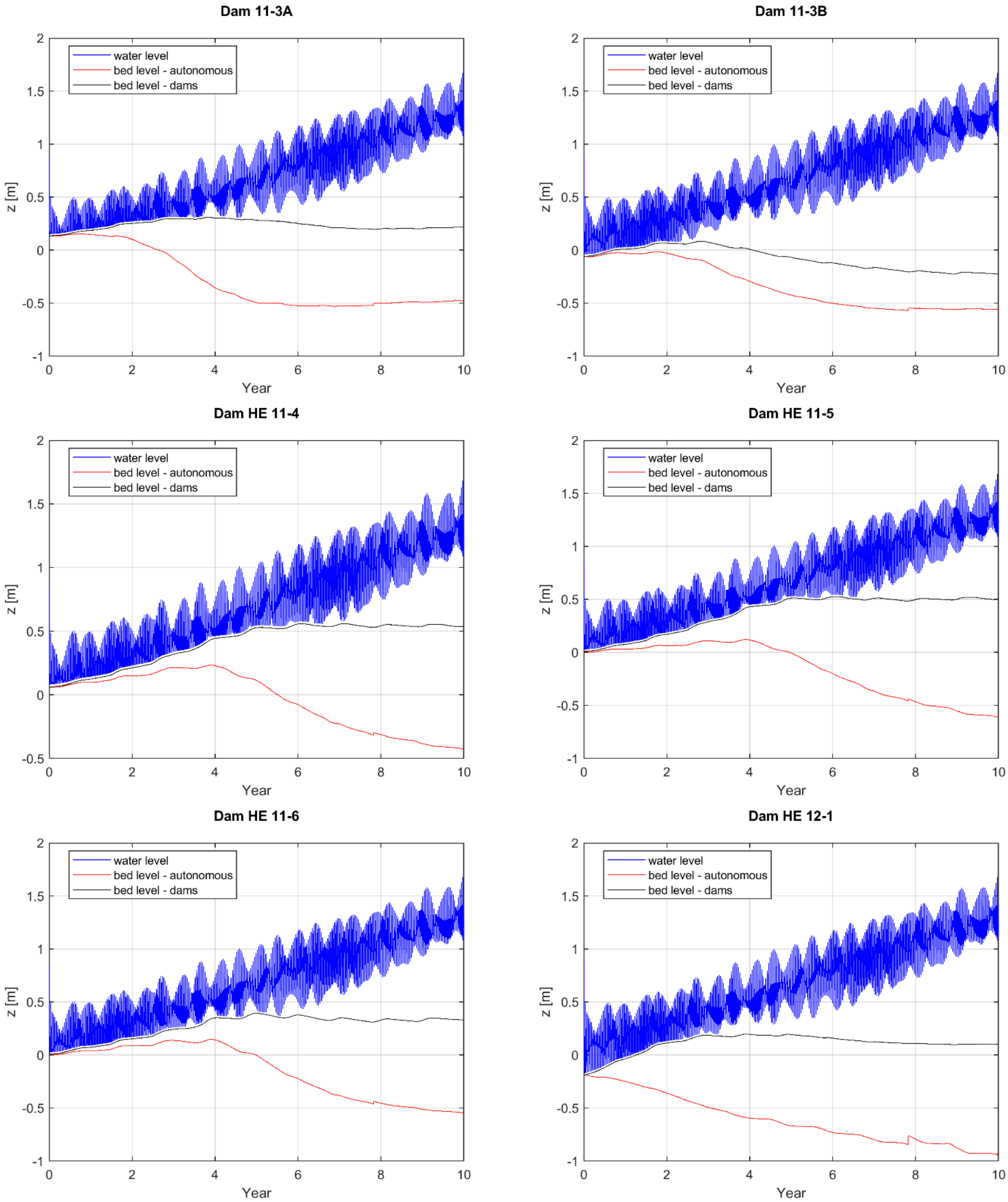

Figure E.38: Bed level development over time throughout the simulation for the worst-case scenario at observation points behind the permeable structures. The blue line gives the tidal water level including relative sea level rise (on hydrodynamic timescale), the red line shows the bed level of the autonomous development and the black line shows the bed level with permeable structures. The subpanels show structures 11-3A (top left), 11-3B (top right), 11-4 (middle left), 11-5 (middle right), 11-6 (bottom left) and 12-1 (bottom right).

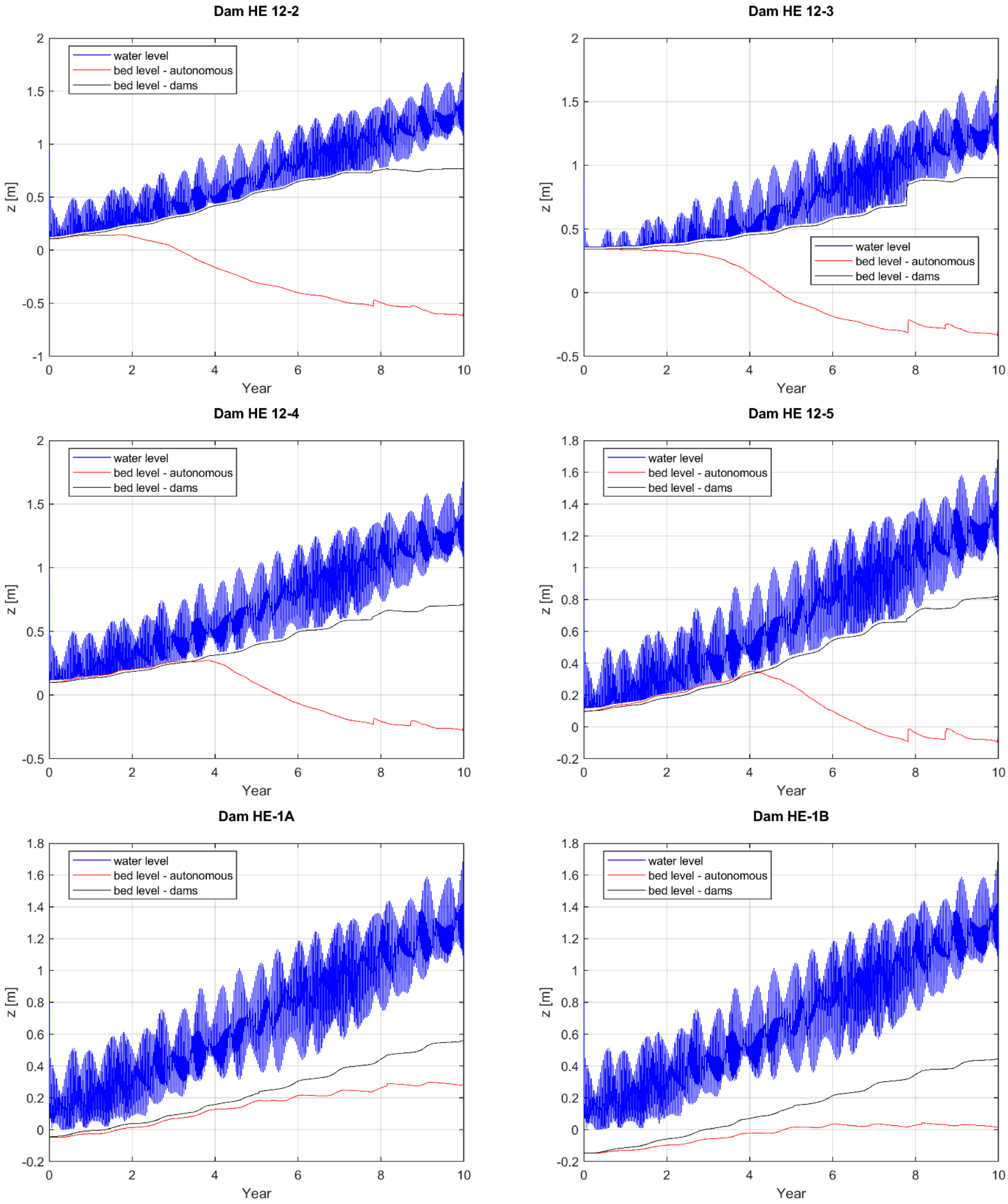

Figure E.39: Bed level development over time throughout the simulation for the worst-case scenario at observation points behind the permeable structures. The blue line gives the tidal water level including relative sea level rise (on hydrodynamic timescale), the red line shows the bed level of the autonomous development and the black line shows the bed level with permeable structures. The subpanels show structures 12-2 (top left), 12-3 (top right), 12-4 (middle left), 12-5 (middle right), HE-1A (bottom left) and HE-1B (bottom right).

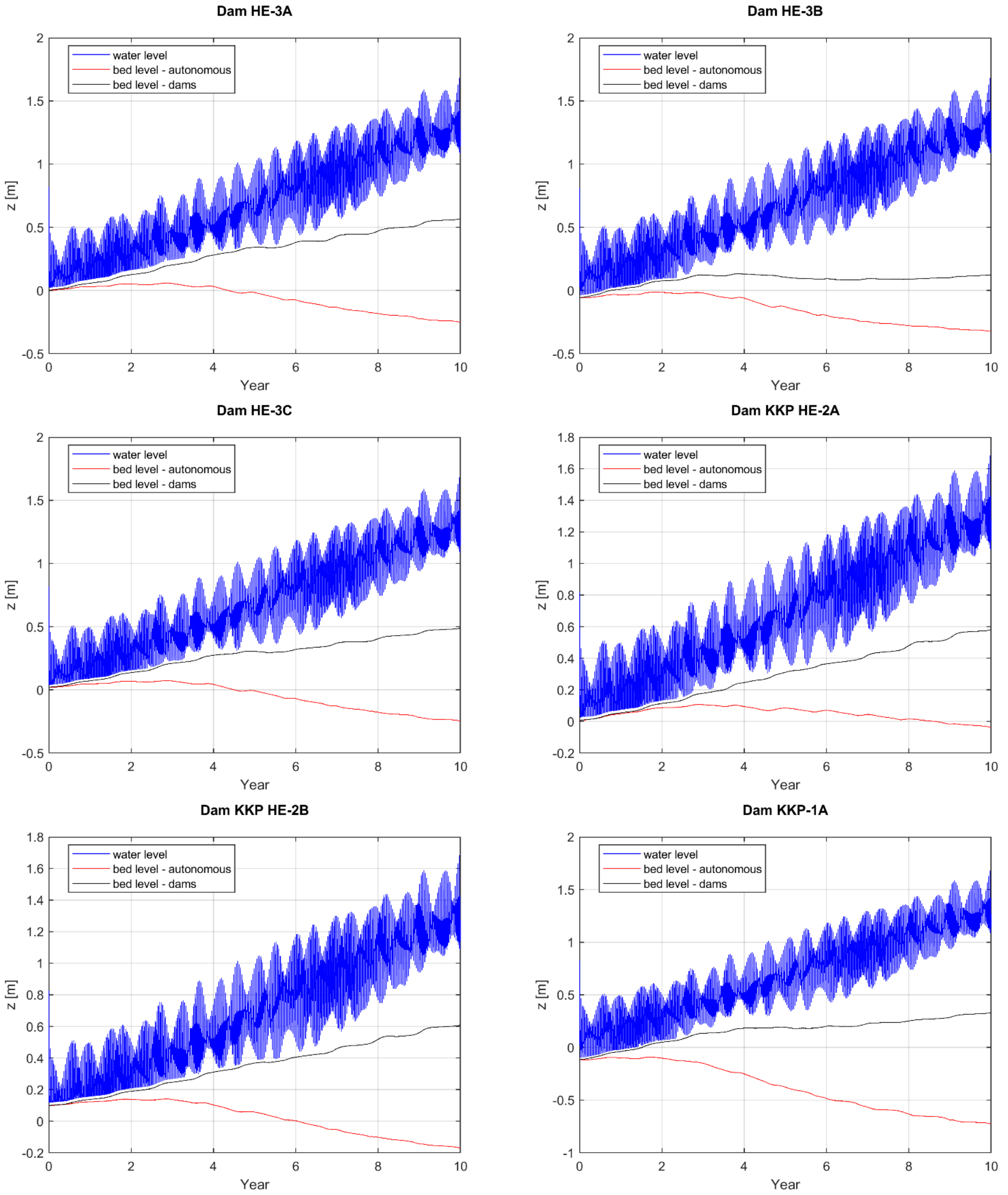

Figure E.40: Bed level development over time throughout the simulation for the worst-case scenario at observation points behind the permeable structures. The blue line gives the tidal water level including relative sea level rise (on hydrodynamic timescale), the red line shows the bed level of the autonomous development and the black line shows the bed level with permeable structures. The subpanels show structures KKP HE-2A (top left), KKP HE-2B (top right), HE-3A (middle left), HE-3B (middle right), HE-3C (bottom left) and KKP-1A (bottom right).

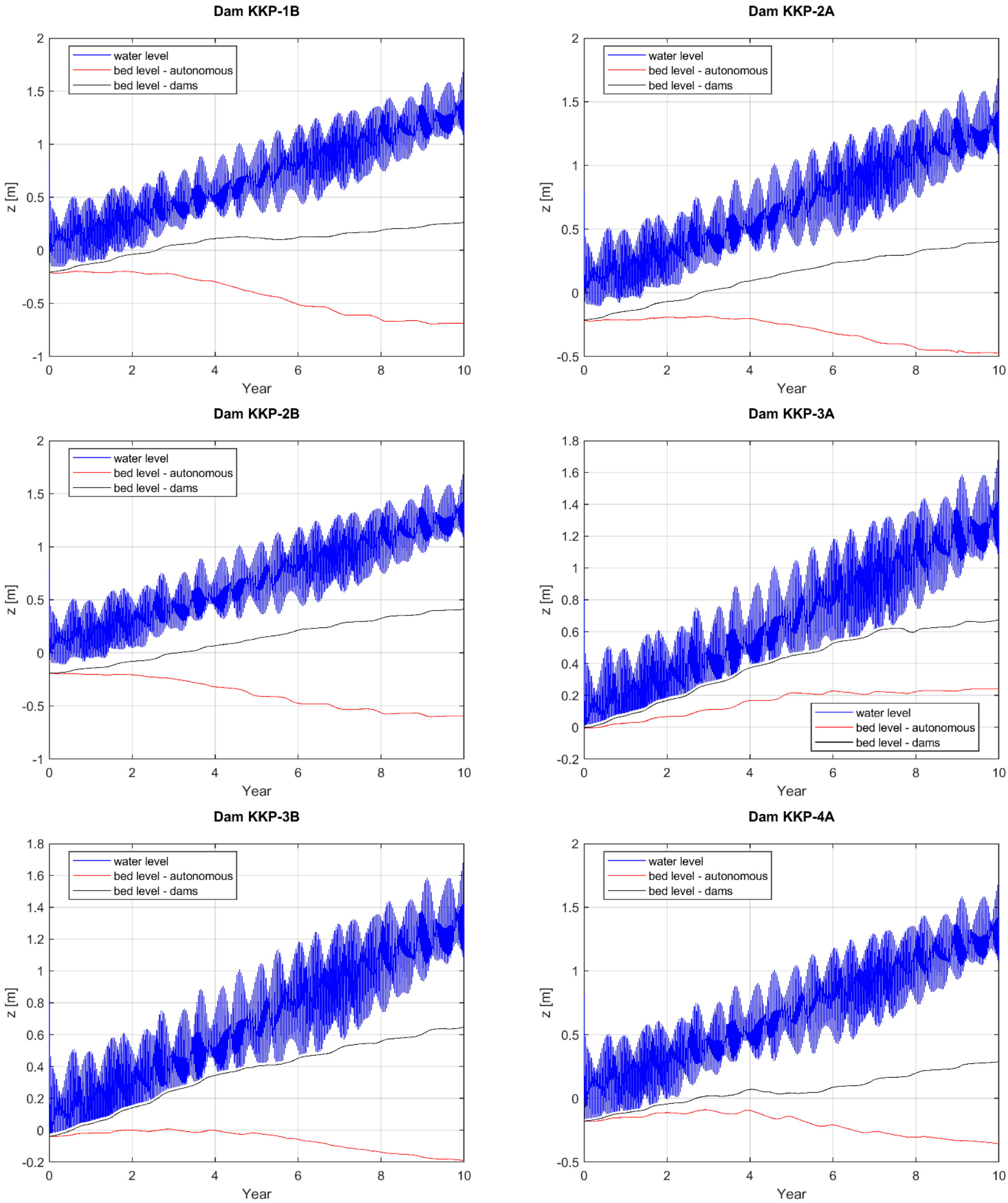

Figure E.41: Bed level development over time throughout the simulation for the worst-case scenario at observation points behind the permeable structures. The blue line gives the tidal water level including relative sea level rise (on hydrodynamic timescale), the red line shows the bed level of the autonomous development and the black line shows the bed level with permeable structures. The subpanels show structures KKP-1B (top left), KKP-2A (top right), KKP-2B (middle left), KKP-3A (middle right), KKP-3B (bottom left) and KKP-4A (bottom right).

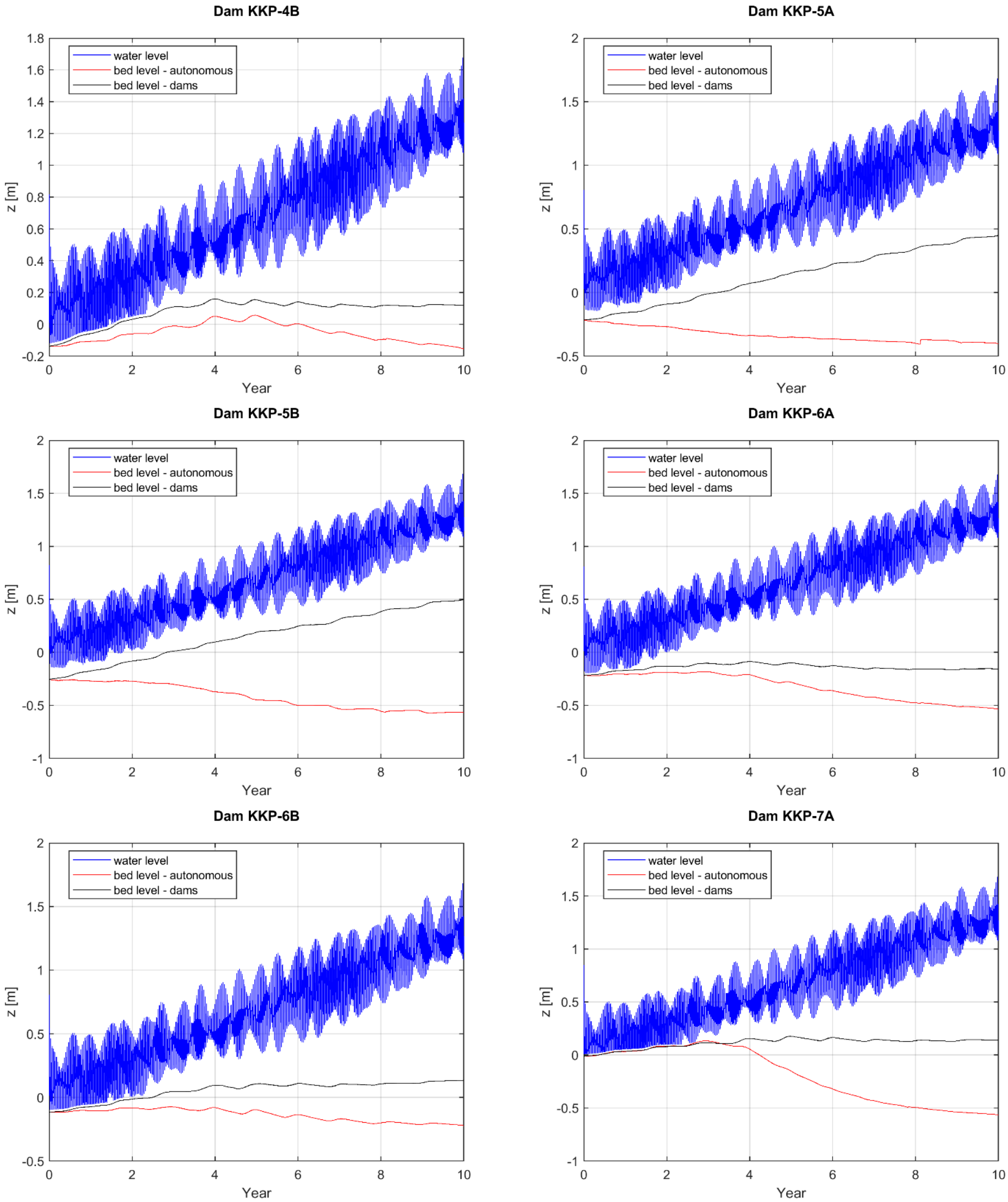

Figure E.42: Bed level development over time throughout the simulation for the worst-case scenario at observation points behind the permeable structures. The blue line gives the tidal water level including relative sea level rise (on hydrodynamic timescale), the red line shows the bed level of the autonomous development and the black line shows the bed level with permeable structures. The subpanels show structures KKP-4B (top left), KKP-5A (top right), KKP-5B (middle left), KKP-6A (middle right), KKP-6B (bottom left) and KKP-7A (bottom right).

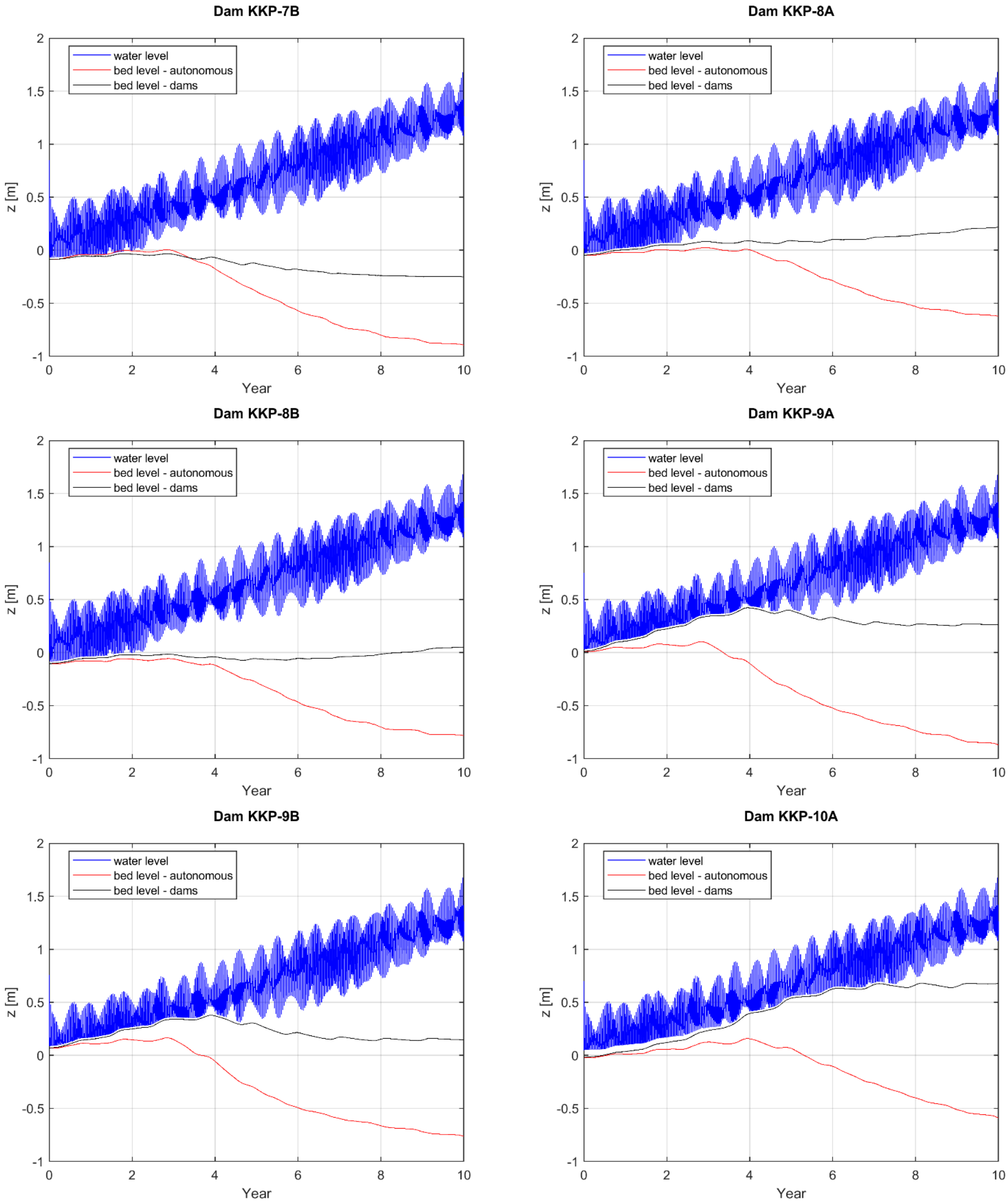

Figure E.43: Bed level development over time throughout the simulation for the worst-case scenario at observation points behind the permeable structures. The blue line gives the tidal water level including relative sea level rise (on hydrodynamic timescale), the red line shows the bed level of the autonomous development and the black line shows the bed level with permeable structures. The subpanels show structures KKP-7B (top left), KKP-8A (top right), KKP-8B (middle left), KKP-9A (middle right), KKP-9B (bottom left) and KKP-10A (bottom right).

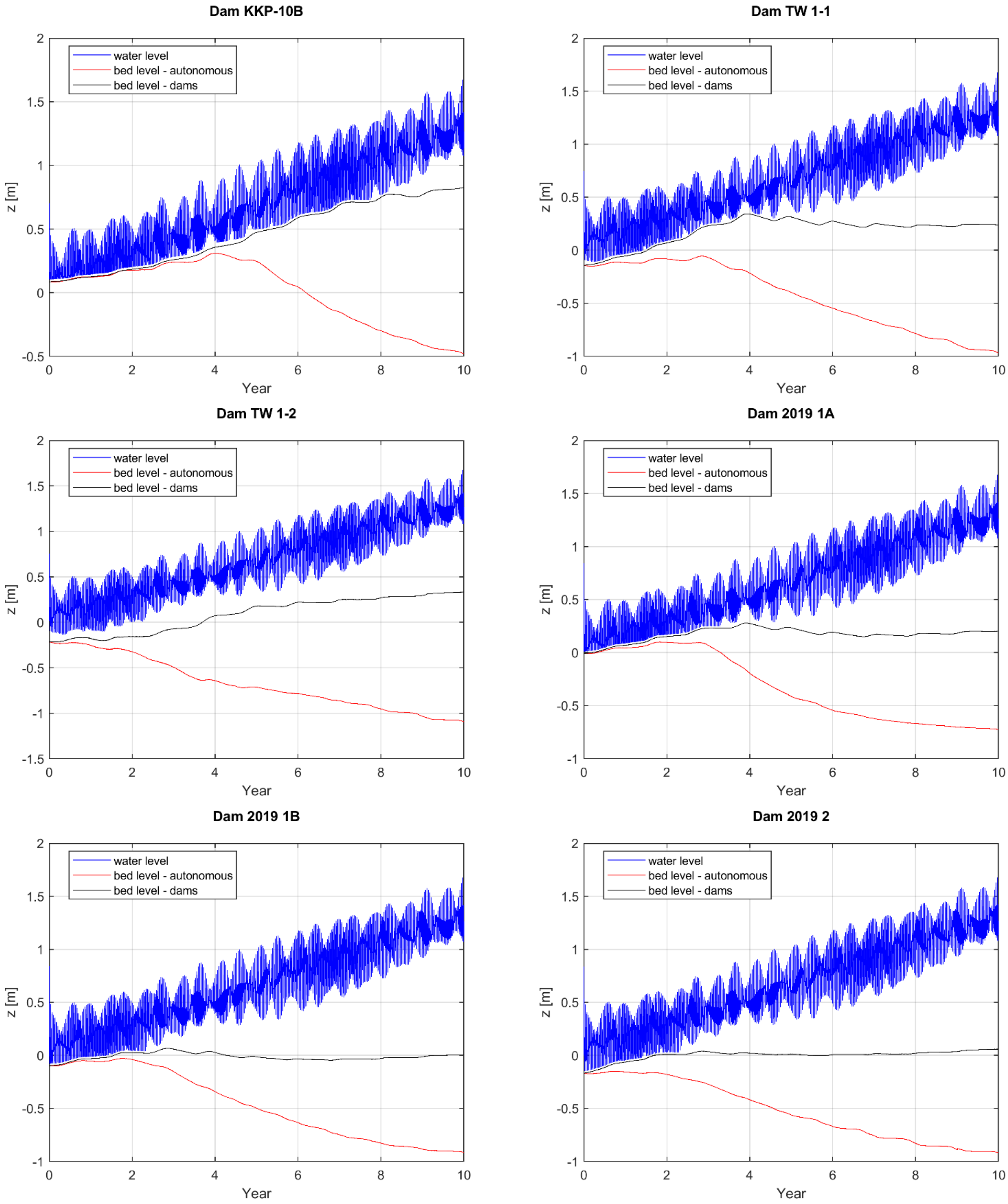

Figure E.44: Bed level development over time throughout the simulation for the worst-case scenario at observation points behind the permeable structures. The blue line gives the tidal water level including relative sea level rise (on hydrodynamic timescale), the red line shows the bed level of the autonomous development and the black line shows the bed level with permeable structures. The subpanels show structures KKP-10B (top left), TW 1-1 (top right), TW 1-2 (middle left), 2019-1A (middle right), 2019-1B (bottom left) and 2019-2 (bottom right).

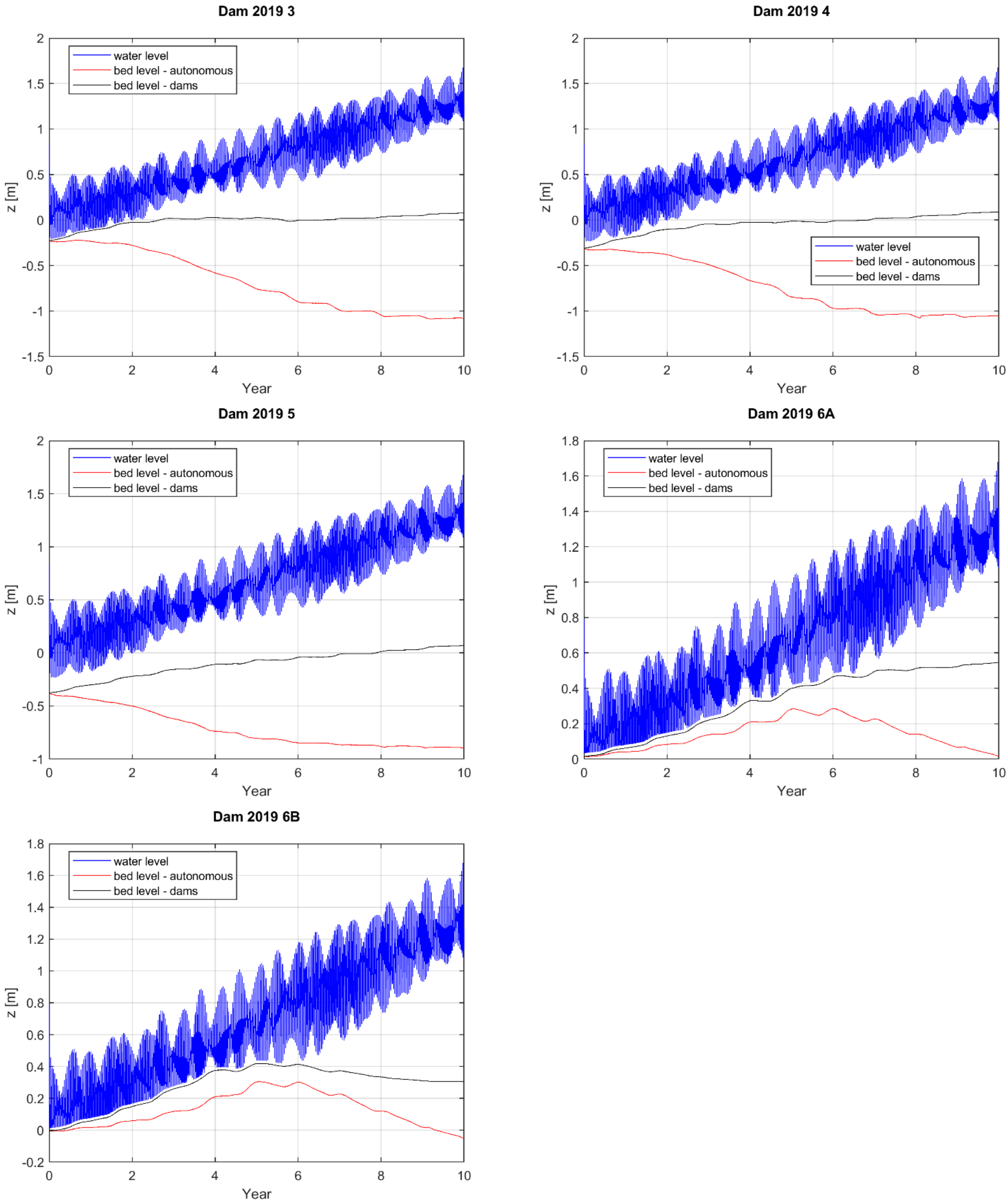

Figure E.45: Bed level development over time throughout the simulation for the worst-case scenario at observation points behind the permeable structures. The blue line gives the tidal water level including relative sea level rise (on hydrodynamic timescale), the red line shows the bed level of the autonomous development and the black line shows the bed level with permeable structures. The subpanels show structures 2019-3 (top left), 2019-4 (top right), 2019-5 (middle left), 2019-6A (middle right) and 2019-6B (bottom left).

Table E.3: Total bed level change at the observation points behind the permeable structures at the end of the worst-case scenario simulation

Observation point	Autono-mous	Permeable structures	Difference	Observation point	Autono-mous	Permeable structures	Difference
1A	-0,06	0,70	0,76	KKP-9A	-0,92	0,26	1,19
1B	0,35	0,69	0,33	KKP-9B	-0,86	0,09	0,95
3A	-0,28	0,70	0,97	KKP-10A	-0,61	0,73	1,34
3B	-0,64	0,35	0,98	KKP-10B	-0,60	0,78	1,39
HE-1A	0,34	0,66	0,32	11-1	-0,31	0,41	0,72
HE-1B	0,16	0,64	0,48	11-2	-0,69	0,47	1,15
KKP HE-2A	-0,05	0,62	0,68	11-3A	-0,62	0,09	0,72
KKP HE-2B	-0,29	0,55	0,84	11-3B	-0,49	-0,15	0,34
HE-3A	-0,28	0,60	0,88	HE 11-4	-0,52	0,49	1,01
HE-3B	-0,28	0,19	0,47	HE 11-5	-0,66	0,52	1,18
HE-3C	-0,29	0,50	0,79	HE 11-6	-0,57	0,35	0,92
KKP-1A	-0,64	0,47	1,11	HE 12-1	-0,82	0,29	1,11
KKP-1B	-0,50	0,49	0,99	HE 12-2	-0,77	0,68	1,45
KKP-2A	-0,28	0,65	0,93	HE 12-3	-0,70	0,59	1,29
KKP-2B	-0,43	0,63	1,06	HE 12-4	-0,41	0,64	1,05
KKP-3A	0,26	0,72	0,46	HE 12-5	-0,22	0,76	0,98
KKP-3B	-0,17	0,72	0,89	TW 1-2	-0,93	0,57	1,50
KKP-4A	-0,19	0,49	0,67	TW 1-1	-0,89	0,40	1,29
KKP-4B	-0,02	0,26	0,28	2019 1A	-0,72	0,23	0,95
KKP-5A	-0,20	0,70	0,90	2019 1B	-0,83	0,12	0,95
KKP-5B	-0,33	0,79	1,12	2019 2	-0,78	0,24	1,02
KKP-6A	-0,33	0,06	0,39	2019 3	-0,88	0,32	1,20
KKP-6B	-0,10	0,26	0,36	2019 4	-0,77	0,41	1,18
KKP-7A	-0,56	0,17	0,73	2019 5	-0,54	0,46	1,01
KKP-7B	-0,82	-0,16	0,66	2019 6A	-0,01	0,55	0,56
KKP-8A	-0,58	0,29	0,88	2019 6B	-0,08	0,31	0,39
KKP-8B	-0,70	0,18	0,88	**average**	**-0,44**	**0,44**	**0,88**